

JOINTS OF COMPOSITE CONSTRUCTION IN MARINE STRUCTURES

A thesis submitted for the degree of  
Doctor of Philosophy in the  
Faculty of Engineering of  
the University of London

by

Fatemeh Haj Sayed Javadi, BSc, MSc, DIC

Imperial College of Science and Technology,  
London.

February, 1979

TO MY PARENTS

## ABSTRACT

Offshore platforms in the North Sea are generally subjected to high cyclic loads which cause extreme fatigue problems particularly at the intersections of steel tubular members. In view of the shortcomings of these more traditional tubular joints, a new approach is suggested and developed in this thesis and that is the use of composite joints.

The structural complexity of the proposed composite joints required the development of a special purpose computer system for stress analysis. The computer system includes a doubly curved thin shell element (Semi Loof shell) used in conjunction with the newly developed hexahedral solid element (Semi Loof solid), thus permitting composite thin steel and thick concrete forms to be analysed.

Various numerical examples were selected to establish the validity and generality of the newly developed solid element. The element passes the patch test with rectangular, parallelogram, arbitrary quadrilateral and general hexagonal geometries. Mixed meshes consisting of Semi Loof shell and Semi Loof solid elements also passed the patch test.

An experimental study was carried out on straight tubular composite connections and comparison of the results with the finite element results verified the accuracy of the newly developed Semi Loof solid element.

Having thus established the performance and validity of the finite element system various types of tubular connections and tubular joints suitable for use in the construction or repair of pipe lines and offshore structures were analysed. Certain conclusions were drawn with respect to the design, fabrication and installation of the proposed composite connections in the construction and repair of North Sea structures.

## INDEX

	<u>Page</u>
ABSTRACT	3
ACKNOWLEDGEMENTS	10
NOTION	11
CHAPTER 1. GENERAL INTRODUCTION	13
1.1 Introduction	13
1.2 Review of previous work on tubular joints	15
1.2.1 Static experimental studies	15
1.2.2 Static analytical studies	18
1.2.3 Experimental fatigue studies	20
1.2.4 Fatigue life prediction	22
1.3 Material selection for platform joints	24
1.3.1 Behaviour of steel	24
1.3.2 Behaviour of concrete	26
1.4 Conclusions	28
1.5 Objectives and scope of the present research	28

	<u>Page</u>
CHAPTER 2. FINITE ELEMENT ANALYSIS	30
2.1 Introduction	30
2.2 Review of previous work on the finite element analysis of joints	32
2.3 Finite element program	36
2.3.1 Finite elements	36
2.3.2 Input facilities and mesh generation	37
2.3.3 Solution facilities	39
2.3.4 Output facilities	40
2.4 Theory of Semi Loof shell element	42
2.5 Program verification	49
2.6 Conclusions	50
CHAPTER 3. THE SEMI LOOF SOLID ELEMENT	51
3.1 Introduction	51
3.2 History	53
3.3 Requirements	56
3.4 Theory for constrained solid elements	57
3.4.1 Basic assumptions	57
3.4.2 Nodal configuration and sign convention	57
3.4.3 Shape functions	58
3.4.4 Element stiffness formulation	61
3.4.5 Unconstrained displacement field	62
3.4.6 Jacobian matrix	67

	<u>Page</u>
3.4.7 Strain displacement relations	70
3.4.8 Kinematic constraints	73
3.4.9 Numerically integrated stiffness matrix	76
3.4.10 Nodal and pressure loading	77
3.5 Reduced numerical integration and spurious mechanism	79
3.6 Global stresses	82
3.7 Numerical results	83
3.7.1 Patch tests	83
3.7.2 Convergence studies	84
3.8 Conclusions	86
CHAPTER 4. EXPERIMENTAL STUDY OF THE COMPOSITE CONNECTIONS	87
4.1 Introduction	87
4.1.1 Objectives of the experimental tests	87
4.1.2 Composite connection layout and forms of construction	88
4.2 Model scale and materials	90
4.2.1 Grout properties	90
4.2.2 Steel properties	91
4.3 Instrumentation	92
4.3.1 Displacements	92
4.3.2 Strains	92
4.3.3 Data logger	92

	<u>Page</u>	
4.4	Loading procedure	93
4.5	Small scale models	94
4.5.1	Effect of tube and sleeve geometry on bond strength	95
4.5.2	Effect of length/diameter ratio on bond strength	96
4.5.3	General behaviour of tests	97
4.6	Large scale model	98
4.6.1	Variation of strains and displacements in large scale model	99
4.6.2	General behaviour of large scale test	99
4.7	Conclusions	101
CHAPTER 5.	FINITE ELEMENT ANALYSIS OF COMPOSITE TUBULAR JOINTS	102
5.1	Introduction	102
5.2	Composite straight tubular connections	103
5.2.1	Finite element analysis of steel tubes connected by a steel sleeve filled with concrete	103
5.2.2	Finite element analysis of steel tubes connected by a prestressed concrete sleeve	106
5.2.3	Discussion and conclusions	107



	<u>Page</u>
5.3 Composite tubular T-joints	110
5.3.1 Finite element analysis of a T-joint with a concrete collar	111
5.3.2 Finite element analysis of a T-joint with a steel collar filled with concrete	112
5.3.3 Discussion and conclusions	112
5.4 Composite tubular K-joint	114
5.4.1 Finite element analysis of a K-joint with a concrete collar	114
5.4.2 Discussion and conclusions	115
5.5 Conclusions	116
CHAPTER 6. GENERAL CONCLUSIONS	117
6.1 Summary of work	117
6.2 Concluding remarks	118
6.3 Future experimental work	119
APPENDIX 1. T, Y and K joint geometric formulation	120
APPENDIX 2. Determination of principal strains and stresses	123
APPENDIX 3. Various designs for composite tubular joints	125
REFERENCES	127
TABLES	139
FIGURES	145
PLATES	218

## ACKNOWLEDGEMENTS

The author wishes to express her gratitude to the following:-

Professor A.J. Harris, Head of Concrete Structures and Technology section of the Civil Engineering Department, Imperial College, who supervised the project and provided helpful suggestions from time to time during the course of the study.

Dr. A.C. Cassell, who also supervised this work, and for his encouragement and advice on many aspects of this project.

The Science Research Council for their financial support and also sponsorship of the experimental work.

Dr. L.P.R. Lyons for his advice during the finite element research and for making available the use of his finite element system.

The technical staff of the Engineering Concrete and Structures Laboratories without whose experience and technical abilities the experiment content of the thesis would not have been possible. In this context special mention must be made of Messrs. J. Neale and R.W. Loveday.

Mr. M. Kubba Concrete D.I.C. student for his help in conducting experiment.

Mrs. H. Guile who traced the figures.

Mr. F. Milsom who took the photographs.

Finally, Miss C.D.M. Collins who typed the manuscript.

## NOTATION

$a_o$	initial crack size
$a_{cr}$	the critical crack size
B	strain-displacement matrix
C	carbon
$c_r$	chromium
cu	copper
$d_i$	unit displacement vector at a point i
D	modulus matrix
E	modulus of elasticity
e	eccentricity of a branch from central axis of chord
$\bar{F}$	element nodal force vector
J	the Jacobian matrix
$\vec{J}$	vector of covariant base vectors
$\vec{j}$	vector of contravariant base vectors
$K^e$	element stiffness matrix
L	Loof shape functions
$M_x$	flexural moment per unit width perpendicular to the x-direction at Loof point
$M_n$	manganese
$M_o$	molybdenum
N	shape functions
$N_i$	nickel
$P_{xi}, P_{yi}, P_{zi}$	applied nodal loads along the x,y and z axes at point i, respectively
t	thickness of shell
u,v,w	global displacement components at a point
V	vanadium

$W$	shape function array
$W^*$	constrained shape function array
$W_A, W_B$	partitions of the shape function array which refer to the wanted and unwanted variables respectively
$\gamma_{xy}$	shearing components of strain in the xy plane
$\gamma_{xz}, \gamma_{yz}$	transverse shear strain components in the xz and yz planes respectively
$\delta$	vector of global displacements
$\delta^e$	vector of global displacements for an element
$\delta_A, \delta_B$	element displacements associated with the wanted and unwanted variables
$\epsilon$	strain vector
$\epsilon_x, \epsilon_y, \epsilon_z$	normal components of strain in the x, y and z directions respectively
$\xi$	natural coordinate in the xi direction
$\eta$	natural coordinate in the eta direction
$\zeta$	natural coordinate in the zeta direction
$\theta_x, \theta_y$	rotations of normals to the mid-surface about the x and y axes respectively
$\nu$	poisson's ratio
$\sigma$	stress matrix
$\sigma'$	global stress matrix
$\sigma_x, \sigma_y, \sigma_z$	normal components of stress in the x and y directions respectively
$\tau$	shearing stress
$\tau'$	global shearing stress

## CHAPTER 1

## GENERAL INTRODUCTION

## 1.1 INTRODUCTION

Increasing power consumption and the importance of petroleum for the production of energy are reflected in the increase of crude oil exploration. New discoveries have been found under the sea in the shallow regions of the Gulf of Mexico, the North Sea, the Persian Gulf, the coasts of Gabon, Nigeria and Senegal and more recently in Alaska.

The first drilling rig in the Gulf of Mexico was installed in 1947, and in the following years rapid progress took place not only in the number of platforms constructed, but also in the water depths in which platforms were installed, for example, in the years 1955, 1965 and 1967 depths of 33, 95 and 133 meters were reached.

In August 1972, Amoco installed the first jack-up gas production platform in 25 meters of water in the Laman Bank of the United Kingdom section of the North Sea. This installation was the start of the rapid development which has recently resulted in the installation of a Chevron platform in 168 meters of water in the Ninian Field.

The North Sea and Eastern and Western Canada, where the number of installations is increasing, have the most hostile marine environments with severe waves, Fig. (1,1), and deep water. As the water depths increase in this hostile environment, so do the structural complexities, and there is an increasing need for more economical and efficient

designs. Structures in the North Sea are generally subjected to dynamic loads which cause extreme fatigue problems, particularly at the intersections of tubular members (tubular joints). Various problems, such as cracking and even complete separation at the intersection of tubular joints, have been cited in the literature.

In view of the shortcomings of the more traditional tubular joints, a new approach is suggested and developed in this thesis and that is the use of composite joints. Accordingly, this thesis is concerned with the design, analysis and testing of a range of suitable composite joint configurations.

In this chapter a general review of joint problems in respect of analytical and experimental studies is carried out.

In chapter 2 the finite element method for shell analysis is reviewed. A description of Semi Loof shell is presented and the finite element method is extended to analyse both shell and solid elements.

In chapter 3 the theory of the newly developed Semi Loof solid element is described together with the extensive series of tests carried out to establish the validity of the proposed element formulation.

In chapter 4 an extensive series of experimental tests carried out on straight tubular connections are described. Several small scale and one larger scale specimens were tested.

In chapter 5 the elastic behaviour of straight tubular connections and tubular joints is discussed.

In chapter 6 concluding remarks of a general nature are made together with recommendations for future research.

## 1.2 REVIEW OF PREVIOUS WORK ON TUBULAR JOINTS

Most joints in offshore platforms are complicated and consist of many interconnecting members. The lack of suitable analytical tools for the analysis of such complex structures has, in the past, meant that most information available on the stress distribution in tubular joints was obtained by experimental methods. However, a small number of analytical studies have been carried out on tubular joints.

### 1.2.1 *Static Experimental Studies*

During the last four decades extensive and varied experimental studies have been carried out on typical T, Y and K joints.

Roark<sup>1.1</sup> measured the effect of a concentrated external load applied normal to the surface of thin walled cylinders, from which he derived empirical expressions for circumferential and longitudinal stresses of T joints.

Later Schoessow and Koaistra<sup>1.2</sup> collected very extensive empirical data by studying a specimen which consisted of a 1.35 m diameter cylindrical shell to which two 0.3 m diameter tubes were symmetrically attached. The two branches were loaded in tension, compression, longitudinal bending and circumferential bending. Electrical strain gauges were placed on the inside and outside surfaces of the branch and chord tubes.

In the studies conducted by Bryant and Pease<sup>1.3</sup> attempts have been made to compare stresses computed theoretically with those determined experimentally. The test consisted of unreinforced T-joints 0.175 m outside diameter chord where strains were measured using electrical resistance strain gauges.

Subsequently, the experimental results were compared with values derived from the Bijlaard <sup>1.4</sup> equations with fair agreement. A series of tests on T-specimens was also conducted at the Southern Methodist University <sup>1.3</sup>, with only one of nine specimens being instrumented with strain gauges. From these tests, a relationship between failure load and wall thickness/diameter ratio was derived.

Toprac <sup>1.5</sup> conducted a study of the strength and rigidity of tubular joints. Tubes of 0.1 m and 0.2 m diameter were welded to make angles of 90° and 135° with each other respectively. These tests were basically concerned with the moment rotation of the joint and the value of plastic moment.

Beale and Toprac <sup>1.6</sup> later carried out a two phase research project on tubular joints. Phase one involved seven joints with various geometrical properties, tested within the elastic range and with each subjected to four loading conditions (direct tension, direct compression, longitudinal moment and circumferential moment). All of these specimens were strain gauged, and subsequently they were loaded to failure with a tensile load on the brace. The experimental results for the stresses in a T-joint indicated that inadequacies existed in the then popular theoretical method of Bijlaard's. However comparing the results predicted by Dundrova's equation <sup>1.7</sup> indicated a comparatively good correlation between theory and experiment. The second phase of the project expanded to cover Y and K specimens and the Dundrova equation was used for correlation. The vertical and horizontal displacements were obtained after



application of each load increment, also observations were made on the stress coats after each increment of load to determine the direction of principal stress. The variation of stress with respect to geometrical properties was studied and empirical equations for T and Y joints were derived, together with an approximate evaluation for K joints. However investigations carried out by other researchers have subsequently proved the inapplicability of this empirical equation for large diameter K joints.

An 'ideal' T-joint was constructed and tested at Oak Ridge National Laboratories <sup>1.8</sup>. The joint was formed by welding together two thick-walled carbon steel cylinders. The weldment was annealed and the inner surface machined by boring. The joint was annealed a second time and the outer surface machined by turning on a lathe, milling and finally by hand finishing in the junction region. The absence of a weld toe permitted gauges to be placed within 1/8 of an inch from the point of intersection of the branch and chord. Strain gauge data were assimilated for 13 load cases, six branch loads, six chord loads and an internal pressure.

An experimental study of the effect of stiffening rings on the strength of a Y-joint was carried out by Miller and Trammel <sup>1.9</sup>. A 1.35 m chord diameter was used to allow access to develop full penetration welds. The joint was subjected to combinations of axial load, longitudinal and circumferential moment but did not produce any guide to the number and size of stiffening rings required.

### 1.2.2 *Static Analytical Studies*

Early attempts at analysis of tubular joints began with the solution of classical equations for cylindrical thin shells, such as Donnell's equation <sup>1.10</sup> and Flugge's equation <sup>1.11</sup>.

Yuan <sup>1.12</sup>, using both the Donnell and Flugge equations analytically, studied cylinders subjected to diametrically opposed concentrated loading.

Bijlaard <sup>1.3,1.4</sup> used an equation similar to Donnell's equation with the displacement represented by a double Fourier series in a natural coordinate system lying on the shell surface. This equation overcomes some of the known inaccuracies of Donnell's equation for long shells. For tubular T-joints in which the branch was subjected to an axial load, the load transmitted to the cylinder was assumed to be radially directed and uniformly distributed over a square area.

Although the above theories have done much to further the understanding of the behaviour of tubes subjected to external load, several limitations in their range of application have been found.

An improved representation of the stresses in a T-joint has been presented by Dundrova <sup>1.7</sup>. In this analysis, loads were transmitted to the chord along the line of intersection with the branch, and it was assumed that the chord was subjected only to forces directed parallel to the branch axis. Dundrova extended the analysis to Y and K joints. In all of these connections, compatibility of the displacements in the axial direction of a branch was maintained between the branches and the chord. However the flexural interaction between a

branch and chord was not considered.

Scordelis and Bouwkamp's<sup>1.13</sup> analytical study of a tubular joint was based on Donnell's equation. This analysis was improved to accept five different types of loading viz, radial load, tangential load, transverse moment load, longitudinal moment load and radial moment load, and this was achieved by applying the load in the form of associated Fourier series. The results derived from analysis showed an inherent improvement by correct evaluation of the load transfer from branch tube to the chord member over previous methods.

It is apparent that the classical methods of shell analysis which have been used by previous investigators deal with the tubular joint problem only approximately because of the difficult boundary conditions at the cylinder intersection line. These methods have considered only the axial stiffness of the branch in computing the forces transmitted by the branch to the chord and have neglected the flexural stiffness at the chord-branch intersection.

The problems associated with classical methods of analysis have been gradually overcome with the emergence of the finite element method. The finite element method has been developed and applied to tubular joint problems since the latter part of the last decade. A literature survey of this method is presented in chapter 2.

### 1.2.3 *Experimental Fatigue Studies*

Many structures suffer a reduction in strength after being subjected to cyclic loading. This phenomenon is known as fatigue, and is essentially a process of crack initiation and subsequent propagation.

The fatigue strength of platforms designed to operate in the North Sea is critical compared with those for other marine areas.

The first study on the behaviour of T-joints under cyclic loading was made at the University of Texas <sup>1.14</sup> and considered the influence of geometrical stress concentration on fatigue in lower range of cycles (about  $10^5$  cycles). The results indicated the considerable effect of geometrical parameters on fatigue and also emphasised that the effect of weld profile and stress range should not be neglected. This project was later expanded to investigate the effect of stress range and weld profile (convex weld surface or concave weld surface <sup>1.15</sup>), which showed that almost all the crack initiated at the stress concentration point in the chord wall.

A research team at the University of California <sup>1.16</sup> also reported the importance of stress concentration and its influence on the fatigue behaviour of joints.

In the United Kingdom research was carried out on the effect of eccentricity on K joints <sup>1.17</sup> and it was reported that the highest fatigue strength was obtained when branches overlap each other at the intersection whereas the lowest fatigue life occurred when they were separated.

Later a random load fatigue test was conducted on a tubular welded T-joint subjected to in-plane bending <sup>1.18</sup> . The purpose of the test was to develop techniques able to predict the fatigue life of a typical joint. It was noted that the life of a joint was dependent on the crack propagation through the wall of the tube but the tests failed to provide a basis for the prediction of the fatigue life of joints in general.

A series of fatigue tests under constant and variable amplitude loading were carried out to evaluate the suitability of Miner's Rule <sup>1.19</sup> for cumulative fatigue damage calculation <sup>1.20</sup> . Very good correlation of data was obtained from constant-amplitude fatigue tests and the AWS design curve <sup>1.21</sup> which suggests that AWS design curves are a safe criterion for fatigue analysis. Comparison of variable-amplitude data also suggests that Miner's Rule was a safe criterion for cumulative damage calculations.

The scatter of the results observed in various fatigue tests mentioned in this review could be due to the fact that most of the available data of welded connection relates to test specimens with small diameters, which are not in every respect representative of the joints in offshore structures. Most of the experiments were performed under constant stress amplitude and high frequency, whereas an offshore structure is subjected to random loading with fairly low frequency. A number of other factors influencing the fatigue behaviour, such as corrosion, growth of marine organisms and low temperature which should also be simulated in laboratory experiments.

#### 1.2.4 Fatigue Life Prediction

The service life of tubular connections subjected to fatigue can be determined with the aid of either S-N curves and the damage assessment rule or fracture mechanics methods.

##### (i) S-N Curves and Damage Assessment Rule:

A commonly used fatigue characteristic of a material subjected to repeated cycles of stress of a constant magnitude is known as the S-N curve. S is taken as the hot spot stress and N the number of cycles to failure. A typical S-N curve is shown in Fig. (1,2). The difficulties in determining the hot spot stress at a tubular intersection have now been substantially solved with the advent of the finite element method.

The most generally applied damage assessment rule to the design of offshore structures is the Palmgren-Miner linear damage rule. This rule defines the fraction of the fatigue life consumed by a given stress range in one year as the ratio of  $n_i$ , the number of cycles in the stress range  $i$  occurring in one year to the  $N_i$ , the number of cycles required in that stress range to cause failure. The total damage per year is given by the sum of the fractions of consumed life.

$$\text{Damage in one year} \quad \sum_{i=1}^m \frac{n_i}{N_i} < 1 \quad (1.1)$$

where  $m$  is the number of stress ranges considered. When the cumulative damage reaches unity the structure's life time is considered to be complete.

## (ii) Fracture Mechanics:

Fatigue is usually considered to be a two stage process consisting of crack initiation and crack propagation. In welded steel structures crack initiation is assumed to have occurred due to the presence of weld defects so that the whole of the fatigue life of a welded connection can be considered as being taken up by crack propagation.

The fracture mechanics method uses a factor called the stress intensity factor ( $K_i$ ) to describe the stress field near the crack tip. The stress intensity factor is a function of geometry, crack size, and the loading condition.

Having the stress intensity factor for the material and assuming that the material is behaving elastically through to failure, it is a relatively simple matter to predict life. Assuming some starting point  $a_o$  (the initial crack size) and end point  $a_{cr}$  (the critical crack size), the crack growth rate can be expressed as

$$\frac{da}{dN} = C(\Delta K_i)^m \quad (1.2)$$

where  $C$ ,  $m$  are material constants. The life due to crack propagation can be obtained by integration

$$N_f = \int dN = \frac{1}{C} \int_{a_o}^{a_{cr}} \frac{da}{(\Delta K_i)^m} \quad (1.3)$$

The value of the stress intensity factor can be found theoretically for a simple welded joint by using the finite element method.

In the case of a complicated joint a detailed three-dimensional finite element analysis in the region of the crack, which takes account of weld profile and provides for singularity at the crack tip is required to evaluate the stress intensity factor, this has proved to be very difficult, costly and time consuming. Therefore the stress intensity factor for the joint has usually been obtained from experimental data <sup>1.22</sup> .

The fracture mechanics approach is in principle superior to the S-N curve method but it is not sufficiently operational for complex joints and even an analysis of a simple T-joint is costly and time consuming. The fracture mechanics technique is relatively new and untried for joints and further work is required to confirm its applicability.

### 1.3 MATERIAL SELECTION FOR PLATFORM JOINTS

Offshore platforms are subjected to wide variations in loading and this places severe demands on such structures and the materials from which they are built.

Criteria for joint design and material selection are now discussed with respect to static strength, fatigue resistance, fabrication and economy.

#### 1.3.1 *Behaviour of Steel*

(i) Static strength - A fundamental requirement for the satisfactory behaviour of tubular structures is adequate static strength of the joints.

A study <sup>1.23</sup> on the most appropriate steels for North Sea construction recommended the production of a very high



ductility steel and this is designated BS 50D grade.

(ii) Fatigue Behaviour - The fatigue strength of a tubular joint depends on such factors as, ultimate yield stress, stress range, joint geometry, corrosion and sea temperature. The geometrical factors affecting joint strength are the diameter/thickness ratio, the overlapping and spacing of the tubes at the joint, the joint eccentricity and the distance from adjoining joints.

A survey <sup>1.24</sup> of the fatigue behaviour of different steels showed that the fatigue resistance of steel with a yield strength of up to 350 N/mm<sup>2</sup> (50 Ksi) increased significantly and approximately in proportion to the yield strength. However, for steels with a yield strength of 420 N/mm<sup>2</sup> (60 Ksi) or higher there is no marked improvement in the fatigue resistance.

(iii) Fabrication - A property required of a steel during the construction of an offshore structure is that it should be capable of being formed into tubular components. This implies that the steel must be resistant to deterioration during hot and cold forming and be capable of being welded under site conditions. Experience indicates that limiting the carbon equivalent (C.E ) to a maximum of 0.45% where

$$C.E = C + \frac{Mn}{6} + \frac{Cr + Mo + V}{5} + \frac{Ni + Cu}{15}$$

can be a most useful guideline in selecting steel for tubular joints.

(iv) Economy - The structure should serve the intended purpose in a safe and efficient manner under the environmental conditions involved, and should be constructed and maintained at minimum cost. All steel platforms at present use steel plate as the construction material and welding for joining the segments. The cost of the steel and the subsequent costs of fabrication are dependent to a high degree on the properties of the steel chosen. The correct choice of steel is obviously of significant importance. A major cost which must also be considered is that of underwater welding during the maintenance of an offshore structure.

### 1.3.2 *Behaviour of Concrete*

Marine structures in reinforced concrete have been in existence for over 70 years and have proved to be exceptionally durable in this harsh environment <sup>1.25</sup> .

Prestressed concrete structures have been in use for about 40 years and have also exhibited excellent durability <sup>1.26</sup> .

(i) Static Strength - Normal concrete with high compressive strength  $35-50 \text{ N/mm}^2$  (5-7 Ksi) possesses poor flexural, shear and tensile properties. It is necessary to improve these properties to justify the use of concrete for the construction of joints. The tensile strength of concrete could be improved by using steel fibres to reinforce the cement. Other alternatives could be the use of multiaxial prestressing or structural steel cover plates and stiffeners, all producing a triaxial state of stress.

(ii) Fatigue Behaviour - Under cyclic loading the fatigue endurance of concrete in compression is higher than that of steel <sup>1.27</sup> . The fatigue failure of concrete is not as critical as steel, which is of a brittle nature.

In a corrosive environment the fatigue endurance of steel can drop considerably, whereas concrete being dense and relatively impermeable to the corrosive environment can even offer an effective protection system to the steel <sup>1.28</sup> .

(iii) Fabrication - Concrete has the property that it can be formed into any complex geometrical shape of any size and this is an important advantage for joint construction.

(iv) Economy - The utilisation of concrete for offshore platforms has the advantage of low initial cost. The use of traditional civil engineering labour and methods of construction, in place of the highly skilled welder, can produce concrete structures which are more economical than steel structures.

Experience gained with concrete platforms already installed, indicates that the maintenance cost for concrete platforms is far below that for steel. A conservative estimate would be in the range of 1% of construction cost compared with 5% for maintenance of a steel jacket <sup>1.29</sup> . This lower maintenance cost of concrete could be attributed to its progressive mode of failure compared with the sudden collapse which can occur with steel structures in fatigue failures. This progressive failure mode of concrete enables repairs to be carried out in situ before more significant and expensive damage occurs.

#### 1.4 CONCLUSIONS

An investigation of the literature on tubular joints, as used in North Sea platforms, indicated that welded steel joints suffer seriously from low fatigue resistance due to the high stress concentration at the weld toes. A possible practical solution is to construct composite joints with steel and concrete. The use of concrete in the region of high stress of a joint, spreads the load over a greater area thus reducing the stress concentration. Furthermore, the concrete can support the walls of steel tubes and reduces the high local deformations.

Composite joints might reasonably be expected to perform well in service due to the fatigue endurance of concrete, the low initial costs, the low maintenance costs, the corrosion resistance, the large energy absorption and the high strength carrying capacity. These attributes are derived from the inherent qualities of both the concrete and the steel.

#### 1.5 OBJECTIVES AND SCOPE OF THE PRESENT RESEARCH

Failures in welded steel joints in offshore platforms have been reported in increasing numbers in recent years. As a result of these failures more efficient alternative joints of composite construction are proposed in this thesis. The efficiency, safety and economy of the proposed family of composite joints is explored by reference to both analytical and experimental studies. These studies cover a wide range of composite connections employed in both the repair and construction of various elements of marine structures, including tubular nodal joints, straight tubular connections and pipe lines.

The analysis is carried out using the finite element method and for this purpose a new solid element is developed which can be combined with an existing generally curved shell element as required for composite construction. A special purpose mesh generation program is developed to reduce the manual intervention during the data preparation for a finite element analysis.

## CHAPTER 2

## FINITE ELEMENT ANALYSIS

## 2.1 INTRODUCTION

The stress analysis of tubular joints with two or more cylindrical shell surfaces intersecting at a node, is of an extremely complex nature. The classical methods of shell analysis can only deal with the problem approximately, because of the unknown boundary conditions at the intersection line.

The advent of the finite element method and flat shell elements has in recent years enabled engineers to approximately analyse tube intersection problems with their complex geometry and boundary conditions. However, in order to effectively apply the finite element method to the analysis of composite tubular joints a doubly curved thin shell element and a compatible solid element are essential. The Irons Semi Loof shell element, the best thin shell element currently available, can be employed to idealise the steel tubes. The Semi Loof solid element, developed and presented in this thesis, can be employed to idealise the concrete sections.

A semi automatic mesh generation program was developed to minimise the manual effort required in the preparation of data for a finite element analysis. This mesh generation facility can take account of the geometries of cylindrical surfaces and intersection lines for any composite tubular joint configuration.

A linear elastic analysis of a welded T-joint was carried out to verify the accuracy of the Semi Loof shell element by comparison with an experimental model. This analysis also served to establish the utility of the mesh generation program.

## 2.2 REVIEW OF PREVIOUS WORK ON THE FINITE ELEMENT ANALYSIS OF JOINTS

At the beginning of the last decade at the University of California, some attempts were made to analyse T, Y and K joints by the finite element method. In this analysis the curved surface was approximated by flat elements.

The first attempt <sup>2.1</sup> used a triangular flat plate element with five degrees of freedom at each node. The element stiffness properties were derived from membrane and bending element stiffnesses. The two types considered were the Turner and Clough membrane element with two degrees of freedom (u,v) at each node, and the Clough and Tocher bending element with three degrees of freedom ( $w, \theta_x, \theta_y$ ) at each node. The effect of a branch member in a T-joint was included by a constant uniform load applied on the chord around the intersection line. The analytical results derived from a reasonable refined mesh showed a fair agreement with experimental results for a T-joint.

The next attempt to analyse a tubular joint <sup>2.2</sup> used as a basis a triangular flat shell element formed from the constant strain triangular (CST) membrane element combined with the Hsieh, Clough, Tocher (HCT) bending triangle. Four of these membrane/bending triangles were then used to construct a quadrilateral shell element with a non-planar central node. This quadrilateral shell element was used to analyse a K-joint. The finite element program was divided into two overlays on a CDC 6400 computer and this allowed a half-bandwidth of 230 to be accommodated. The K-joint was analysed by a substructure technique.



Later an improvement in the analysis of tubular joints was achieved by using flat triangular and quadrilateral shell elements developed by Johnson <sup>2.3</sup>. The quadrilateral element was constructed of four constrained linear strain membrane triangles (CLST) plus four bending triangles (HCT) with five degrees of freedom at each node (20 d.o.f. total). A K-joint with separate branches was analysed and the results compared favourably with Bouwkamp's experimental test <sup>2.4</sup>. Although the correlation of results demonstrated the excellent capabilities of the quadrilateral element, a small inaccuracy arose due to the absence of the third rotational degree of freedom which introduced constraints on the bending of the branch elements adjacent to the intersection line.

The aforementioned families of flat plate elements provided only an approximate idealisation of a curved shell surface and this is inherently inaccurate. Furthermore this type of element has the disadvantage of creating incompatibilities at a shell intersection line.

Early attempts to analyse tubular joints were somewhat hindered by the computational demands associated with the large number of elements required to model the curved geometry and structural behaviour of the joint.

A crossed joint of equal diameter tubes was analysed using the (SATE) finite element program <sup>2.5</sup>, and the results were compared with the results derived from a parallel experiment. A curved triangular shell element developed by Visser <sup>2.6</sup> was used to study the local stress

pattern in the cross-joint with specific weld sizes. This triangular element has three transitional degrees of freedom at the mid side nodes (u,v,w) and six degrees of freedom at the corner nodes (u,v,w,  $m_1, m_2, m_3$  where m are moments). This element was also used for the analysis of stiffened and unstiffened T and K joints <sup>2.7</sup>. However a fine mesh idealisation was required to obtain agreement with the experimental results. The thickness of the elements in the intersection region was increased by 1.1 to 1.5 times the normal wall thickness to allow for the influence of the weld size.

A three-dimensional hexahedral isoparametric element with a total of 48 degrees of freedom developed by Dovey, was used for the stress analysis of grouted and ungrouted connections <sup>2.8</sup>. An accurate computation of the stress concentration factors in chords and branches was achieved by correct idealisation of the weld zones. A special purpose mesh generation routine automatically generated the weld profile geometry according to AWS guidelines, while Greste's mesh generation <sup>2.3</sup> generated the mesh numbers and coordinates. The coordinates of the weld toe, root and intermediate nodal points, were automatically computed depending on the local dihedral angle between the tangent planes of the intersecting cylindrical surfaces. The mesh idealisation for this program, when compared with previous finite element analyses <sup>2.1-3</sup> of joints, requires far less elements. Nevertheless the element's large number of degrees of freedom made substructuring and optimum node numbering of vital importance.

Recently, a shell and solid element has been used to study non-linear behaviour of T-joints <sup>2.9</sup>. An elastic analysis of a joint was carried out using a shell element constructed of CST membrane element and Zienkiewicz's non-conforming bending element to provide data for a local non-linear analysis of the area near the intersection line. An isoparametric solid element with 63 degrees of freedom which was subdivided into layers throughout the thickness to represent the spread of plasticity, was used for local non-linear analysis. This non-linear approach made the ultimate load study of joints possible only for marine regions where fatigue is not a dominant feature.

The sophisticated thin shell element developed by Irons was applied to T-joint analysis <sup>2.10</sup>. The results derived from a fine mesh (with 60 elements) compared well with Oak Ridge Laboratory experimental results.

## 2.3 FINITE ELEMENT PROGRAM

To apply the finite element method effectively to the analysis of composite tubular joints attention should be given to the choice of finite elements, the mesh generation routine, the input and output facilities and the computational efficiency of the program.

### 2.3.1 *Finite elements*

A careful study of the published behaviour of existing thin shell elements in joint analysis, resulted in the choice of Iron's Semi Loof shell element.

This element has the advantage that it will produce accurate results with only a medium mesh and can idealise sharp corners and intersecting shell surfaces.

In order to model the concrete parts in the finite element analysis of composite tubular joints, a three-dimensional solid element which could be mated with the Semi Loof shell element was required. Since no such element existed a new Semi Loof solid element was developed. The nodal configuration is based on the twenty node isoparametric solid element but has an additional eight rotations on the top surface to attain both  $C^0$  continuity and a semblance of  $C^1$  continuity with the Semi Loof shell element. The theory and verification of this new mixable solid element, Semi Loof solid, is presented in the following chapter.

### 2.3.2 *Input Facilities and Mesh Generation*

To achieve a satisfactory analysis of a tubular joint, the finite element mesh should exhibit the following properties:

(i) Since the highest stress gradients occur in the immediate vicinity of the branch to chord connections, the elements should become smaller and more concentrated in these regions.

(ii) Near the ends of the chord and the branches where the stresses are more uniformly distributed the elements may be considerably larger and therefore the mesh coarser, though not to such an extent that the curved surface is poorly described.

(iii) The nodes should be numbered so as to achieve the smallest possible bandwidth for the stiffness matrix, when a banded solution procedure is used.

(iv) The elements should be numbered or presented so as to achieve the smallest possible front width for the stiffness matrix, when a frontal solution procedure is used.

A semi-automated mesh generation routine was developed to provide data for typical T, Fig. (2,1), Y and general K, Fig. (2,2), joints. The degree of refinement of the mesh can be chosen by the user. The user can also decide on the discretization of mesh, when comparison with experimental results are involved. For example, the strain gauge locations can be adjusted to match an element node or vice versa, in order to simplify the interpolation of results.

To generate the coordinate data the user specifies the x and z coordinates (elevation) of element corner nodes. The program then generates the three-dimensional coordinates of the element corner and mid-side node, computes the node coordinates along the intersection line and then generates the node coordinates of the branches automatically. The formulae for the coordinates of nodes on the intersection line for T, Y and general K joints are presented in Appendix 1.

The input parameters required for a T-joint are;

- (i) The length of the branch,  $l$ .
- (ii) The length from the centre of coordinates system along the chord to the central axis of the branch,  $l_b$ .
- (iii) The radius of branch and chord,  $r$  and  $R$ .
- (iv) The number of elements along the intersection line,  $n$ .
- (v) The first and last node numbers on the intersection line,  $N_1$  and  $N_2$ .

A typical T-joint is shown in Fig. (2,3).

The input parameters required for a Y-joint are;

- (i) The length of the branch,  $l$ .
- (ii) The length from centre of coordinates system to the axis of branch,  $l_b$ .
- (iii) The branch inclination with respect to the chord,  $\phi$ .
- (iv) Radius of branch and chord,  $r$  and  $R$ .
- (v) Number of element at the intersection line,  $n$ .

- (vi) First and last node numbers on the intersection line,  $N_1$  and  $N_2$ .

A typical Y-joint is shown in Fig. (2,4).

The input parameters required for a K-joint with positive or zero eccentricity are, a combination of T and Y or Y and Y joint mesh generators.

Parameters required for a K-joint with negative eccentricity are;

- (i) The branches inclination with respect to chord,  $\phi_1$  and  $\phi_2$ .
- (ii) The lengths of branches,  $l_1$  and  $l_2$ .
- (iii) The length from centre of coordinates system,  $l_{b_1}$  and  $l_{b_2}$ .
- (iv) Radius of the branches,  $r_{b_1}$  and  $r_{b_2}$  and radius of chord,  $R$ .
- (v) First, mid and last node numbers on intersection line,  $N_1-N_6$ .
- (vi) The coordinate  $X$  of point  $N_2$ .

A typical K-joint is shown in Fig. (2,5).

### 2.3.3 *Solution Facilities*

A finite element idealisation of composite tubular joints, even with optimum numbering of the nodes, produces a stiffness matrix with a large bandwidth. In order to accommodate this large bandwidth an efficient, practically unlimited, bandwidth equation solver<sup>2.11</sup> was implemented in the finite element program. This solution processor enables analyses of composite joint meshes

consisting of large numbers of Semi Loof solid elements (68 DOF) and Semi Loof shell elements (32 DOF).

A computer subroutine was written to store the equations in blocks and the operations are only performed on non-zero figures. The available high speed core of computer is used in an optimum way by calculating the maximum block size possible. A comparison of the block solution with the frontal solution showed that an equal amount of computer time was required. The main difference between the two methods is that the block solution requires optimum node numbering whereas the front solution requires optimum element numbering.

#### 2.3.4 *Output Facilities*

To simplify the interpolation of finite element results the von Mises stresses (inside and outside surfaces) of Semi Loof shell are computed from the moments and membrane stresses, according to the following formula for shells:

$$\sigma_x = \pm \frac{6}{t^2} M_x + \sigma_{x_m}$$

$$\sigma_y = \pm \frac{6}{t^2} M_y + \sigma_{y_m}$$

$$\sigma_{xy} = \pm \frac{6}{t^2} M_{xy} + \tau_{xy_m}$$

in which  $t$  is the shell thickness and  $\sigma_{x_m}$ ,  $\sigma_{y_m}$  and  $\tau_{xy_m}$  are membrane stresses. The positive and negative signs are for the outside and inside surfaces respectively.



Principal stresses for Semi Loof shell are computed from  $\sigma_x$ ,  $\sigma_y$  and  $\sigma_{xy}$  using Mohr's circle and similarly for the Semi Loof solid from  $\sigma_x$ ,  $\sigma_y$ ,  $\sigma_z$ ,  $\sigma_{xy}$ ,  $\sigma_{yz}$ ,  $\sigma_{zx}$  using standard transformation relationships, Appendix 2.

## 2.4 THEORY OF SEMI LOOF SHELL ELEMENT

The quadrilateral Semi Loof shell has three types of nodes,

(i) Corner and midside nodes at which three global displacement components ( $U_i, V_i, W_i$ ) are taken as nodal variables.

(ii) Loof nodes which are located at the Gaussian quadrature positions for two point integration along the element sides. Consequently the two nodes along a side are positioned at a distance of  $1/2 \sqrt{3}$  side length, from centre. The nodal parameters at Loof node,  $j$ , are chosen to be the two rotations  $\theta_{xz}^j, \theta_{yz}^j$  which are respectively normal and parallel to the element edge and are expressed with respect to a local coordinate system defined by the orthogonal unit vector systems ( $\hat{X}, \hat{Y}, \hat{Z}$ ).

(iii) The central node at which the nodal variables are chosen to be the three global displacement components together with the two rotations,  $\theta_{xz}^9$  and  $\theta_{yz}^9$ .

The element has a total 43 degrees of freedom which will later be condensed to 32 by the prescription of appropriate constraints on the shear behaviour of the element.

The two families of shape functions are the corner-midside nodes family <sup>2.12</sup>  $N_i(\xi, \eta)$  where  $i = 1$  to 8, and the Loof family <sup>2.13</sup>  $L_j(\xi, \eta)$ , including the central node, where  $j = 1$  to 9.

A preliminary requirement is the generation of the local coordinate system ( $\hat{X}, \hat{Y}, \hat{Z}$ ) at Gauss and Loof points. Denoting the global displacements of point P ( $x, y, z$ )

by

$$\{d\} = \begin{bmatrix} u \\ v \\ w \end{bmatrix} \quad (2.1)$$

considering the shape function  $N$  then,

$$\{d\} = [N] \{\delta^e\} \quad (2.2)$$

The displacement components in each of the local directions  $x$ ,  $y$  and  $z$  are denoted by  $u$ ,  $v$  and  $w$  respectively and are obviously projections of  $\{d\}$  on the unit base vectors and therefore given by the scalar product;

$$u = \{x\}^T \{d\} = \{x\}^T [N] \{\delta^e\} \quad (2.3)$$

with similar expressions for  $v$  and  $w$ .

In order to accomplish in-plane derivatives of  $u$  and  $v$ , with respect to local directions based on eqn. (2.3), the formulation

$$\frac{\partial u}{\partial x} = \{x\}^T \left[ \frac{\partial N}{\partial x} \right] \{\delta^e\} \quad (2.4)$$

where

$$\begin{bmatrix} \frac{\partial N_i}{\partial x} \\ \frac{\partial N_i}{\partial y} \end{bmatrix} = \begin{bmatrix} \xi.\hat{X} & \xi.\hat{Y} \\ \eta.\hat{X} & \eta.\hat{Y} \end{bmatrix}^{-1} \begin{bmatrix} \frac{\partial N_i}{\partial \xi} \\ \frac{\partial N_i}{\partial \eta} \end{bmatrix} \quad (2.5)$$

is desired.

The out of plane derivatives  $\frac{\partial u}{\partial z}$ ,  $\frac{\partial v}{\partial z}$  require special attention. The deformation is as

$$\frac{\partial u}{\partial z} = \left(\frac{\partial u}{\partial z}\right)^L + \left(\frac{\partial u}{\partial z}\right)^N \quad (2.6)$$

where the first term relates to the contributions from the rotations at the Loof and central nodes and the second term denotes the contribution from the displacements of the corner and midside and central nodes. In order to evaluate the first term, a vector,  $T^j$ , is defined at each Loof node and central node,  $j$ , as follows:

$$T^j = t^j \hat{Z}^j \quad (2.7)$$

where  $t^j$  is the shell thickness at node  $j$ .

The rotation shared by adjacent elements can be expressed by means of the vector,  $R^j$ , as

$$R^j = T^j \times Y^j \quad (2.8)$$

and the slope along the element edge, at node  $j$ , is given by

$$S^j = t^j \hat{Y}^j \quad (2.9)$$

with the aid of these vectors the first term in eqn. (2.6) can be expressed as

$$\left(\frac{\partial u}{\partial z}\right)^L = \sum_{j=1}^9 \left[ \{R^j\}^T \{x\} \frac{L^j}{t} \theta_{xz}^j + \{s^j\}^T \{x\} \frac{L^j}{t} \theta_{yz}^j \right] \quad (2.10)$$

A similar expression exists for  $\left(\frac{\partial v}{\partial z}\right)^L$ . Using eqn. (2.7) the vector T at any point can be interpolated as

$$T = \sum_{j=1}^9 L^j T^j \quad (2.11)$$

The vector thickness T is in general not normal to the mid surface, which implies that a relative displacement of two points (say A and B), A not orthogonally above B confined to the plane XZ, is

$$\left(\frac{\partial u}{\partial z}\right)_{xz}^N = \frac{U_B - U_A}{t} = \frac{T_x}{t} \frac{\partial u}{\partial x} \quad (2.12)$$

where t is the shell thickness at the point in question and  $T_x$  is the component of T along the local x-axis. Adding the correction (Kirchhoff and Love assumption) gives

$$\left(\frac{\partial u}{\partial z}\right)^N = \frac{1}{t} \left\{ T_x [x]^T \left(\frac{\partial N}{\partial x}\right) + T_y [x]^T \left(\frac{\partial N}{\partial y}\right) \right\} \{\delta^e\} \quad (2.13)$$

A similar expression can be written for  $\left(\frac{\partial v}{\partial z}\right)^N$ .

The degrees of freedom corresponding to the displacements of the central node are combined to create a deflection normal to the element at its centre, the in-plane components are then discarded. Of the remaining 43 degrees of freedom a further 11 variables are eliminated to give a final total of 32 degrees of freedom for the element,

which are; 24 displacement components, with respect to the global axes at the corner and midside nodes, 8 rotations normal to the element edge at each Loof node (i.e.  $\theta_{xz}$ ).

The eleven constraints fall into the following three classes:

(i) The eight unwanted rotations at the Loof nodes. The slope of the normal in the side direction generates a shear strain  $\gamma_{yz}$ . It is natural to constrain it by putting  $\gamma_{yz} = 0$  at Loof points knowing that the lateral deflections  $W$  are identical for neighbouring elements. Furthermore one can argue that as  $W$  varies quadratically with  $y$  and because the shear  $\gamma_{yz}$  is constrained to zero at both Loof points, it follows that a patch test will succeed, whatever three final constraints are chosen <sup>2.14</sup>.

(ii) The two rotations at the centre. The shear vector in plane  $xy$  is

$$\gamma = \hat{X} \gamma_{xz} + \hat{Y} \gamma_{yz} \quad (2.14)$$

The unit vector  $\hat{X}_9$  and  $\hat{Y}_9$  at centre  $\xi = \eta = 0$  with reference to the Kirchhoff assumption is;

$$\int \hat{X}_9 \cdot \gamma \, d(\text{area}) = \int \hat{Y}_9 \cdot \gamma \, d(\text{area}) = 0 \quad (2.15)$$

(iii) The bubble function  $(1-\xi^2)(1-\eta^2)$ . The function has negative curvature in both the  $\xi$  and  $\eta$  directions. Therefore it seems highly probable that the

total curvature

$$\frac{\partial^2 w}{\partial x^2} + \frac{\partial^2 w}{\partial y^2} \quad (2.16)$$

is negative almost everywhere. As there is no rotation and  $u = v = 0$  at the central point, therefore shear corresponding to slope  $W_x$  is  $\gamma_{xz} = W_x + U_z$ . Now the expression in the shears that corresponds to the total curvature in the same way, is

$$\frac{\partial \gamma_{xz}}{\partial x} + \frac{\partial \gamma_{yz}}{\partial y} = \nabla \cdot \vec{\gamma} \quad (2.17)$$

It would be reasonable to integrate  $\nabla \cdot \vec{\gamma}$  over the area, to generate an appropriate constraint

$$\int \nabla \cdot \vec{\gamma} \, d(\text{area}) = 0 \quad (2.18)$$

This was the constraint originally used, but when the thickness is constant, by using Green's theorem the constraint can be transformed to

$$\int t(\gamma_{xz}) \, d(\text{boundary}) = 0 \quad (2.19)$$

The eleven constraint equations can be written in matrix form as

$$\left[ \begin{array}{c|c} C_A & C_B \end{array} \right] \begin{Bmatrix} \delta_A \\ -\delta_A \\ \delta_B \end{Bmatrix} = 0 \quad (2.20)$$

where  $\{\delta_A\}$  represents the 32 degrees of freedom to be retained,  $\{\delta_B\}$  denotes the ones to be eliminated and  $[C]$  is a (11 x 43) constraint matrix. The element stiffness matrix is computed using a five point integration rule. To date this rule has not revealed any mechanisms.



## 2.5 PROGRAM VERIFICATION

In order to establish the validity of the computer code and to assess the accuracy of the Semi Loof shell element an analysis of a tubular T-joint was carried out and compared with experimental results <sup>2.3</sup>.

Finite element analyses of a T-joint subject to internal pressure with coarse, medium and fine mesh idealisations were carried out, the latter is shown in Fig. (2,1). Surface stresses are compared with experimental values in Figs. (2,6) to (2,9). In each case the axial stress is directed along the section at which the stresses are plotted and the hoop stress is perpendicular to the section. The region of greatest interest is the vicinity of the chord-branch intersection where the chord-branch intersection induces high stresses. The finite element results and experimental values compared favourably for the fine mesh idealisation of 60 Semi Loof shell elements.

## 2.6 CONCLUSIONS

The practical application of Semi Loof shell and solid elements to the analysis of arbitrary joints requires a computer program with special mesh generation facilities, high computational efficiency and extensive input and output facilities. Such capabilities are especially important because of the complexities of three-dimensional meshes, the large number of linear equations that must be solved and because of the quantity of stress and displacement information that can be produced by the Semi Loof shell and Semi Loof solid elements.

The equation solving algorithm used, has the capability of accommodating essentially unlimited bandwidth in 50,000 decimal central memory locations of the Cyber 174 or CDC 6500 computers at Imperial College. This solution facility offers the possibility of analysing various ranges of joint configurations limited only by the computing cost.

A practical application of the computer program is illustrated by reference to the analysis of a T-joint.

## CHAPTER 3

## THE SEMI LOOF SOLID ELEMENT

## 3.1 INTRODUCTION

In order to apply the finite element method effectively to the analysis of composite tubular joints, finite elements with a good performance and a sound theoretical basis are required. For the thin shell part of the joint an element which could satisfy these requirements is the non-conforming Semi Loof shell element developed by Irons. For the thick concrete part of the joint the familiar 20-node isoparametric solid element could be appropriate. However, the Semi Loof shell and the 20-node isoparametric solid element cannot strictly be mixed at the interface between the steel and concrete due to the lack of continuity between the elements which causes gross errors on their interface. Accordingly, a new special purpose Semi Loof solid element has been developed which permits the analysis of combined shell and solid problems.

Irons' thin shell element is a non-conforming quadratic Ahmad type element, which uses low order integration and can accommodate multiple shell junctions. This element is the first of the Ahmad family to pass the patch test with general quadrilateral geometry. The Semi Loof shell element has eight nodes with  $u$ ,  $v$  and  $w$  as deflections in the global  $x$ ,  $y$  and  $z$  directions. This would be sufficient for a membrane shell  $c^{(0)}$  continuity, but to provide a semblance of  $c^{(1)}$  continuity the 8 normal slopes

in local directions at the Loof nodes have been added in a non-conforming way so that the slopes are continuous only at the Loof nodes. The 32 degrees of freedom for the element should be sufficient to define linear stress fields both in membrane and bending actions. Irons grouped the two rotations at the Loof nodes along a side as "mid side" variables, for convenience, as if they are operated at the mid side node, Fig. (3,1).

The new Semi Loof solid element should possess a top surface nodal configuration and response identical with that of the Semi Loof shell element and a bottom surface nodal configuration and response that is identical with that of 20-node isoparametric solid element, Fig. (3,2). The nodal configuration for the proposed solid element is based on the familiar 20-node isoparametric solid element, but has additional rotational degrees of freedom at the Loof nodes on the top surface to ensure a semblance of  $c^{(1)}$  continuity, Fig. (3,2). The formulation includes shear deformations and the element is coded into a shape function subroutine. The use of a shape function subroutine combined with numerical integration means that any matrix can easily be formed and ensures that the element will be easy to implement in existing finite element systems.

### 3.2 HISTORY

This section looks into the history and development of the techniques which characterize the second generation of isoparametric elements for shell analysis.

In 1966 H.W. Loof<sup>3.1</sup> conceived the idea of connecting non-conforming elements at Gauss points along the inter-element boundaries to minimize the virtual work generated by the non-conformity. A few years later the Ahmad membrane stack was devised using vectorial arguments for the first time in finite element history<sup>3.2</sup>.

The Ahmad element has 40 degrees of freedom and to make it sufficiently stiff in bending for thin shells a factor of 1.2 was introduced to simulate parabolic shear distribution.

The Discrete Kirchhoff Assumption is being used increasingly for thin shells and plates. This assumption, first applied to plates and shells by Love and Kirchhoff, means that straight lines normal to the middle surface before deformation remain straight and normal to the middle surface and unchanged in length after deformation. The Discrete Kirchhoff Assumption sometimes produces elements with exceptionally good performance<sup>3.3, 3.7, 3.9</sup>.

A careful survey of integrating rules by Too<sup>3.4</sup> showed that 2 x 2 Gaussian integration gives remarkably improved results in the Ahmad stack provided that the final stresses are calculated at the same 2 x 2 points.

A further development in 1973 by Baldwin, Razzaque and Irons <sup>3.5</sup> led to the introduction of the first delinquent plate element (an approximately integrated isoparametric element with the Discrete Kirchhoff Assumption). Then Razzaque <sup>3.6</sup> developed and coded the delinquent Ahmad shell element. In both of these elements the Kirchhoff assumption was applied by constraining the shears to the zero at the 2 x 2 Gauss points, and this enabled the superfluous degrees of freedom to be discarded (a translation and rotation at each mid side node). However, the patch test was satisfied only for parallelogram geometry. Later for the Semi Loof shell Irons constrained the slopes at the Loof points (Gauss point at the edge  $\frac{L}{2\sqrt{3}}$  either side of mid side point) to exactly zero and now the patch test was successful in general quadrilateral geometry.

Irons found that by using a constraint which relates to a side rather than to the surface one ensures that the discarded degree of freedom takes the same constrained values in the neighbouring element. Therefore the constraint does not destroy the patch test behaviour so the continuity is guaranteed. Also to succeed in the quadrilateral patch Test W must be able to respond quadratically in x, y. Accordingly the bubble function was

$$w = (1-\xi^2)(1-\eta^2) \quad \text{at } \xi = 0, \eta = 0 \quad (3.1)$$

added as an extra initial degree of freedom and later constrained <sup>3.7,3.8</sup>.

Semi Loof shell element is one of the latest elements in the evolution process of the above concepts. The most recent is the ISOFLEX family of plate bending elements developed on similar concepts by Lyons<sup>3.9</sup>.

### 3.3 REQUIREMENTS

The requirements for a Semi Loof solid element may be summarised as follows;

(i) The element should be capable of representing curved boundaries when necessary.

(ii) The nodal configuration should be such that a Semi Loof shell element can be mated with the top surface and an isoparametric solid element can be mated with the bottom surface.

(iii) The equations produced should not be ill-conditioned and fail for certain geometries.

(iv) The element should be easy to implement and computationally efficient.

(v) The element should pass the patch test for general hexahedral geometry both on its own and when mixed with the Semi Loof shell element and the 20-node isoparametric solid element.



### 3.4 THEORY FOR CONSTRAINED SOLID ELEMENT

The theory given in the subsequent section introduces a new vectorial approach for the formulation of a solid element. The variation of a displacement and its derivatives within the element are specified independently by suitable shape functions. The independent displacements and rotations are then constrained to be compatible at the Loof points on the top surface of the solid element with the Semi Loof shell surface.

#### 3.4.1 *Basic Assumptions*

The following assumptions are traditional for an elastic solid element with shear deformations;

(i) The displacements within the deformed body are linearly related to the forces (Hooke's Law).

(ii) The deflections are small and linearly related to the strains within the deformed body.

#### 3.4.2 *Nodal Configuration and Sign Convention*

The element has three global displacements  $u, v, w$  at twenty corner and mid side nodes. These sixty variables are necessary and sufficient to ensure  $c^{(0)}$  compatibility at the edges of the neighbouring solid and shell elements. The top surface of the solid has additional local rotations at the two Loof points along each side.

Noticing that solid elements experience shearing deformations, whereas the shell does not, it is clearly impossible to say that the normal slopes  $(\frac{\partial u}{\partial z}, \frac{\partial v}{\partial z})$  on the top surface of the solid and on the shell surface would agree after deformation. However it is conceivable to equate the

slopes of the top surface ( $\frac{\partial W}{\partial x}, \frac{\partial W}{\partial y}$ ) of the solid and at the shell surface.

The sign convention for rotations along an edge of Semi Loof solid and of a Semi Loof shell element are identical; that is a rotation according to the right-hand screw rule where the vector direction along an edge is defined by ascending node numbers.

### 3.4.3 Shape Functions

In order to implement any displacement formulation, a set of suitable interpolation functions should be chosen. The functions can vary to ensure continuity in linear, parabolic and cubic forms.

$$(\text{Displacement}) = \sum N_i (\text{Displacement at node } i) \quad (3.2)$$

Two families of interpolating functions are necessary to define the deflections and rotations independently.

(i) Solid shape function:

Using three normalized coordinates ( $\xi, \eta, \zeta$ ) the quadratic solid element (20-node) shape functions can be expressed in the following way:

$$N_i = \frac{1}{8} (1 + \xi_0) (1 + \eta_0) (1 + \zeta_0) (\xi_0 + \eta_0 + \zeta_0 - 2)$$

$$\xi_0 = \xi \xi_i \quad \eta_0 = \eta \eta_i \quad \zeta_0 = \zeta \zeta_i \quad (3.3)$$

for the 8 corner nodes.

and for a typical mid side node

when

$$\xi_i = 0 \quad , \quad \eta_i = \pm 1 \quad \zeta_i = \pm 1$$

$$N_i = \frac{1}{4} (1 - \xi^2) (1 + \eta_0) (1 + \zeta_0) \quad (3.4)$$

eqn. (3.4) maintains the inter-element continuity.

This family of shape function are identical to the second order serendipity rectangle <sup>3.10</sup>, in 3D this becomes

(3.5)

(ii) Loof shape function:

The polynomial terms of second family of shape function, which only operates on the top surface, are as follows:

(3.6)

Bubble function term

The Loof family,  $L_j(\xi, \eta)$ ,  $j = 1$  to 9 has been taken from the Semi Loof shell element for compatibility between the two elements<sup>3,8</sup>, a typical shape function shown in Fig. (3,3) is

$$L_1 = \frac{3}{32} (3\eta^2 - \xi^2) + \frac{1}{8} \left[ -3\eta(1 - \xi^2) - \sqrt{3}\xi \left\{ 3\eta^2 - \eta - 1 - \frac{3\eta}{2}(\eta^2 - \xi^2) \right\} \right] \quad (3.7)$$

By adding an extra degree of freedom at the central node of the element top surface ( $\xi = 0, \eta = 0, \zeta = 1$ ) in a direction normal to this surface ensures that the patch test succeeds for quadrilateral geometry. This extra degree of freedom is introduced by use of the bubble function

$$L_9 = (1 - \xi^2)(1 - \eta^2) \quad (3.8)$$

The zero value of the bubble function along all boundaries does not affect inter-element continuity. For a hexahedron to pass a flexural patch test, the element should respond with  $w = \text{quadratic in } x, y$ . Therefore the term  $\xi^2 \eta^2$  is required and rotations at the central node are now derived from bubble function.

#### 3.4.4 Element Stiffness Formulation

The displacement field can be expressed in terms of a set of discrete nodal displacements,  $\delta^e$ , by use of shape function,  $N$

$$\delta = N \delta^e \quad (3.10)$$

and the strains are defined as

$$\epsilon = B \delta^e \quad (3.11)$$

where  $B$  is a matrix which depends on the shape functions  $N$  and its derivatives with respect to global coordinates.

The element stress components  $\sigma$  are given by the usual equation

$$\begin{Bmatrix} \sigma_x \\ \sigma_y \\ \sigma_z \\ \sigma_{xy} \\ \sigma_{yz} \\ \sigma_{zx} \end{Bmatrix} = \begin{bmatrix} D_x & D_1 & D_1 & 0 & 0 & 0 \\ & D_y & D_1 & 0 & 0 & 0 \\ & & D_z & 0 & 0 & 0 \\ & & & D_{xy} & 0 & 0 \\ & & & & D_{yz} & 0 \\ & & & & & D_{zx} \end{bmatrix} \begin{Bmatrix} \epsilon_x \\ \epsilon_y \\ \epsilon_z \\ \gamma_{xy} \\ \gamma_{yz} \\ \gamma_{zx} \end{Bmatrix} \quad (3.12)$$

where for an isotropic material

$$D_x = D_y = D_z = \frac{E(1-\nu)}{(1+\nu)(1-2\nu)}$$

$$D_1 = \frac{E\nu}{(1+\nu)(1-2\nu)}$$

$$D_{xy} = D_{yz} = D_{zx} = \frac{E}{2(1+\nu)}$$

E is elastic modulus and  $\nu$  is Poisson's ratio.

The element stiffness matrix can be derived from eqns. (3.10) and (3.12) as

$$K^e = \int B^T D B d(\text{vol}) \quad (3.13)$$

### 3.4.5 Unconstrained Displacement Field

The unconstrained nodal configurations and coordinates systems are shown in Fig. (3,4).

The strain-displacement relationship can be written in matrix form for the corner and mid-side nodes with three degrees of freedom as follows;

$$\begin{Bmatrix} \epsilon_x \\ \epsilon_y \\ \epsilon_z \\ \gamma_{xy} \\ \gamma_{yz} \\ \gamma_{xz} \end{Bmatrix} = \begin{bmatrix} \frac{\partial}{\partial x} & 0 & 0 \\ 0 & \frac{\partial}{\partial y} & 0 \\ 0 & 0 & \frac{\partial}{\partial z} \\ \frac{\partial}{\partial y} & \frac{\partial}{\partial x} & 0 \\ 0 & \frac{\partial}{\partial z} & \frac{\partial}{\partial y} \\ \frac{\partial}{\partial z} & 0 & \frac{\partial}{\partial x} \end{bmatrix} \begin{Bmatrix} u \\ v \\ w \end{Bmatrix} \quad (3.14)$$

where  $u$ ,  $v$  and  $w$  are respectively the  $x$ ,  $y$  and  $z$  components of displacement.

For the top surface midside nodes, the strains due to discrete nodal variables are;

$$\begin{Bmatrix} \epsilon_x \\ \epsilon_y \\ \epsilon_z \\ \gamma_{xy} \\ \gamma_{yz} \\ \gamma_{xz} \end{Bmatrix} = \begin{bmatrix} \frac{\partial}{\partial x} & 0 & 0 & 0 & 0 & 0 & 0 & 0 \\ 0 & \frac{\partial}{\partial y} & 0 & 0 & 0 & 0 & 0 & 0 \\ 0 & 0 & \frac{\partial}{\partial z} & 0 & 0 & 0 & 0 & 0 \\ \frac{\partial}{\partial y} & \frac{\partial}{\partial x} & 0 & 0 & 0 & 0 & 0 & 0 \\ 0 & \frac{\partial}{\partial z} & \frac{\partial}{\partial y} & L_i & 0 & L_j & 0 & 0 \\ \frac{\partial}{\partial z} & 0 & \frac{\partial}{\partial x} & 0 & L_i & 0 & L_j & 0 \end{bmatrix} \begin{Bmatrix} u \\ v \\ w \\ \theta_{xi} \\ \theta_{yi} \\ \theta_{xj} \\ \theta_{yj} \end{Bmatrix} \quad (3.15)$$

for the two Loof points  $i$  and  $j$  assigned to the mid-side node. These physical quantities have been stored in the Displacement Matrix in the following order.

(i) Direct Strain: The value of the resultant global displacement  $u$  at some arbitrary point (XI) in response to a unit displacement in the same direction has been stored in the first row of the displacement matrix. Accordingly, the values of  $v$ ,  $w$  have been stored in the succeeding rows. So, for a given displacement vector  $\vec{d}_i$  at a node, there is a displacement vector  $N_i d_i$  at an arbitrary point (XI). Now by using the scalar product all the displacements and their first order derivatives would be:

$$\begin{aligned}
u &= \sum_{i=1}^{i=n} N_i d_i \hat{X} \\
v &= \sum_{i=1}^{i=n} N_i d_i \hat{Y} \\
w &= \sum_{i=1}^{i=n} N_i d_i \hat{Z} \\
u_x &= \sum_{i=1}^{i=n} N_{ix} d_i \hat{X} \\
v_x &= \sum_{i=1}^{i=n} N_{ix} d_i \hat{Y} \\
\bar{w}_x &= \sum_{i=1}^{i=n} N_{ix} d_i \hat{Z} \\
u_y &= \sum_{i=1}^{i=n} N_{iy} d_i \hat{X} \\
v_y &= \sum_{i=1}^{i=n} N_{iy} d_i \hat{Y} \\
w_y &= \sum_{i=1}^{i=n} N_{iy} d_i \hat{Z} \\
u_z &= \sum_{i=1}^{i=n} N_{iz} d_i \hat{X} \\
v_z &= \sum_{i=1}^{i=n} N_{iz} d_i \hat{Y} \\
w_z &= \sum_{i=1}^{i=n} N_{iz} d_i \hat{Z}
\end{aligned} \tag{3.16}$$



where  $\hat{X}$  = outward pointing normal in the tangent plane at the element boundary

$\hat{Y}$  = axis along the boundary in the tangent plane at the element boundary

$\hat{Z}$  = normal to  $\hat{X}$ ,  $\hat{Y}$  surface (top surface of solid element) and  $n$  is number of nodes.

The technique to create a  $\{\hat{X}, \hat{Y}, \hat{Z}\}$  set of vectors at a node will be described later.

(ii) Shearing Strain: Considering a deformed cross section of a plate as shown in Fig. (3,5). The rotation of  $\phi_x$  can be expressed as the sum of the rotation of the mid surface  $\frac{\partial w}{\partial x}$  plus a straight line rotation which represents a uniform shear through the thickness.

$$\theta_x = \frac{\partial u}{\partial z}$$

$$\phi_x = \frac{\partial w}{\partial x} + \theta_x \quad (3.17)$$

In thin shell theory plane sections remain plane and shear deformations are not permitted which requires some internal restraint ( $\phi_x = 0$ ). For thick elements this internal restraint is relaxed so that when shear deformation takes place the rotation of the normal  $Z$  at any Loof point,  $j$ , is described by a vector in the local coordinate system

$$Z_j (\vec{r}_j \quad \vec{s}_j \quad \vec{z}_j) \quad (3.18)$$

where  $\vec{r}_j$  is the rotation about the axis  $OX$

$\vec{s}_j$  is the rotation about the axis  $OY$

$\vec{z}_j$  is the rotation about the axis  $OZ$  as demonstrated in Fig. (3,6).

$\vec{r}_j$  is the unit rotation shared with neighbouring elements and can be expressed as

$$\vec{r}_j = \vec{Z}_j \wedge \vec{Y}_j \quad (3.19)$$

The rotation along the edge  $s_j$  (a variable destined to be eliminated) is

$$\vec{s}_j = \vec{r}_j \wedge \vec{Z}_j \quad (3.20)$$

But the rotation of  $Z$  at any integration point ( $i$ ) would be

$$Z_i = Z_j \tilde{R}(\theta) = (\vec{r}_i \ \vec{s}_i \ \vec{z}_i) \quad (3.21)$$

$\tilde{R}(\theta)$  is the transformation matrix from Loof local coordinates system to integration point coordinates system and  $\theta$  is the angle between  $Z_i$ ,  $Z_j$ , which for a flat element is zero.

In general  $Z(\vec{r} \ \vec{s} \ \vec{z})$  represents the rotation at Loof or at Gauss point respectively. Now, the rotations  $\theta_x$  and  $\theta_y$  can be introduced as follows

$$\begin{aligned} \theta_x &= \sum_{i=1}^{i=n} L_i \begin{bmatrix} \vec{r} \\ \vec{s} \\ \vec{z} \end{bmatrix} \hat{X}_i \\ \theta_y &= \sum_{i=1}^{i=n} L_i \begin{bmatrix} \vec{r} \\ \vec{s} \\ \vec{z} \end{bmatrix} \hat{Y}_i \end{aligned} \quad (3.22)$$

where  $n$  = number of Loof or Gauss points, or as;

$$\vec{\Delta} = \sum_{i=1}^{i=n} L_i \vec{\Delta}_i \begin{bmatrix} \hat{X} \\ \hat{Y} \end{bmatrix} \quad (3.23)$$

The normal displacement contribution to transverse shear strains at any point from eqn. (3.16) are:

$$\gamma_{xz} = \frac{\partial u}{\partial z} + \frac{\partial w}{\partial x} = \sum N_{iz} \vec{d}_i \hat{X} + \sum N_{ix} \vec{d}_i \hat{Z} \quad (3.24)$$

$$\gamma_{yz} = \frac{\partial v}{\partial z} + \frac{\partial w}{\partial y} = \sum N_{iz} \vec{d}_i \hat{Y} + \sum N_{iy} \vec{d}_i \hat{Z}$$

By adding the rotation of the normal to the normal displacement, the complete shearing strain formula can be obtained

$$\begin{bmatrix} \gamma_{xz} \\ \gamma_{yz} \end{bmatrix} = \sum L_i \vec{\Delta}_i \begin{bmatrix} \hat{X} \\ \hat{Y} \end{bmatrix} + \sum N_{iz} \vec{d}_i \begin{bmatrix} \hat{X} \\ \hat{Y} \end{bmatrix} + \begin{bmatrix} \sum N_{ix} \\ \sum N_{iy} \end{bmatrix} \vec{d}_i \hat{Z} \quad (3.25)$$

#### 3.4.6 Jacobian Matrix

It is now necessary to establish the relationship between natural (curvilinear) coordinate and local coordinate systems. The  $x$ ,  $y$  and  $z$  coordinates at a point  $\xi$ ,  $\eta$  and  $\zeta$  can be given as

$$\begin{bmatrix} x \\ y \\ z \end{bmatrix} = \sum_{i=1}^{i=n} N_i \begin{bmatrix} x \\ y \\ z \end{bmatrix}_i \quad (3.26)$$

where the shape function (N) are in terms of the natural  $\xi$ ,  $\eta$  and  $\zeta$  coordinates and the summation is taken over n nodes on the element periphery which are sufficient to define the element geometry.

By the use of partial differentiation rules <sup>3.10</sup> the three-dimensional transformation relationship derives as

$$\begin{bmatrix} \frac{\partial N_i}{\partial x} \\ \frac{\partial N_i}{\partial y} \\ \frac{\partial N_i}{\partial z} \end{bmatrix} = [J]^{-1} \begin{bmatrix} \frac{\partial N_i}{\partial \xi} \\ \frac{\partial N_i}{\partial \eta} \\ \frac{\partial N_i}{\partial \zeta} \end{bmatrix} \quad (3.27)$$

where

$$[J]^{-1} = \frac{1}{\det[J]} \begin{bmatrix} \frac{\partial y}{\partial \eta} \cdot \frac{\partial z}{\partial \zeta} - \frac{\partial y}{\partial \zeta} \cdot \frac{\partial z}{\partial \eta} & \frac{\partial y}{\partial \zeta} \cdot \frac{\partial z}{\partial \xi} - \frac{\partial y}{\partial \xi} \cdot \frac{\partial z}{\partial \zeta} & \frac{\partial y}{\partial \xi} \cdot \frac{\partial z}{\partial \eta} - \frac{\partial y}{\partial \eta} \cdot \frac{\partial z}{\partial \xi} \\ \frac{\partial x}{\partial \zeta} \cdot \frac{\partial z}{\partial \eta} - \frac{\partial x}{\partial \eta} \cdot \frac{\partial z}{\partial \zeta} & \frac{\partial x}{\partial \eta} \cdot \frac{\partial z}{\partial \xi} - \frac{\partial x}{\partial \xi} \cdot \frac{\partial z}{\partial \eta} & \frac{\partial x}{\partial \xi} \cdot \frac{\partial z}{\partial \zeta} - \frac{\partial x}{\partial \zeta} \cdot \frac{\partial z}{\partial \xi} \\ \frac{\partial x}{\partial \eta} \cdot \frac{\partial y}{\partial \zeta} - \frac{\partial x}{\partial \zeta} \cdot \frac{\partial y}{\partial \eta} & \frac{\partial x}{\partial \zeta} \cdot \frac{\partial y}{\partial \xi} - \frac{\partial x}{\partial \xi} \cdot \frac{\partial y}{\partial \zeta} & \frac{\partial x}{\partial \xi} \cdot \frac{\partial y}{\partial \eta} - \frac{\partial x}{\partial \eta} \cdot \frac{\partial y}{\partial \xi} \end{bmatrix} \quad (3.28)$$

A geometrical interpretation of the Jacobian is that the rows of  $J$  constitute three vectors which are tangential to the coordinate curves  $\xi$ ,  $\eta$  and  $\zeta$  at the point of intersection and are known as the covariant base vectors, Fig. (3,7).

$$[J] = \begin{bmatrix} \vec{J}_\xi \\ \vec{J}_\eta \\ \vec{J}_\zeta \end{bmatrix} \quad (3.29)$$

On inspection it can be seen that the definition of local axes  $(\hat{X}_i \ \hat{Y}_i \ \hat{Z}_i)$  would be derived from base covariant vectors as follows:

$$\hat{Z} = \frac{\vec{J}_\xi \wedge \vec{J}_\eta}{|\vec{J}_\xi \wedge \vec{J}_\eta|} \quad (3.30)$$

which is normal to top surface of element and  $Y$  tangent to the side at loof nodes

$$\hat{Y} = \frac{\vec{Y}}{\sqrt{\left(\frac{\partial x}{\partial \eta}\right)^2 + \left(\frac{\partial y}{\partial \eta}\right)^2 + \left(\frac{\partial z}{\partial \eta}\right)^2}} \quad (3.31)$$

and finally

$$\hat{X} = \hat{Y} \wedge \hat{Z} \quad (3.32)$$

The vector  $X$  is pointing out of the element side, Fig. (3,8), at the Loof nodes, where the corner node numbers are ascending, otherwise by swopping the coordinate

system the consistency between the two elements is insured.

Also the columns of  $[J]^{-1}$  constitute three vectors which are normal to the coordinate surfaces  $\xi = \text{constant}$ ,  $\eta = \text{constant}$  and  $\zeta = \text{constant}$  and are known as contra-variant base vectors which can be written as

$$\begin{aligned}
 [J]^{-1} &= \frac{1}{\det[J]} \left[ \begin{array}{c} \vec{J}_\eta \wedge \vec{J}_\zeta, \quad \vec{J}_\zeta \wedge \vec{J}_\xi, \quad \vec{J}_\xi \wedge \vec{J}_\eta \end{array} \right] \\
 &= \left[ \vec{j}_\xi, \quad \vec{j}_\eta, \quad \vec{j}_\zeta \right] \quad (3.33)
 \end{aligned}$$

and the symbol  $\wedge$  signifies a vector cross product.

#### 3.4.7 Strain Displacement Relations

The 78 unconstrained nodal variables for Semi Loof solid have been illustrated in Fig. (3,4). The relationship of all the unconstrained variables and derivatives, at any point  $\xi$ ,  $\eta$  and  $\zeta$  within the element, to the discrete nodal displacements can be concisely presented in the following order

$$\{U\} = [N] \{\delta\} \quad N \text{ is } (12 \times 78) \quad (3.34)$$

A typical partition for a node with 3 d.o.f. is







### 3.4.8 Kinematic Constraints

The unconstrained nodal variables for the Semi Loof solid element, Fig. (3,4) are now reduced to the constrained nodal configuration of Fig. (3,9). Ten constraints are required to produce an element, whose degrees of freedom on the top surface correspond with those of the Semi Loof shell element. The degrees of freedom and the constraints are introduced to duplicate so far as possible the behaviour of the Semi Loof shell surface on the top surface of the solid. Therefore if A and B are the neighbouring Loof points on the shell and the solid elements the relative angular displacement ( $\theta$ ) of adjacent edges can be prescribed to zero.

$$\begin{aligned}
 (\theta)^A - (\theta)^B &= 0 \\
 \therefore (\theta)^A &= (\theta)^B
 \end{aligned}
 \tag{3.38}$$

Considering the rotation terms of the Semi Loof shell the above constraints also mean securing the  $w$ ,  $\frac{\partial w}{\partial x}$ ,  $\frac{\partial w}{\partial y}$  continuity between shell and solid at corner and mid-side nodes.

Several tests of element performance with different constraints showed that the reproduction of the central  $w$  on the top surface of the solid element caused ill conditioning. This degree of freedom on shell element helps in providing constant flexural curvature of the shell mid surface.

The following set of constraints are such that the element passes the patch test for arbitrary hexagonal geometry and for mixed Semi Loof solids and shells.

The list of the constraints are as follows;

(i) The Loof Rotations (2 constraints along each edge):

In Semi Loof solid elements the relative angular rotation is constrained to zero at the two Loof points on each edge of top surface of the element. These boundary constraints have the advantage of being identical for two adjacent elements. The top surface slope ( $\frac{\partial W}{\partial y}$ ) due to the rotations at the Loof points are constrained to be identical to the top surface slope ( $\frac{\partial W}{\partial y}$ ) due to the displacements at the corner and mid-side nodes.

(ii) The Two Rotations at the Centre (2 constraints):

The work produced during rigid body displacement of an element by proposed rotation equality is to be zero. Therefore, by numerical integration of

$$\vec{\theta} = \hat{X} \cdot \theta_x + \hat{Y} \cdot \theta_y \quad (3.39)$$

over the top surface of element, the total work is equal to zero.

$$\int_{\text{area}} \hat{X}_9 \vec{\theta} d(\text{area}) = 0$$

$$\int_{\text{area}} \hat{Y}_9 \vec{\theta} d(\text{area}) = 0 \quad (3.40)$$

From eqns. (3.36) and (3.40) by extracting the appropriate columns and transforming the edge tangential rotation and integrating the rotation force over the area, one can derive the following equation

$$\begin{array}{c} \left[ \begin{array}{c|c} C_A & \\ \hline & C_B \end{array} \right] \begin{bmatrix} \delta_A \\ \hline \delta_B \end{bmatrix} = \begin{bmatrix} 0 \\ 0 \end{bmatrix} \end{array} \quad (3.41)$$

$10 \times 68$        $10 \times 10$

where  $\delta_A$  are the wanted variables and  $\delta_B$  are the unwanted variables. From eqn. (3.41) the discarded variables can be expressed in terms of the others as

$$\delta_B = -C_B^{-1} C_A \delta_A \quad (3.42)$$

By introducing the eqn. (3.42) to (3.35) and (3.36) the constrained displacement array

$$W^* = \{W_A - W_B C_B^{-1} C_A\} \quad (3.43)$$

and eqn. (3.10) would be expressed as

$$\delta^* = W^* \delta_A \quad (3.44)$$

the inversion of the matrix  $C_B$  followed by a matrix multiplication for the product  $C_B^{-1} C_A$  can be solved by the Gauss elimination or Faddeeva scheme <sup>3.11</sup>.

### 3.4.9 Numerically Integrated Stiffness Matrix

From eqns. (3.13) and (3.27) the stiffness matrix can be expressed as

$$K^e = \int_{-1}^{+1} \int_{-1}^{+1} \int_{-1}^{+1} B^T D B [J]_{3 \times 3} d\xi d\eta d\zeta \quad (3.45)$$

or in submatrix form

$$K_{ij}^e = \int_{-1}^{+1} \int_{-1}^{+1} \int_{-1}^{+1} B_i^T D B_j [J] d\xi d\eta d\zeta \quad (3.46)$$

where  $K_{ij}^e$  is a typical submatrix linking nodes  $i$  to  $j$ .

Integration of the stiffness coefficients is carried out numerically, so if eqn. (3.46) is replaced by a weighted summation of the values at a certain Gauss point in the element

$$K^e = \sum_{i=1}^n W_p [ B_p^T D B_p [J] ] \quad (3.47)$$

Where  $B_p$  is evaluated at the appropriate integration point with coordinates  $(\xi_p, \eta_p, \zeta_p)$  and  $W_p$  are the corresponding weight coefficients at this point.

### 3.4.10 Nodal and Pressure Loading

The Semi Loof solid at present accepts only the following constituents:

$$\bar{F} = \bar{F}_1 + \bar{F}_2 \quad (3.48)$$

where  $\bar{F}_1$  and  $\bar{F}_2$  are the consistent nodal forces associated with concentrated nodal loads and distributed surface pressures respectively.

The vector  $\bar{F}_1$  will consist of three force components for corner and mid-side nodes with three degrees of freedom and five for top surface mid-side nodes with five degrees of freedom.

$$\bar{F} = \begin{Bmatrix} \bar{f}_1 \\ \vdots \\ f_i \\ \vdots \\ \vdots \\ f_{20} \end{Bmatrix} \quad \text{with } \bar{f}_i = \begin{Bmatrix} P_{xi} \\ P_{yi} \\ P_{zi} \end{Bmatrix} \quad 3 \text{ d.o.f} \quad (3.49)$$

$$\text{and } \bar{f}_i = \begin{Bmatrix} P_{xi} \\ P_{yi} \\ P_{zi} \\ (M_x)_1 \\ (M_x)_2 \end{Bmatrix} \quad 5 \text{ d.o.f}$$

The consistent nodal forces  $\bar{F}_2$  due to a distributed pressure  $p$  over the top surface ( $\zeta = +1$ ) can be determined simply as

$$\bar{F} = - \int_{\text{area}} W^T p \, d(\text{area}) \hat{Z} \quad (3.50)$$

where  $W$  here refers to the first column of shape function array and  $p$  which varies over the surface and can be interpolated from the values specified at the nodes as

$$p = \sum_{i=1}^{i=8} N_i p_i \quad (3.51)$$

where  $N_i$  here refers to the standard shape function for an eight node isoparametric element.

The integration in eqn. (3.50) is carried out numerically and concurrently with the stiffness integration.

### 3.5 REDUCED NUMERICAL INTEGRATION AND SPURIOUS MECHANISMS

The stiffness matrix of the Semi Loof solid element is obtained by numerical integration of eqn. (3.47). Three different integration rules have been used and are presented in the general form:

$$\begin{aligned}
 & \int_{-1}^{+1} \int_{-1}^{+1} \int_{-1}^{+1} f(x,y,z) \, dx dy dz = A_1 f(0,0,0) \text{ (1 term)} \\
 & + B_6 \{f(-b,0,0) + f(b,0,0) + f(0,-b,0) + \dots \quad 6 \text{ terms}\} \\
 & + C_8 \{f(-c,-c,-c) + f(c,-c,-c) + \dots \quad 8 \text{ terms}\} \\
 & + D_{12} \{f(-d,-d,0) + \dots + f(d,0,-d) + \dots \quad 12 \text{ terms}\} \\
 & \hspace{20em} (3.52)
 \end{aligned}$$

The rules are listed below:

Rule 8G (The 2 x 2 x 2 product - Gauss Rule)

$$A_1 = 0, B_6 = 0, C_8 = 1.0, c = 0.57732$$

$$D_{12} = 0$$

This is the most popular and economical one with good results and rapid convergence. However this reduced rule does not prevent spurious mechanism occurring. Ideally the stiffness matrix for an element should have a rank of (the number of nodal variables) - (the number of rigid body motion available <sup>3.7</sup>).

The Semi Loof solid element therefore requires a rank of  $68 - 6 = 62$  and each integration point can contribute at most 6, (the rank of the elasticity matrix).

Hence the  $2 \times 2 \times 2$  Gauss integration rule should permit the occurrence of at least (14) spurious mechanisms.

Rule 27G - ( $3 \times 3 \times 3$  product - Gauss Rule)  
which is exact for polynomial of fifth order in each direction <sup>3.10</sup>.

$$A_1 = 0.70233196$$

$$B_6 = 0.43895747$$

$$C_8 = 0.17146776$$

$$D_{12} = 0.27434842$$

$$b = c = d = 0.77459667$$

The  $3 \times 3 \times 3$  Gauss integration rule would provide adequate rank thus avoiding spurious mechanism but it could be very costly in computer time. However in the search for more economical rules giving the same order of accuracy as the Gauss  $3 \times 3 \times 3$  rule, but cheaper, one can try the 14 point rule <sup>3.12, 3.13</sup> given originally by Hammer and Stroud and the slightly cheaper, slightly less accurate, 13 point rule given originally by Stroud <sup>3.14</sup>.

Rule 13 - The (13) point rule is defined by the following coordinates and weighting coefficients



(0, 0, 0) Coeff. A

$\pm (\lambda, \xi, \xi), \pm (\xi, \lambda, \xi), \pm (\xi, \xi, \lambda)$ , Coeff. B

$\pm (\mu, \mu, \lambda), \pm (\mu, \gamma, \mu), \pm (\gamma, \mu, \mu)$ , Coeff. C

$\lambda =$	0.88030430	$\xi =$	- 0.49584802
$\mu =$	0.79562143	$\gamma =$	0.025293237
A =	1.68421056	B =	0.54498736

C = 0.507644216

Rigid body tests showed that the (13) point rule does not prevent the occurrence of spurious mechanism totally, although it reduces their number.

Rule 14 - with  $B_6 = 0.886426503$

b = 0.795822426 ,  $C_8 = 0.335180055$

and c = 0.758786911

Accurate to complete quintic, like 27G, with the same Gaussian efficiency and considerably cheaper effort.

Several rigid body tests showed that the 14 point rule of integration prevented the occurrence of spurious mechanism.

### 3.6 GLOBAL STRESSES

The strain components of interest are in the directions (x,y,z), local coordinates, so as to be consistent to the Semi Loof shell assumption. The stresses corresponding to these are defined by a matrix  $\{\sigma\}$  in local coordinates.

These are indeed directly of interest but as the directions of local axes are not easily visualised at Gauss points or nodes, it is convenient to transfer the components to the global system using the following formulation.

$$[\sigma']_{3 \times 3} = \begin{bmatrix} \hat{X} & \hat{Y} & \hat{Z} \end{bmatrix}_{3 \times 3} * [\sigma]_{3 \times 3} * \begin{bmatrix} \hat{X} & \hat{Y} & \hat{Z} \end{bmatrix}_{3 \times 3}^T \quad (3.53)$$

where

$$[\sigma'] = \begin{bmatrix} \sigma'_x & \tau'_{xy} & \tau'_{xz} \\ \tau'_{xy} & \sigma'_y & \tau'_{yz} \\ \tau'_{xz} & \tau'_{yz} & \sigma'_z \end{bmatrix}$$

The nodal stresses can be calculated by extrapolating the stresses at Gauss points to the nodes.

The stresses calculated at a nodal point where several elements meet can then be averaged.

In typical solid structures the stress in a global system does not, however, give a clear picture of stresses. The principal stress routine and principal strain routine would derive the principal stresses or strains correspondingly, where direction cosines of such stresses or strains are also obtained (see Appendix 1).

### 3.7 NUMERICAL RESULTS

Various numerical examples were selected to establish the validity and generality of the proposed formulation.

#### 3.7.1 *Patch Tests*

The element passed the patch test with rectangular, parallelograms, trapezoidal and arbitrary hexagonal geometry as demonstrated, Figs. (3,10) to (3,14).

In order to check against the occurrence of mechanisms the rectangular and quadrilateral patch tests were repeated in the form of rigid body tests. In these tests a sufficient number of boundary constraints were prescribed to produce a statically determinate system, together with the external forces (the computed reactions derived from the patch test) acting on the patch. If there is any chance of a singular assembled stiffness matrix then this procedure would encourage it to occur.

However, as stated in the previous section, the rigid body test showed that the element has at least 14 mechanisms when  $2 \times 2 \times 2$  point Gaussian integration is being used. The 13 point rule also showed some mechanisms, when the 14 point rule and the 27 Gaussian rule did not show any singularity in the stiffness matrix.

A careful study of the behaviour of a patch of elements using different integration rules showed that all the patch tests with elements integrated by the 14 point rule were passed successfully. Furthermore, the 14 point rule is more economical than the 27 point Gaussian rule.

A series of mixed patch tests were carried out to establish the mixability of the Semi Loof solid element

with the Semi Loof shell element. The rectangular and general hexagonal mixed patch tests were successful.

### 3.7.2 Convergence Studies

#### (i) Cantilever Beam

A cantilever beam, shown in Fig. (3,15), illustrates the element accuracy for plane stress structures. The results for two different loading conditions and for two different meshes are shown in Table (3-1). The results compare favourably with the exact theoretical solution, the standard isoparametric quadrilateral element (Q4), and the Wilson incompatible element (Q6) <sup>3.15,3.16</sup>.

#### (ii) Plane Stress Cantilever Beam

A plane stress cantilever subjected to the point load at the free end, is shown in Fig. (3,16). The results compared favourably with the exact solution and the Semi Loof shell element <sup>3.17</sup>.

#### (iii) Cantilever Beam

The out-of-plane performance of the Semi Loof solid was tested for meshes with varied length/thickness ratios. The performance of the element as a thick element also compared with thick beam theory <sup>3.18</sup>, with the twenty nodes isoparametric brick element, and with both parallelogram (PQC3) and quadrilateral (QLC3) elements <sup>3.19</sup> (both include shear deformation). The results are shown in Tables (3-2) and (3-3).

The Semi Loof solid gives superior results as shown in Fig. (3,17) for very thick elements (shear dominated area) and slightly superior in almost thin elements (bending dominated area) over twenty nodes isoparametric brick element.

(iv) Simply Supported Thick Plate

A simply supported square plate was analysed using a 1 x 1, 2 x 2, 4 x 4 and 6 x 6 mesh of elements. A comparison with thick plate theory <sup>3.20-3.24</sup> and twenty node isoparametric brick element is shown in Fig. (3,18). A Semi Loof solid showed a better convergence than a twenty node brick element.

(v) Composite Beam

A composite plated beam was analysed using six Semi Loof shell and six Semi Loof solid elements as shown in Fig. (3,19). The deflection at the centre derived from finite element analysis compared favourably with the experimental results <sup>3.25</sup>.

(vi) A Cylinder under Uniform Axial Load

A cylinder subjected to uniform axial load (p) at both ends is shown in Fig. (3,20). A quarter of the circumferential cross-section was idealised by eight elements and one element used longitudinally as shown in Fig. (3,21). Symmetrical boundary conditions were applied on all the four cut edges. The results plotted in Fig. (3,22) show good correlation with results from the twenty node isoparametric brick element and classical shell theory.

### 3.8 CONCLUSIONS

(i) The formulation for a special Semi Loof solid element has been developed and presented. The new element is capable of being mixed with the Semi Loof shell element and the twenty node isoparametric solid element as may be required in the analysis of composite structures.

(ii) The criteria for convergence are satisfied according to the patch test and there are no limitations such as low rank and spurious mechanisms.

(iii) The results of the numerical examples establish the validity of the formulation for an extensive range of single material and composite structural problems and the results are an improvement over the twenty node solid element. The element performs well even for a coarse mesh idealisation.

(iv) The Semi Loof solid element has been coded into a shape function subroutine which with the use of numerical integration is easy to implement and computationally efficient.

## CHAPTER 4

EXPERIMENTAL STUDY OF THE  
COMPOSITE CONNECTIONS

## 4.1 INTRODUCTION

To investigate the applicability of composite connections an experimental test program was undertaken.

This chapter describes the manufacture, instrumentation and testing arrangement for the 12 models of Phase 1, 2 models of Phase 2 and the large-scale model of Phase 3, which simulate different forms of composite connections. These connections are studied with particular attention being given to the axial and circumferential strains and stresses, bond stress of concrete, displacement and the composite behaviour of steel and concrete.

4.1.1 *Objectives of the Experimental Tests*

The limited funds available allowed an experimental program to be conducted only on straight tubular composite connections. The construction and testing of these straight tubular connections, gave some insight into the possible construction procedure and provided in depth information on their structural behaviour. The choice of straight tubular connections as opposed to the more commonly used T or K joints was for reasons of economy and of the difficulty in physically understanding the structural action of the latter, due to the indeterminate triaxial stress effects and the composite behaviour of steel and concrete in areas of high stress concentrations. Furthermore, a

need existed for simple model tests to be conducted in which the effects on the composite behaviour of varying the various parameters are immediately obvious. The general objectives of the tests were therefore;

(i) To develop a construction procedure for straight tubular connections with the generality necessary to cope with construction and repair of straight tubular connections and pipe lines in deep water.

(ii) To provide comprehensive experimental data against which the analytical approach derived earlier in this thesis could be checked and also to elucidate on aspects of the behaviour not directly apparent from current finite element methods, for example the effect of shear connections and welded end rings.

(iii) To examine the non-linear behaviour of connections, in particular the effects of the concrete cracking.

#### 4.1.2 *Composite Connection Layout and Form of Construction*

Phase I - The specimens were constructed of two equal diameter tubes placed in a steel sleeve which was then grouted to form connection, Plate 1. The sleeve was carefully positioned and grouted to ensure a near perfect symmetry with a constant thickness of grout. A series of twelve small scale tests were carried out, with various geometries and types of surface roughness to determine an optimum configuration for the large scale test to follow.



Phase 2 - It was proposed that the serviceability of a connection could be improved by welding two steel rings to the extremities of the sleeve to contain the grout in a triaxial manner. To verify this proposal two small scale tests with a welded ring at the end were carried out, Plate 2.

Phase 3 - This large scale model was instrumented with strain gauges, Fig. (4,1), to measure the variation in strains along the length of steel tube and sleeve, Plate 3.

## 4.2 MODEL SCALE AND MATERIALS

The choice of scale depended upon the following:

(i) Minimum possible distance between steel tube and sleeve to accommodate the grout.

(ii) Magnitude of loads readily available in the laboratory.

Consequently the small scale of 1:20 and large scale of 1:5 based on original tube diameter of 1,000 mm were chosen.

It was also decided at an early stage that the mix most suitable and easy to pump for the construction of the connections was a fine sand (25-100) and Portland cement mixture to represent concrete parts of the models and steel tubes for steel parts of the models.

### 4.2.1 Grout Properties

The grout used for the small scale models was a 1:2 cement-sand with a free  $w/c$  ratio of 0.49, FEBMIX plasticiser (5.6 cc to each 1 kg of cement) was added. The sand used was a fine sand passing (25-100) grade. This was mixed with ordinary Portland cement. Test cubes were made from the grout mix which gave an average value of  $34.5 \text{ N/mm}^2$  compressive cube strength for 28 days.

The grout used for the large scale model was a 1:1.5 cement-sand mixed with a free  $w/c$  ratio of 0.48 and FEBMIX plasticiser (5.6 cc to each 1 kg of cement) was added. The sand was a fine sand passing (25-100) grade. This was mixed with ordinary Portland cement. Test cubes were made from the mix used for casting the model, which gave an average value of  $30 \text{ N/mm}^2$  at 14 days.

#### 4.2.2 *Steel Properties*

The steel used for the manufacture of the small scale composite connections was cut from standard scaffolding steel tubes which were machine turned to give the required diameters and thicknesses.

The steel used for large scale models was chosen from standard pipes used in North Sea construction. Table (4-1) shows the diameters and thicknesses of the tubes used. Values of yield stress and other information given by supplier is shown in Table (4-2). Tensile specimens were cut from each of the tubes used and elasticity modulus was calculated.

Further tests were carried out to check the strength of the pipes and sleeve and it was found that the average yield stresses of the pipe and sleeve were  $340.37 \text{ N/mm}^2$  and  $384.00 \text{ N/mm}^2$  respectively.

### 4.3 INSTRUMENTATION

No instrumentation was used for the small scale tests. The large scale model was instrumented to measure displacements and strains. The instrumentation was concentrated at sections which were thought likely to be highly stressed. The instrumentation was attached to the internal and external faces of the tubes and the external face of the sleeve.

#### 4.3.1 *Displacements*

The displacements at both ends of the large scale sleeve were measured using two dial gauges of 0.001 of an inch sensitivity as the load increased.

#### 4.3.2 *Strains*

The T.M.L. electrical resistance strain gauges type PC.5.11 were used for strain measurements. The gauge factor was approximately 2.04 with a tolerance of  $\pm 1\%$ . Cross gauges (biaxial) were used to derive axial and hoop stresses. Owing to the axial symmetry it was felt rosettes were unnecessary.

#### 4.3.3 *Data Logger*

A data logging system, a 70 channel Solartron logger, was used for this project. This system incorporates fast scanning speeds, print out and punch tape output, so that temperature changes do not affect the measured parameter values during the scanning period. The experiment took place in one morning so that a temperature compensating dummy gauge was not required.

#### 4.4 LOADING PROCEDURE

A simple uniaxial 50 ton pullout machine was used to test the small scale models, Plate 4. Consequently the pullout forces that caused any significant slip and ultimate loads were recorded.

The loading rig for the large scale model was made of two vertical steel frames which could move longitudinally without any friction. Both ends of the pipes were horizontally secured at the centres of the frames through special holes, and 12 jacks each with 20 tons capability providing a total of 240 tons pushed the two frames apart and this therefore pulled out the connections, Plate 5.

The load was applied in increments of 13.2 tons and loading was sustained for a few minutes before each set of instrument readings. Large strains were noticeable as the load increased and after the eleventh increment of load (145 tons) a crack appeared on the weld between the sleeve and external ring at approximately 150 tons load. At this stage the loading was removed and reapplied with the same increments up to 79.2 tons. During the next increment at approximately 84 tons, the bond between the steel and the concrete was broken and the concrete started to slip out from the sleeve, Plate 6.

#### 4.5 SMALL SCALE MODELS

The Phase 1 small scale models were categorised into four groups;

Group 1 - Three models with various lengths of sleeve (2D, 2.5D and 3D) were tested. The specimens of this group were dipped in a sea water bath before grouting for three weeks to give a roughened surface to the steel tubes. The test results showed that the maximum equivalent bond strength was obtained when the  $L/D_I$  ratio was equal to 2.5. No slip was noticed during testing and failure occurred when one of the pipes pulled out of the joint.

Group 2 - Three models were similar to those of Group 1 except that the sleeve had a larger internal diameter which left a gap of 12.2 mm for the grout. The models were treated in the same manner as in Group 1. Again, maximum ultimate bond strength was obtained at  $L/D_I$  ratio of 2.5.

Group 3 - Three models had the same dimensions as Group 1. However the outside surface of the pipes and the inside surface of the sleeve had additional rings of protruding teeth, 2 x 2 mm square at a 20 mm spacing, and the teeth on the inside surface of the sleeves alternated with the teeth on the outside surface of the pipes. Test results showed a significant increase in ultimate bond strength over the previous models. Two modes of failure can be seen on Plates 7 and 8.

Group 4 - Three models similar to Group 3 models but with a larger sleeve diameter which allowed 12.2 mm grout thickness were tested. The maximum equivalent bond strength

was obtained when the  $L/D_I$  ratio was equal to 2. Plate 9 shows the mode of failure for  $L/D_I$  ratio of 3 and the position of shear connectors for this model.

In Phase 2 testing two specimens with rings welded at both extremities were tested. The diameters and thickness of tube and sleeve, the size and number of shear connectors and the thickness of grout were exactly the same as the first specimen of Group 3 ( $L = 2D$ ). In addition a 3.2 mm thick steel ring was welded to the end of the sleeve to contain the grout triaxially. One of the models had the ring welded to the tube and sleeve, whereas in the second model the ring was welded only to the sleeve. The first model failed at approximately 11.75 tons when the steel tube yielded and failed. The second model, with the steel ring welded to the sleeve, like the first, also showed an improvement in ultimate load capacity compared with with the Group 3 model.

The behaviour of the models was studied with particular attention being given to the ultimate equivalent bond strength and its relationship with radial stiffness, length/diameter ratio and with shear connectors. Table (4-3) shows the value of the ultimate axial loads, the geometrical properties and the associated ultimate equivalent bond strength for each of the small scale models tested.

#### 4.5.1 *Effect of Tube and Sleeve Geometry on Bond Strength*

The test results showed that the ultimate bond strength is extremely sensitive to model geometry and the radial stiffnesses of the sleeve, tube and grout. The

radial stiffness of the tube or sleeve in terms of a uniformly distributed radial force  $F$ , and radial deflection  $\Delta$ , is proportional to Young's modulus  $E$ , and the thickness to diameter ratio ( $t/D$ ) of the tube. If the radial stiffness of the complete connection is considered, a stiffness factor,  $K$ , proportional to the radial stiffness of the grout and steel cylinders can be derived. A linear relationship <sup>4.1,4.2</sup> exists between the ultimate bond strength and the radial stiffness factor for a given set of conditions (i.e. grout strength, surface roughness and length of connection). The stiffness factor  $K$  is given by:

$$S = \frac{F}{\Delta} \approx E \frac{t}{D} \quad (4.1)$$

$$K = S_{\text{grout}} + \left( \frac{1}{S_{\text{tube}}} + \frac{1}{S_{\text{sleeve}}} \right)^{-1}$$

is plotted against ultimate bond strength in Fig. (4,2). It was noticed from this diagram that shear connectors improve the performance of connection several times.

#### 4.5.2 *Effect of Length/Diameter Ratio on Bond Strength*

The length to diameter ratios in the range of  $2 < L/D_I < 3$  were chosen for the composite connection tests. The ultimate bond stress is plotted against  $L/D_I$  ratio in Fig. (4,3). The results indicate a slight reduction in bond stress with increasing length although the maximum values occur at different ( $L/D_I$ ) ratios for each of the test groups.



#### 4.5.3 *General Behaviour of Tests*

Most of the models with shear connectors exhibited large reserves of strength and in many cases the ultimate load was sustained over displacements of several millimeters. The behaviour of Groups 1 and 2 was more erratic owing to the sudden breakage of the chemical bond (the adhesion or glueing by the cement gel to the steel) and of the friction due to concrete shrinkage..

The behaviour of the Group 3 and 4 models with shear connectors was different because there was a large post ultimate reserve of strength. Failure took place on the grout and sleeve interface by crushing the grout ahead of the weld bead. In most cases, near the ends of the connection, diagonal cracks formed across the annulus originating from weld bead positions.

A significant increase in the strength of the connection was achieved by triaxial action of the grout due to the presence of welded rings at both extremities of the sleeve. A model with similar geometrical and physical properties to one of the Phase 1 models but with a 3.2 mm thickness steel ring welded lightly to the tube and the sleeve showed a 180% increase in strength over a similar model. Failure occurred in the steel tube without any noticeable effect on the connection.

#### 4.6 LARGE SCALE MODEL

In Phase 3 of testing a large scale specimen was tested. The outside surface of tubes and the inside surface of the sleeve were furnished circumferentially with 5 mm height and 5 mm width of weld beads at 70 mm spacing. The weld beads on the tubes were located mid-way between the weld beads of the sleeve. A ring made of 6 mm thick steel plate was welded to both extremities of the sleeve and to the tubes. Holes on the end ring of the connection allowed the grout mix to be pumped into the cavity between the tubes and the sleeve.

This model carried a substantial load in tension and failure occurred when the total load on the model reached 150 tons, that is 81% of the yield load of the tube, when fracture of the weld between the sleeve and tubes occurred. A tolerance of 1-5 mm between the sleeve and tube which had been filled with weld deposits may have caused the failure of the connection earlier than expected. However, the connection still exhibited a high reserve of strength and was again capable of carrying a load up to 84 tons. At this load the bond between the sleeve and the grout failed, Plate 10. This model was extensively covered with electrical strain gauges. The locations of the strain gauges on the external surface of the sleeve are shown on Plate 11. A total of 35 axial and 35 circumferential strain gauge elements were used on this model. The location and numbering of the biaxial strain gauges on the inside and outside of the tube and outside of the sleeve are shown in Fig. (4,1).

#### 4.6.1 *Variation of Strains and Displacements in Large Scale Model*

The behaviour of the model is studied with particular attention being given to the distributions of axial and hoop strains and stresses, principal stresses, displacements and bond between concrete and steel.

Before the results were plotted, the readings from gauges which drifted more than  $30 \mu\epsilon$  were rejected. Out of a total of 70 strain gauge elements on this model, one had a drift larger than  $30 \mu\epsilon$  on three successive readings and in this case the results obtained were from one of the reserve gauges. However, reserve gauges were present as a precaution against drift and failure, the alternative readings were invariably available.

Figs. (4,4) and (4,5) show the overall axial strain distribution and Figs. (4,6) and (4,7) show the overall circumferential strain distributions for different load cases.

Longitudinal extensions of the sleeve are plotted in Fig. (4,8).

#### 4.6.2 *General Behaviour of Large Scale Test*

A high post ultimate reserve of strength was observed in the large scale composite connection and this was due to the following;

The steel cylinder with its high strength and ductility suppressed the development of cracks in concrete until the mechanical bond was broken and crushing of concrete occurred.

The cracked concrete could carry high shear stress by an arching action which delayed failure.

The presence of two welded rings at both extremities of the sleeve increased the strength of the connections due to the triaxial effect on the concrete.

#### 4.7 CONCLUSIONS

The ultimate bond strength of composite connections depends on many parameters including, the radial stiffness of the connection, the length/diameter ratio of the connection, the grout strength and the size and number of shear connectors.

The use of shear connectors provides a high ultimate strength which is not affected by shrinkage or expansion of the grout and can be sustained over large displacements.

A significant increase in the strength of composite connections can be achieved by the use of steel rings welded to both extremities of the sleeve which fully confines the concrete. This also assures complete waterproofing when the connection is used for pipe lines in deep water.

## CHAPTER 5

FINITE ELEMENT ANALYSIS  
OF COMPOSITE TUBULAR JOINTS

## 5.1 INTRODUCTION

The newly developed Semi Loof solid element was described and verified by reference to classical problems and convergence tests (chapter 3). However in order to further verify the proposed element formulation and the validity of the associated computer code, the large scale model test described in chapter 4, was analysed and the results are presented and compared in this chapter.

Having thus established the performance and validity of the proposed Semi Loof solid element, various types of tubular connections and tubular joints, suitable for use in the construction or repair of pipelines and offshore structures, were analysed. Information on the displacement and stress distributions is presented in this chapter and the effect of including concrete is shown. From these analyses certain conclusions are drawn with respect to the design, fabrication and installation of the proposed composite connections in the construction and repair of North Sea structures.

## 5.2 COMPOSITE STRAIGHT TUBULAR CONNECTIONS

An analytical study of two types of composite straight tubular connections was carried out. The two types of construction considered were, steel tubes connected by a steel sleeve filled with cement grout, with or without welded end rings, and steel tubes connected by a prestressed concrete sleeve with or without steel encasement. The geometrical and material properties were as for the large scale model of chapter 4, which allows a comparison between finite element results and experimental results.

The connections were analysed for loadings at 45% of the estimated ultimate loads, in order to ensure that joint behaviour was predominantly elastic. The stress distributions shown subsequently were plotted from the values available at the Gauss points for both shell and solid elements.

### 5.2.1 *Finite element analysis of steel tubes connected by a steel sleeve filled with concrete*

Finite element analyses of the (1:5 scale) composite tubular connections were carried out using 42 Semi Loof shell and 30 Semi Loof solid elements. The mesh incorporated elements over a quarter of tube and nine shell elements over the half length of tube together with five solid elements along the connection length. Only one quarter of the structure was analysed to take advantage of the double symmetry of the structure, Fig. (5,1).

The shear connectors (weld beads) were not modelled in the finite element idealization and a perfect bond state between the steel and concrete was assumed.

In order to ascertain whether undesirable stress concentrations were likely to arise under operating conditions, two types of loading were considered.

Load case 1 - an axial load along the connection caused by tensile end forces of 79.2 tons (790 KN), which is approximately 45% of the yield loading ( $P_y$ ) of the pipes.

Load case 2 - a constant bending moment along the length of the connections was applied by end moments of 13.75 KN.M and this is approximately 10%<sup>†</sup> of the full plastic moment ( $M_p$ ) of the pipes for pipe lines. End moments of 27.50 KN.M, which is approximately 20% of the full plastic moment ( $M_p$ ) of the pipes for straight tubular connections.

The longitudinal stresses of the inside and the outside surfaces of the steel tube and the sleeve subjected to axial load are shown in Figs. (5,2) to (5,4). The largest stress concentration factor was found to be 1.13. The variation of longitudinal tensile stresses in the concrete is shown in Fig. (5,5). The analysis was then extended to a model with welded steel rings at the extremities of the sleeve and a considerable reduction in the

---

<sup>†</sup>0.10  $M_p$ , is the largest fluctuating moment likely to be permitted in pipe lines for a fatigue life of  $10^8$  cycles<sup>5.1</sup>.



longitudinal tensile stress of the concrete was observed, Fig. (5,5), however the effect on the stresses in the tube and sleeve was not so marked. The results of this second analysis were compared with the experimental results, reported in chapter 4. Axial strains in the steel tube are shown in Fig. (5,6). Close agreement between the analytical results and model experimental results was obtained except in the vicinity of the weld in the sleeve where a high strain concentration was detected by the electrical strain gauges. Circumferential strains in the steel tube are shown in Fig. (5,7). Analytical results were in close agreement with the model experimental results. Longitudinal expansions of the sleeve versus load cases are plotted in Fig. (5,8).

The analysis of the composite connection was also carried out subjected to a factored load combination ( $P_y + 10\% M_p$ ) for pipe line connections. The largest stress concentration factor of 1.35 on the outside surface of the tube was caused by local bending near the end of the connection. It can therefore be concluded that the additional bending moment increased the tensile stresses of the steel and concrete by a maximum of 18%.

This analysis was repeated for straight tubular connections as found in platforms subjected to a factored load combination of ( $P_y + 20\% M_p$ ). The largest stress concentration factor of 1.56 was calculated on the outside surface of the tube.

### 5.2.2 *Finite element analysis of steel tubes connected by a prestressed concrete sleeve*

Finite element analyses of several prestressed composite connections were carried out idealizing only one-eighth of the connection with 27 Semi Loof shell and 30 Semi Loof solid elements by taking advantage of the triple symmetry, Fig. (5,9). To find a suitable prestressing force and an appropriate number of tendons several connections were analysed. The prestressing tendons were idealized by point loads acting axially at the mid-thickness of the concrete.

Longitudinal stresses of the inside and the outside surfaces of the steel subjected to several prestressing forces are shown in Figs. (5,10) and (5,11).

The variation of stress concentration factors, the ratio of maximum axial stress to the nominal axial stress, versus prestressing forces are shown in Fig. (5,12).

Longitudinal stresses in concrete for various prestressing forces are shown in Fig. (5,13).

It was noted that connections with smaller numbers of tendons around the periphery produced high stress concentration on the steel tube. It can be argued that the connection with the lower stress concentration factor and with adequate compressive stress of concrete is the least vulnerable to cyclic loading damage and best suited to the North Sea environment.

### 5.2.3 *Discussion and Conclusions*

The experimental tests and the finite element analyses of the composite connections with steel encasement provided sufficient evidence to allow this connection to be used for permanent repairs and tie-ins of subsea pipe lines and straight tubular connections on offshore platforms.

The fabrication process would start by welding vertical rings (with holes for grouting) in two halves to the two halves of sleeve, leaving an appropriate connection length. The sleeve would then be placed and welded to the pipe at the side of the opening.

The two halves of the sleeve and rings are then welded together. These welds should withstand the bending moments produced by cyclic forces. The gap is then pumped full with high strength grout. Proper sealing of the pipe is required to prevent oil or gas chemical action on the cement grout.

The prestressed connection also can be used to reinforce or repair subsea pipe lines and straight tubular connections on offshore platforms. Prestressing can be accomplished in either of two ways, depending on the economics, the size of the member and the environment.

The prestressed connection with the concrete collar is particularly suitable for large diameter tubes in platform structures. Post tensioning tendons are stressed uniaxially after the concrete has been cast and attained sufficient strength to safely withstand the prestressing force.

The pretensioned-strand system can be used for smaller diameter pipes in connection with a steel sleeve filled with concrete. A steel sleeve and end rings are welded to the pipe. A number of strands are arranged in a circle and anchored safely to the end rings with nuts on washers, so that the extra cost of anchorage blocks can be avoided. The tendons are then tensioned and the gap between sleeve and pipe grouted. When the grout has set and tension in the strands is released the grouted connection goes into compression. This prestressed connection secures watertightness in deep water. Where the water pressure can cause serious problems<sup>5.2,5.3</sup> in exposed concrete surfaces.

The following conclusions can be drawn from the above discussion and the finite element analyses of composite connections:

(i) The finite element results of composite connection with steel encasement compared favourably with the experimental results.

(ii) Welded end rings with some stiffness endured the relative movement between concrete and steel tubes producing compressive stress in concrete which delayed the bond failure. This implies that higher stress levels can be imposed. A similar observation was made during the experimental program.

(iii) In practice, to ensure composite action between concrete and steel as assumed in the numerical examples, the surfaces of the steel tube and sleeve should be furnished with shear connectors. The mechanical shear

connectors should be designed to resist all the interface forces arising from composite actions between the concrete and steel tube.

(iv) In the case of prestressed connections high compressive stresses in the concrete were observed.

(v) A more rapid diminution of axial stress in the tube inside the encasement was observed in the prestressed connections compared to other composite connections. It was also noted that the prestressing forces caused local bending beyond the sleeve. It is likely that this local bending was due to the method of applying prestressing forces in the analysis.

(vi) Concrete compressive stresses, induced due to the presence of mechanical shear connectors, welded end rings and prestressing, allow a much shorter connection to be made. This implies savings during fabrication and installation.

(vii) Advantage can be taken of a longer fatigue life due to the high fatigue endurance of concrete in compression.

(viii) In connections in which steel surrounds the concrete, a higher compressive triaxial stress state is achievable under large loads. This increases the strength of the connection.

### 5.3 COMPOSITE TUBULAR T-JOINTS

Finite element analyses of composite T-joints with a concrete collar and a steel collar filled with concrete were carried out and compared with welded joint results computed for a T-joint subjected to a branch axial force. Because the finite element discretization models the welded T-joint as an ideal intersection of two tubes, it would be appropriate first to establish the validity of the analysis by comparison with experimental data from such an idealized joint. The Oak Ridge National Laboratory's ideal T-joint<sup>5.4,5.5</sup> is shown in Fig. (5,14). The joint was cantilevered at one end of the chord and subjected to an axial load applied at the end of the branch. Attached to each of the unsupported pipe ends was a heavy end plate which constrained the pipe end to remain a plane circle and largely restrained rotation of the pipe wall about the axes in the plane of the end plate. For both the chord and the branch the radius to thickness ratio was 50.0 which places this shell structure well within the range of what are usually regarded as thin shells. The finite element analysis was carried out with 60 Semi Loof shell elements, Fig. (5,15). Analytical results of the surface longitudinal and transverse stresses for the branch axial load of 100 lb (445 N), 25% of the branch yield load, were compared with experimental values in Figs. (5,16) to (5,18). In each case the longitudinal stress was directed along the section at which the stresses were plotted and the transverse stress was perpendicular to the section. A hot spot stress value of about  $8765 \text{ lb/in}^2$  ( $60.62 \text{ N/mm}^2$ ) was observed and this value is later compared

with the hot spot stress values derived from various composite T-joints.

### 5.3.1 *Finite element analysis of a T-joint with a concrete collar*

In this joint the highly stressed area in a welded T-joint is covered by an 0.4 in (10 mm) thick concrete collar. A finite element analysis was carried out using 60 Semi Loof shell and 24 Semi Loof solid elements. The mesh idealization is shown in Fig. (5,19). The concrete modulus was taken as 3000 KSi ( $21000 \text{ N/mm}^2$ ) with Poisson's ratio of 0.2.

The effect of the concrete collar on the variation of chord stresses and stresses around the intersection line are shown in Figs. (5,20) and (5,21).

It is apparent that, if the concrete remains bonded to the outside surfaces of the chord and branch members, then significant reductions in the local stresses would be realized. In addition there is a 70% reduction of the hot spot stress value. The maximum shear and tensile normal bond stresses on the inside surface of the concrete were calculated to be  $61 \text{ lb/in}^2$  ( $0.42 \text{ N/mm}^2$ ) and  $247 \text{ lb/in}^2$  ( $1.73 \text{ N/mm}^2$ ) respectively. The concrete stresses in the immediate vicinity of the branch chord intersection are close to the allowable concrete tensile and bond stresses, whereas the maximum steel tensile stress is far from the allowable. It would seem that a non-linear analysis which takes account of the cracking of the concrete and changes in stiffness in solid elements experiencing high tensile stresses would probably show a less substantial reduction in chord stresses

when higher axial load is applied.

### 5.3.2 *Finite element analysis of a T-joint with a steel collar filled with concrete*

In this joint the highly stressed area in a welded T-joint is covered by an 0.6 in (15 mm) thickness of concrete surrounded by an 0.05 in (1.3 mm) steel tube. The finite element analysis was carried out using 84 Semi Loof shell and 48 Semi Loof solid elements. The mesh idealization is shown in Fig. (5,22). The concrete modulus was taken as 3000 Ksi ( $21000 \text{ N/mm}^2$ ) with Poisson's ratio of 0.2.

The effect of a steel collar filled with grout on the variation of chord stresses and stresses around the intersection line are shown in Figs. (5,23) and (5,24). A significant (80%) reduction of hot spot stress values was obtained when compared to a welded T-joint. The maximum shear and tensile normal bond stresses on the inside surface of concrete were calculated to be  $12.9 \text{ lb/in}^2$  ( $0.09 \text{ N/mm}^2$ ) and  $131 \text{ lb/mm}^2$  ( $0.91 \text{ N/mm}^2$ ) respectively.

### 5.3.3 *Discussion and Conclusions*

A requirement exists for an effective method for the repair and strengthening of T-joints in offshore structures. The method proposed in this thesis consists of placing a steel collar around the T-joint and filling the gaps thus created with concrete. A benefit of this approach is the easy casting and fabrication process required. Furthermore, since the strengthening is external to the tubes the main legs of an offshore structure remain uncluttered for easy access.



To ensure composite action between concrete and steel tubes, the surface of the steel tubes should be furnished with mechanical shear connectors. The corroded surface of tubes in offshore platforms generally offers some mechanical connection between the steel and concrete.

To withstand North Sea cyclic loading and the related high bending moments, the steel collar should be walled (that is a lip plate around the periphery of the collar) and welded to the chord and the branch. As an alternative prestressing tendons can be used to produce compression stresses in the concrete thus allowing higher stress levels to be imposed.

The following conclusions can be drawn from the above discussion and the finite element analyses of T-joints:

(i) The presence of concrete in the T-joint with concrete collar reduced the hot spot values of stress around the intersection line.

(ii) A composite T-joint with a steel collar filled with concrete had a higher strength when compared to a composite T-joint without a collar.

(iii) It is likely that the addition of a steel collar suppresses crack initiation and propagation in the concrete surface when a joint is subjected to higher loads.

(iv) The encasement of concrete with a steel collar produces an advantageous triaxial compressive stress state in the concrete.

## 5.4 COMPOSITE TUBULAR K-JOINT

A finite element analysis of a composite K-joint was carried out and the results compared with the results derived from the analysis of a welded K-joint. The validity of the welded K-joint analysis was established by comparison with published experimental data<sup>5,6</sup>. The geometry and loading of the K-joint are shown in Fig. (5,25). The chord and branches are subjected to axial and transverse forces and a transverse moment. In the analysis the right-hand end of the chord and the two branch loads were assumed to be completely free and subjected to end loads, while the left-hand of the chord was assumed to be completely fixed. A finite element analysis of a welded K-joint with an idealization using 245 Semi Loof shell elements was carried out, Fig. (5,26). The maximum principal stresses along the top line of the chord compared well with the experimental values, Fig. (5,27). The displacement along the chord top line is shown in Fig. (5,28). A hot spot stress value of  $32,252 \text{ lb/in}^2$  ( $222.37 \text{ N/mm}^2$ ) was obtained from the analysis.

### 5.4.1 *Finite element analysis of a K-joint with a concrete collar*

In this joint the highly stressed area in a welded K-joint is covered by an 0.8 inch (20 mm) thickness of concrete to form a composite K-joint. The finite element analysis of the joint was carried out using a mesh of 245 Semi Loof shell and 100 Semi Loof solid elements, Fig.(5,29). The concrete modulus was taken as 3000 Ksi ( $21000 \text{ N/mm}^2$ ) with a Poisson's ratio of 0.2.

The effect of the concrete on the variation of chord stresses, the displacements and stresses around the intersection lines are shown in Figs. (5,30) to (5,32). A hot spot stress value of about  $17138 \text{ lb/in}^2$  ( $118.16 \text{ N/mm}^2$ ) was obtained. With reference to this figure it became apparent that, if the concrete remained bonded to the outside surfaces of the chord and branches, a significant (46%) reduction of the hot spot stress value in comparison to a welded K-joint was obtained.

The maximum shear and tensile normal bond stresses on the inside surface of concrete were higher than allowable values.

#### 5.4.2 *Discussion and Conclusions*

The results presented here, for a composite K-joint having simple geometry, serve as an illustration of the analysis technique developed in this thesis which may be applied to joints of considerable complexity, Appendix 3.

The following conclusions can be drawn from the analysis of a composite K-joint;

(i) The thickness of concrete in the model analysed was inadequate since the shear and tensile stresses in the concrete were greater than the allowable values.

(ii) The presence of concrete decreased the hot spot stress values in the steel around the intersection lines.

(iii) Smaller  $W$  displacements were observed in the composite K-joint compared to the welded K-joint.

## 5.5 CONCLUSIONS

The newly developed Semi Loof solid element when combined with the Semi Loof shell element provides an efficient procedure for the analysis of concrete and steel in composite connections. The results derived from the finite element analysis compared closely with the experimental results for a composite connection with a steel sleeve filled with concrete.

From the analysis of various types of composite connections and joints reported in this chapter, it is evident that the proposed finite element method can be used effectively to provide an improved understanding of the structural behaviour.

The proposed finite element method is simple to apply and computationally efficient as was demonstrated in the analysis of a composite K-joint. This problem required an idealization of 245 Semi Loof shell and 100 Semi Loof solid elements with a total of 1297 nodes. The mesh generation routines reduced the data preparation effort to a minimum and the execution time required to produce the results was 3000 sec on a Cyber 174 computer.

## CHAPTER 6

## GENERAL CONCLUSIONS

## 6.1 SUMMARY OF WORK

The work described herein on the linear static analysis of straight tubular members, composite connections and composite tubular joints has involved;

(i) The development of a Semi Loof solid element which is mixable with the Semi Loof thin shell element and is particularly suitable for use in the analysis of composite connections.

(ii) The development of a special purpose mesh generation program which will automatically generate the descriptive data required for a wide range of joint geometries.

(iii) An experimental program to study the composite behaviour of steel and concrete for connections with various physical and geometrical properties.

(iv) The verification of the developed computer program by reference to model experiments.

(v) The application of the computer program to a range of composite connections and joints.

(vi) Discussion with respect to the design, fabrication and installation of the analysed composite connections.

## 6.2 CONCLUDING REMARKS

The Semi-Loof solid element was developed and applied to various composite tubular connections and joints.

The finite element results of several models were compared with theoretical and experimental results, and found to be in close agreement, thus establishing the overall validity of the element and versatility of the finite element program.

The finite element program was used to analyse several composite tubular connections and joints, and the results enabled certain improvements with respect to the design, fabrication and installation to be suggested. The program could therefore be utilized for parametric studies of a series of static linear joints for the formulation of a design guides to estimate stress concentration factors.

The Semi Loof solid finite element can be utilized in conjunction with one of several iterative schemes to incorporate the effect of geometrical and material non-linearity, cracking in concrete, steel plasticity etc. The application of a program containing these effects would be limited by the high computer costs involved in the incremental solution of the non-linear equations.

In this thesis attention has been drawn to the fatigue problem at joint intersections as a result of cyclic forces. The way now appears to be open for the development of time dependent forces acting on joints based on this static program. The fatigue life of a joint can be derived from the fatigue analysis in conjunction with Palmgren-Miner 's rule.

### 6.3 FUTURE EXPERIMENTAL WORK

As a result of the experimental program carried out for this thesis the following suggestions are made for future work. Studies could with advantage be made of:-

- (i) The effect of steel tube diameter/grout thickness ratio on the ultimate strength of straight tubular connections.
- (ii) The effect of the shear connection height/spacing, height/tube diameter and spacing/tube diameter ratios on the ultimate strength of straight tubular composite connections.
- (iii) The effect of shear connection height/spacing, height/tube diameter and spacing/tube diameter ratios and concrete compressive strength on the induced compressive stress of the concrete in straight tubular composite connections.
- (iv) The effect of reinforcing and prestressing the concrete on the ultimate strength of straight tubular composite connections.
- (v) The fatigue performance of composite materials (steel and concrete).
- (vi) The behaviour of straight tubular composite connections under cyclic loading.
- (vii) The behaviour of large scale composite T-joints subjected to branch axial and flexural load (static and dynamic loading).
- (viii) The behaviour of large scale composite K-joints subjected to full platform loads.

## APPENDIX 1

## A1. T, Y AND K JOINT GEOMETRIC FORMULATION

The following formulae provide the value of the coordinates (X,Y, Z) at the intersection line, for any polar position ( $\alpha$ ) around the branch member

(i) T-joint, Fig. (2,1).

$$\begin{aligned} X &= \ell_b + r \cos \alpha \\ Y &= r \sin \alpha \\ \beta &= \text{Arc} \left( \sin \left( \frac{Y}{R} \right) \right) \\ Z &= R \cos \beta \end{aligned}$$

when  $0 < \alpha < 180^\circ$  and  $0 < \beta < 90^\circ$ .

(ii) Y-joint, Fig. (2,2).

The value of ordinate (R) for any polar position ( $\alpha$ ) around the branch member is

$$h = \frac{R}{\sin \phi} [A] + \frac{r}{\tan \phi} [B]$$

where

$$[A] = 1 - \sqrt{1 - \left(\frac{r}{R}\right)^2 \sin^2 \alpha}$$

$$[B] = 1 - \cos \alpha$$



Therefore,

$$X = l_b + \frac{r}{\sin \phi} + R \cot \phi - r (1 - \cos \alpha) \sin \phi - h \cos \phi$$

$$Y = r \sin \alpha \sin \phi$$

$$\beta = \text{Arc} \left( \sin \left( \frac{Y}{R} \right) \right)$$

$$Z = R \cos \beta$$

(iii) K-joint with negative eccentricity, Fig. (2,3)

The value of the x coordinate of the point  $N_2$  can be found graphically<sup>A1.1</sup>, the program then generates the coordinates of the intersection points related to  $X_{N_2}$  as

$$\alpha_{1N_2} = \text{Arc} \cos \left( \frac{X_{N_2} - l_{b1}}{r_1} \right)$$

$$\alpha_{2N_2} = \text{Arc} \sin \left( \frac{r_1 \sin \alpha_1}{r_2 \sin \phi} \right)$$

where the  $\alpha_1$  and  $\alpha_2$  angles vary as

$$180^\circ < \alpha_1 < \alpha_{1N_2}$$

$$\alpha_{2N_2} < \alpha_2 < 0$$

The previously described T-joint and Y-joint geometric formulation can now be used in the above angular domain. The coordinate values of  $N_2$ ,  $N_4$ ,  $N_5$  and  $N_6$  on the intersection line between the two small pipes are

$$X_{N_2} \quad \text{known}$$

$$Y_{N_2} = \sqrt{r_1^2 - X_{N_2}^2}$$

$$Z_{N_2} = l_{b_2} - \frac{r_1 \cos \alpha_2}{\sin \phi} + X_{N_2} \tan \phi$$

$$X_{N_4} = \frac{(l_{b_1} + r_1 - X_{N_2})}{3} + X_{N_2}$$

$$Y_{N_4} = \sqrt{r_1^2 - X_{N_4}^2}$$

$$Z_{N_4} = l_{b_2} - \frac{r_1 \cos \alpha_2}{\sin \phi} + X_{N_4} \tan \phi$$

$$X_{N_6} = l_{b_1} + r_1$$

$$X_{N_6} = 0$$

$$Z_{N_6} = l_{b_2} - \frac{r_1 \cos \alpha_2}{\sin \phi} + X_{N_6} \tan \phi$$

$$X_{N_5} = \frac{2(l_{b_1} + r_1 - X_{N_2})}{3} + X_{N_2}$$

$$Y_{N_5} = \sqrt{r_1^2 - X_{N_5}^2}$$

$$Z_{N_5} = l_{b_2} - \frac{r_1 \cos \alpha_2}{\sin \phi} + X_{N_5} \tan \phi$$

## APPENDIX 2

## A2 DETERMINATION OF PRINCIPAL STRAINS AND STRESSES

The 3D symmetric stress tensor  $[\sigma]$  is

$$\sigma_{ij} = \begin{bmatrix} \sigma_{11} & \sigma_{12} & \sigma_{13} \\ \sigma_{21} & \sigma_{22} & \sigma_{23} \\ \sigma_{31} & \sigma_{32} & \sigma_{33} \end{bmatrix}$$

This tensor can be multiplied by a unit vector  $n_i$  to give the product  $\sigma_{ij} \cdot n_i$ . This product can be rewritten as  $S n_j$ , where  $S$  is a scalar representing the magnitude of the vector and  $n_j$  is a unit vector.

Then

$$\sigma_{ij} n_i = S n_j$$

and

$$(\sigma_{ij} - S \delta_{ij}) n_i = 0$$

The above equation represents a set of three linear algebraic homogeneous equations in the  $n_i$ . A necessary and sufficient condition for a non-trivial solution is that the determinant of the coefficients be zero. The expansion of the determinant yields a cubic equation for  $S$  which is called the characteristic equation of the symmetric tensor  $\sigma_{ij}$ .

$$S^3 - I_1 S^2 + I_2 S - I_3 = 0$$

where

$$I_1 = \sigma_{11} + \sigma_{22} + \sigma_{33} = \Sigma \sigma_{ii}$$

$$I_2 = \sigma_{11} \sigma_{22} + \sigma_{11} \sigma_{33} + \sigma_{22} \sigma_{33} - \sigma_{12}^2 - \sigma_{13}^2 - \sigma_{23}^2 = \frac{1}{2} \Sigma (\sigma_{ii} \sigma_{jj} - \sigma_{ij} \sigma_{ji})$$

and

$$I_3 = \det [\sigma_{ij}]$$

$I_1$ ,  $I_2$  and  $I_3$  are called the basic invariants of the symmetric tensor  $\sigma_{ij}$ <sup>A2.1</sup>. The principal values of the stresses are the roots of the cubic equation.

A similar procedure can be carried out to calculate principal strain values.

## APPENDIX 3

## A3. VARIOUS DESIGNS FOR COMPOSITE TUBULAR JOINTS

The five joint designs which were originally proposed and investigated during the author's M.Sc. project were later modified as a result of discussions with design and construction engineers involved in offshore work. These joints were designed to withstand loadings anticipated in a typical North Sea platform and are now described in this section.

Joint I - This first joint is in essence a steel tube composite with a prestressed concrete casing and is suitable for a jacket structure. The main leg is left entirely free internally and it has simple prestressed bar guides welded onto its outside. The bracing members finish in two simple collars which guide the Macalloy bars, Fig. (A3,1) and Plate 12.

Joint II - This joint is for the same structural members having smaller eccentricity, which has the main leg strengthened with a partial filling of concrete thus saving weight in return for partially blocking the tube. This and the next joint are logical extensions of the practice using concrete-filled composite steel tubes and would employ standard shear connections, Fig. (A3,2).

Joint III - There is a tendency towards larger diameter legs in gravity platforms in order to increase buoyancy. This makes it possible to envisage a partial blockage of the hollow leg without loss of function. The design, shown in

Fig. (A3,3) and Plate 13 is proportionately lighter in weight than the second joint.

Joint IV - This is a different approach to the gravity platform joint where all the steel tubes are stiffened with internal plates and the bracing tubes are finished with curved cylindrical ends to match the main leg, Fig. (A3,4). The composite joint now consists of a sand filled epoxy resin concrete which is prestressed by high strength friction grip bolts to hold the members together.

Joint V - Examination of the previous four joints and discussion with some designers and consultants of offshore practice, led to this joint. The joint has similarities with joint III with additional advantages of external concrete for easy access, a non-structural steel cover to give electrical continuity and resin-bonded filler to allow the concrete to be cast in advance and to accommodate any dimensional inaccuracies in manufacture, Fig. (A3,5).

## REFERENCES

## CHAPTER 1

- 1.1 Roark, R.J. The strength and stiffness of cylindrical shells under concentrated loading, Journal of Applied Mechanics, ASME, p.A-147 (1935)
- 1.2 Schloessow, G.J. and Koaistra, L.F. Stresses in cylindrical shell due to nozzle or pipe connection, TRANS. ASME 67, A-107 (1945)
- 1.3 Toprac, A.A. Stresses at intersection of tubes cross and T-joints, Society of Petroleum Engineers of AIME, SPE 14 12 (May 1966)
- 1.4 Bijlaard, P.P. Stresses from local loadings in cylindrical pressure vessels. TRANS. ASME, 77 (66) (1955)
- 1.5 Toprac, A.A. An investigation of welded steel pipe connections, Welding Research Council Bulletin No. 71 (August 1976)
- 1.6 Beale, L.A. and Toprac, A.A. Analysis of in-plane T, Y and K welded tubular connections, Tech. Rpt. P.550-9 (1967)
- 1.7 Dundrova, V. Stresses at intersection of tubes cross and T-joints, SFRL University of Texas Rpt., P.550-5 (August 1965)

- 1.8 Kuang, J.G , Potvin, A.B. and Leick, R.D. Stress concentration in tubular joints, Offshore Technology Conference 2205. Houston, Texas (1975)
- 1.9 Miller, C.D. and Trammell, J.H. An analytical and experimental study of stiffened tubular joints with multiple branches, Offshore Technology Conference 2101. Houston, Texas (1974)
- 1.10 Donnell, L.H. Stability of thin-walled tubes under torsion, NACA Rpt. No. 479 (1934)
- 1.11 Flügge, W. Statik und dynamic der schalen, Springer, Berlin (1934)
- 1.12 Yuan, S.W. Thin cylindrical shells subjected to concentrated loads, Quarterly of Applied Mathematics, V.4, n.1 (April 1946)
- 1.13 Scordelis, A.C. and Bouwkamp, J.G. Analytical study of tubular Tee-joints, Str. Div, ASCE (1970)
- 1.14 Kurabane, Y , Natarjan, M. and Toprac, A.A. Fatigue Tests of tubular T-joints, University of Texas Rpt. (Nov. 1967)
- 1.15 Natarjan, M. and Toprac. A.A. Research on the fatigue strength of tubular T-joints, University of Texas Rpt (Nov. 1968)
- 1.16 Becker, J.M, Gerberich, W.W. and Bouwkamp, J.G. Fatigue failure of welded tubular joints, Str Div. ST1, ASCE (Jan. 1972)



- 1.17 Eastwood, W. and Wood, A.A. Fatigue strength of welded joints in structural hollow sections, Constructional Steel Work (April 1971)
- 1.18 Hibberal, R.O. and Dover, W.O. Random load fatigue crack growth in T-joints, Offshore Technology Conference 2853. Houston, Texas (1977)
- 1.19 Miner, M.A. Cumulative damage in fatigue, Journal of Applied Mechanics, ASME, vol. 12, p.A-159 (1945)
- 1.20 Martin, T. and McGregor, J. An investigation into the stress distribution and fatigue strength of a welded tubular T-joint, Offshore Technology Conference 2856. Houston, Texas (1977)
- 1.21 American Welding Society, Inc. Structural welding code, AWS D1.1 (Sept. 1972)
- 1.22 Pan, R.B. and Plummer, F.B. A fracture mechanics approach to non-overlapping tubular K-joint fatigue life prediction, Offshore Technology Conference 2645. Houston, Texas (1976)
- 1.23 Chapman, J.A, Clark, A. and Kirkwood, P.R. Steels for North Sea structures, Paper 6, Welding Research Council Bulletin 193 (1974)
- 1.24 Mukhopudhyay, A, Itah, Y. and Bouwkamp, J.G. Fatigue behaviour of tubular joints in offshore structures, Offshore Technology Conference 2207. Houston, Texas (1975)

- 1.25 Hansen, F.J. Utilization for structures in and under the seas, Symposium on Concrete Sea Structures, FIP, Tbibisi, Russia (Sept. 1972)
- 1.26 Bury, M. and Domone, P.L. The role of research in the design of concrete offshore structures, Offshore Technology Conference 1949. Houston, Texas (1974)
- 1.27 Gerwick, B.C. Design and construction of prestressed concrete vessels, Offshore Technology Conference 1886. Houston, Texas (1973)
- 1.28 Browne, R.O. and Domone, P.L. The long-term performance of concrete in marine environment, paper 5, Offshore Structure Conference, ICE (7-8 Oct. 1974)
- 1.29 Rivertz, J.A. The future of concrete structure in offshore technology, Offshore Structure Conference, ICE (1978)

## CHAPTER 2

- 2.1 Greste, O. and Clough, R.W. Finite element analysis of tubular joints, University of California, Berkeley, Rpt. No. 67-7 (April 1967)
- 2.2 Greste, O. A computer program for the analysis of tubular K-joints, University of California, Berkeley, Rpt. No. 69-19 (1969)
- 2.3 Greste, O. Finite element analysis of tubular K-joints, University of California, Berkeley, Rpt. 70-11 (June 1970)
- 2.4 Bouwkamp, J.G. Tubular joints under static and alternating loads, University of California, Berkeley, Rpt. No. 66-15 (June 1966)
- 2.5 Brink, F.I.A. and Van der Krogt, A.H. Stress analysis of a tubular cross-joint without internal stiffening for offshore structures, Welding in Offshore Construction, Welding Institute Conference, Newcastle (Feb. 1974)
- 2.6 Visser, W. On the structural design of tubular joints, Offshore Technology Conference 2117. Houston, Texas (1974)

- 2.7 Kuang, J.G, Patvin, A.B. and Leick, R.D. Stress concentration in tubular joints, Offshore Technology Conference 2205. Houston, Texas (1975)
- 2.8 Liaw, C.Y, Litton, R.W. and Reimer, R.B. Improved finite elements for analysis of welded tubular joints, Offshore Technology Conference 2642. Houston, Texas (1976)
- 2.9 Yasida, K, Inui, T. and Iida, K. Behaviour analysis and crack initiation prediction of tubular T-connections, Offshore Technology Conference 2854. Houston, Texas (1977)
- 2.10 Analysis of T-joint by Semi-Loof shell, rpt. circulated by W.S. Atkins
- 2.11 Wilson, E.L, Bathe, K.J. and Doherty, W.P. Direct solution of large systems of linear equations, Computer and Structures, vol. 4 (1974)
- 2.12 Ahmad, S, Irons, B.M. and Zienkiewicz, O.C. Analysis of thick and thin shell structures by curved finite elements, Int. J. Num. Meth. Engng., vol. 2 (1970)
- 2.13 Loof, L.W. The economical computation of stiffness of large structural elements, Int. Symp. on Use of Comp. in Struct. Eng., University of Newcastle upon Tyne (1966)
- 2.14 Irons, B.M. The Semi-Loof shell element, Finite elements for thin shells and curved members, Edited by Ashwell, D.G. and Gallagher, R.H. John Wiley (1976)

## CHAPTER 3

- 3.1 Loof, H.W. The economical computation of stiffness of large structural elements, Int. Symp. on Use of Comp. in Struct. Eng. University of Newcastle upon Tyne (1966)
- 3.2 Ahmad, S, Irons, B.M. and Zienkiewicz, O.C. Analysis of thick and thin shell structures by curved elements, Int. J. Num. Meth. Engng, vol. 2 (1970)
- 3.3 Stricklin, J.A, Haisler, W.E, Tisdal, P.E. and Gunderson, R. A rapidly converging triangular plate element, AIAAJ, 7, 180 (1969)
- 3.4 Zienkiewicz, O.C, Taylor, R.L. and Too, T. Reduced integration technique in general analysis of plates and shells, Int. J. Num. Meth. Engng, vol. 3 (1971)
- 3.5 Baldwin, J.T, Razzaque, A. and Irons, B.M. Shape function subroutine for an isoparametric thin plate element, Int. J. Num. Meth. Engng. vol. 7 (1973)
- 3.6 Razzaque, A. Finite element analysis of plates and shells, Ph.D. thesis, University of Wales, Swansea (1972)
- 3.7 Irons, B.M. The Semi-Loof shell element, Rpt. CIR/124/70, University of Wales, Swansea (1973)

- 3.8 Irons, B.M. The Semi-Loof shell elements, Finite elements for thin shells and curved members. Edited by Ashwell, D.G. and Gallagher, R.H. John Wiley (1976)
- 3.9 Lyons, L.P.R. A general finite element system with special reference to the analysis of cellular structure, Ph.D. Thesis, Imperial College (1977)
- 3.10 Zienkiewicz, O.C. The finite element method in engineering science, MacGraw Hill (1971)
- 3.11 Faddeva, V.N. Computational methods of linear algebra. Translated from Russian by Benster, C.D. New York Dover (1959)
- 3.12 Helen, T.K. Effective quadrature rules for quadratic solid isoparametric finite elements, Int. J. Num. Meth. Engng, vol. 4 (1972)
- 3.13 Irons, B.M. Quadrature rules for brick based finite elements, Int. J. Num. Meth. Engng., vol. 3 (1971)
- 3.14 Irons, B.M. and Helen, T.K. On reduced integration in solid isoparametric elements when used in shells with membrane modes. Int. J. Num. Meth. Engng., vol.10 (1976)
- 3.15 Wilson, E.L, Taylor, R.L, Doherty, W.P. and Ghaboussi, J. Incompatible displacement models numerical and computer methods in structure mechanics. Academic Press (1973)
- 3.16 Cook, R.D. Concepts and application of finite element analysis, John Wiley & Sons, Inc. (1974)

- 3.17 Analysis of shell structure using general curved shell,  
Atkins Research and AAD Rpt. (1974)
- 3.18 Roark, R.J. Formulation for stress and strain,  
MacGraw Hill (1954)
- 3.19 Sisodiya, R.G, Cheung, Y.K. and Ghabi, A. New finite  
elements with application to box girder bridges,  
Civil Engineering Proceedings, part 2 (1972)
- 3.20 Hinton, E. Flexure of composite laminates using the  
thick finite strip method, Computers and Structures,  
vol. 7, Pergamon Press (1977)
- 3.21 Reissner, E. The effect of transverse shear deformation  
on the bending of elastic plates, J. Appli. Mech. ASME,  
vol. 12 (1945)
- 3.22 Reissner, E. On bending of elastic plates, Quarterly  
of Applied Maths, vol. 5 (1947)
- 3.23 Salerno, V.L. and Goldberg, M.A. Effect of shear  
deformation on the bending of rectangular plates,  
J. Appli. Mech. ASME, vol. 27 (1960)
- 3.24 Discussion by Donnell, L.H. and Reissner, E. J. Appli.  
Mech. ASME, vol. 68 (1946)
- 3.25 Gogoi, S. Integration phenomena in composite beams  
and plates. Ph.D. Thesis, Imperial College (1964)

## CHAPTER 4

- 4.1 Billington, C.J. The integrity of jacket to pile connections, Oceanology International (1978)
- 4.2 Billington, C.J. and Lewis, G.H.G. The strength of large diameter grouted connections, Offshore Technology Conference 3083, Houston, Texas (1978)



## CHAPTER 5

- 5.1 Keller, R.H. and Smith, C.J. A new method for hyperbaric welded pipe line Tie-ins, Offshore Technology Conference 3350, Houston, Texas (1978)
- 5.2 Matsuishi, M, Nishimaki, K, Takeshita, H, Iwata, S. and Suhara, T. On the strength of new composite steel concrete material for offshore structure, Offshore Technology Conference 2804, Houston, Texas (1977)
- 5.3 Matsuishi, M, Nishimaki, K, Takeshita, H, Iwata, S. and Suhara, T. On the new composite steel-prestressed concrete structural module for offshore structures, Offshore Technology Conference 3158, Houston, Texas (1978)
- 5.4 Corum, J.M, Bolt, S.E, Greenstreet, W.L. and Gwaltney, R.C. Theoretical and experimental stress analysis of ORNL Thin-shell cylinder-to-cylinder model no. 1, Oak Ridge National Laboratory, Rpt. 4553 (1972)
- 5.5 Greste, O. Finite element analysis of tubular K joints, University of California, Berkeley.  
PB 193 560 (June 1970)

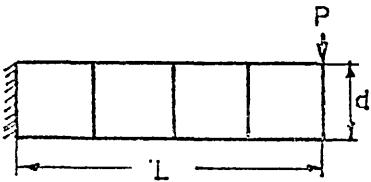
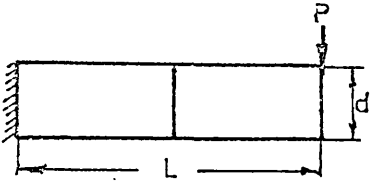
## A P P E N D I C E S

- A1.1 Blodgett, O.W. Design of welded structures  
published by the James F. Lincoln Arc Welding  
Foundation (1967)
- A2.1 Calcate, Lee. R. Introduction to continuum mechanics,  
Princeton, N.J, Van Nostrand (1968)

		V DISPLACEMENT AT i		$\bar{\sigma}_x$ STRESS AT j	
		LOAD A	LOAD B	LOAD A	LOAD B
BEAM THEORY		10.0000	103.000	300.00	4050.00
MESH 1	SL SOLID	10.0076	102.195	300.00	4050.00
	Q 4	6.8100	70.1000	218.20	2945.00
	Q 6	10.0000	101.500	300.00	4050.00
MESH 2	SL SOLID	9.4600	103.100	300.10	4050.70
	Q 4	7.0600	72.300	218.80	2954.00
	Q 6	10.0000	101.300	300.00	4050.00

Table (3-1)

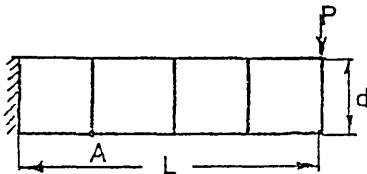
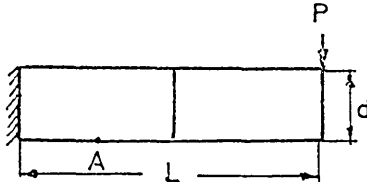
Downward Vertical Displacement at the Free end in Terms of  
 $P/Et$  ( AVERAGE OF DISPLACEMENTS AT TOP AND BOTTOM FOR SOLIDS )

Finite Element Idealization	SPAN L	BEAM THEORY INCLUDING SHEAR DEFORMATION #1	Finite Element Analysis							
			VALUE				% OF BEAM THEORY			
			PQC 3	QLC 3	KHX 20 #2	KHL 20 #3	PQC 3	QLC 3	KHX 20	KHL 20
	2d	36.8	35.382	35.382	40.794	36.860	96.140	96.140	110.850	100.160
	4d	265.6	259.764	259.764	266.807	264.540	97.800	97.800	100.450	99.600
	8d	2067.2	2031.530	2031.520	2065.930	2064.200	98.270	98.270	99.930	99.850
	2d	36.8	36.380	33.765	38.750	36.530	98.850	91.750	105.290	99.260
	4d	265.6	265.160	247.529	265.876	264.198	99.840	93.190	100.100	99.470
	8d	2067.2	2066.800	1935.050	2065.270	2055.940	99.980	93.600	99.960	99.450

- \*1 Thick Beam Theory  $W = W_b + W_s = PL^3/3EI + 5/5(PL/AG)$   
 \*2 20 Node Solid Element  
 \*3 Semi Loof Solid

Table (3-2)

## Stresses at Point A in Terms of $(P/td)$

Finite Element Idealization	SPAN  L	BEAM THEORY INCLUDING SHEAR DEFORMATION *1	Finite Element Analysis							
			VALUE				% OF BEAM THEORY			
			PQC3	QLC3	KHX 20 *2	KHL 20 *3	PQC3	QLC3	KHX 20	KHL 20
	2d	9.00	8.999	9.000	9.000	8.969	99.990	100.000	100.000	99.650
	4d	18.00	18.000	18.000	18.000	17.965	100.000	100.000	100.000	99.800
	8d	36.00	36.000	36.000	36.000	36.135	100.000	100.000	100.000	100.370
	2d	9.00	9.025	9.000	9.000	9.000	100.270	100.000	100.000	100.000
	4d	18.00	18.021	18.000	18.000	18.000	100.110	100.000	100.000	100.000
	8d	36.00	35.990	35.000	36.000	36.000	99.970	100.000	100.000	100.000

- \* 1 THICK BEAM THEORY
- \* 2 20 NODE SOLID ELEMENT
- \* 3 SEMI LOOF SOLID ELEMENT

Table (3-3)

		Do TUBE	t TUBE	Di SLEEVE	t SLEEVE	t CONCRETE
Phase 1	GROUP 1,3	47.625	2.160	60.325	1.650	12.700
	GROUP 2,4	47.625	2.160	73.025	1.650	12.700
Phase 2		47.625	2.160	60.325	1.650	6.350
Phase 3		219.280	8.135	258.000	8.230	19.360

Do = Outside Diameter

Di = Inside Diameter

Table(4-1) - Geometrical Properties of  
Small-Scale and Large-Scale Models (in mm )

API 5L Grade B	Dimension of Test Piece			YIELD LOAD	MAX LOAD	YIELD STRESS	TENSILE STRENGTH	Elongation % on
	WIDTH OR DIAM	THICKNESS	AREA					
	mm	mm	mm <sup>2</sup>	KN	KN	N/mm <sup>2</sup>	N/mm <sup>2</sup>	
SLEEVE	38.70	7.10	275.00	132	180	481	655	38
TUBE	38.60	8.15	315.00	122	164	387	521	38
Chemical Composition %								
	C	Si	Mn	P	S	Cr	Mo	Carbon Equivalent
SLEEVE	.20	.30	.52	.008	.017			C.E = .30
TUBE	.19	.30	.52	.009	.018			C.E = .29

Table (4-2)- Physical and Chemical Properties  
of Large-Scale Model

Small-Scale		D (mm)	t (mm)	L (mm)	A (mm <sup>2</sup> )	F (N)	f <sub>b</sub> <sup>2</sup> (N/mm <sup>2</sup> )	L/D <sub>i</sub>	K <sup>2</sup> (N/mm <sup>2</sup> )
Group 1	1	47.625	6.35	120.650	9025.73	17437.0	1.930	2.00	5943.80
	2	47.625	6.35	152.400	11400.92	21920.8	1.923	2.50	5943.80
	3	47.625	6.35	180.975	13538.60	20924.4	1.545	3.00	5943.80
Group 2	1	47.625	12.70	146.050	10925.88	23913.6	2.189	2.00	7046.68
	2	47.625	12.70	182.563	13657.40	32881.2	2.407	2.50	7046.68
	3	47.625	12.70	219.075	16388.82	38361.4	2.340	3.00	7046.68
Group 3	1	47.625	6.35	120.650	9025.73	62275.0	6.900	2.00	5943.80
	2	47.625	6.35	152.400	11400.92	86188.6	7.560	2.50	5943.80
	3	47.625	6.35	180.975	13538.60	108607.6	8.022	3.00	5943.80
Group 4	1	47.625	12.70	146.050	10925.88	82701.2	7.569	2.00	7046.68
	2	47.625	12.70	182.563	13657.40	85690.4	6.274	2.50	7046.68
	3	47.625	12.70	219.075	16388.82	106614.8	6.505	3.00	7046.68

D = Outside Diameter of Tube  
 D<sub>i</sub> = Inside Diameter of Sleeve  
 t = Thickness of the Grout  
 L = Length of the Sleeve  
 A = Area of Tube and Grout Interface ( $\pi D \times L / 2$ )  
 F = Ultimate Load  
 f<sub>b</sub> = Equivalent Ultimate Bond Strength (F/A)  
 K = Radial Stiffness  
 $[S_{grout} + (1/S_{tube} + 1/S_{sleeve})^{-1}]$

Table(4-3)-Geometrical and Physical Properties of Small-Scale Models



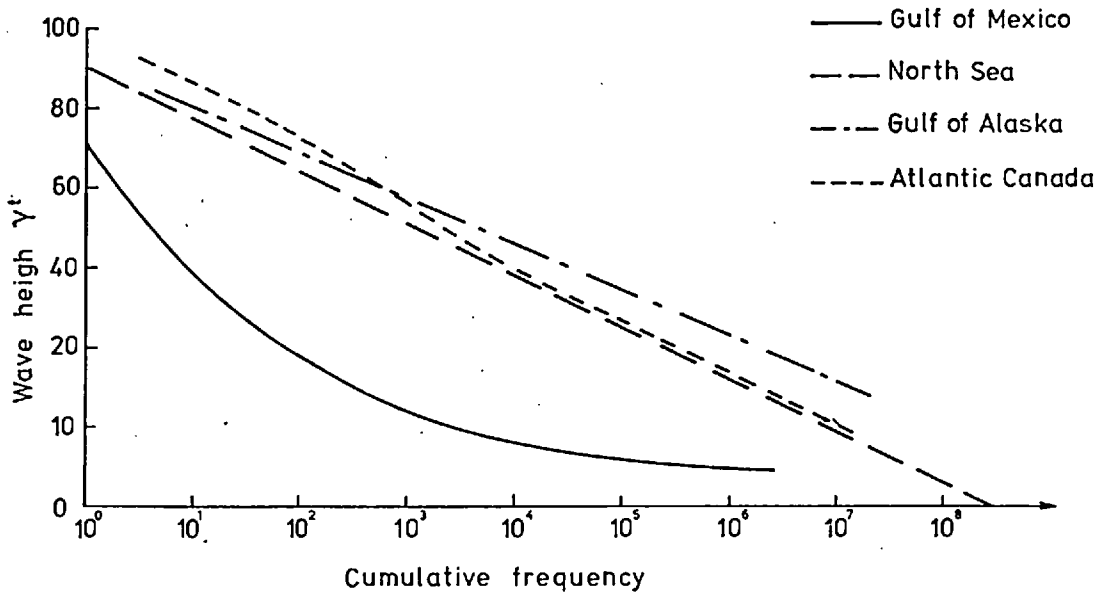


Fig (1,1) Wave height versus frequency for different regions

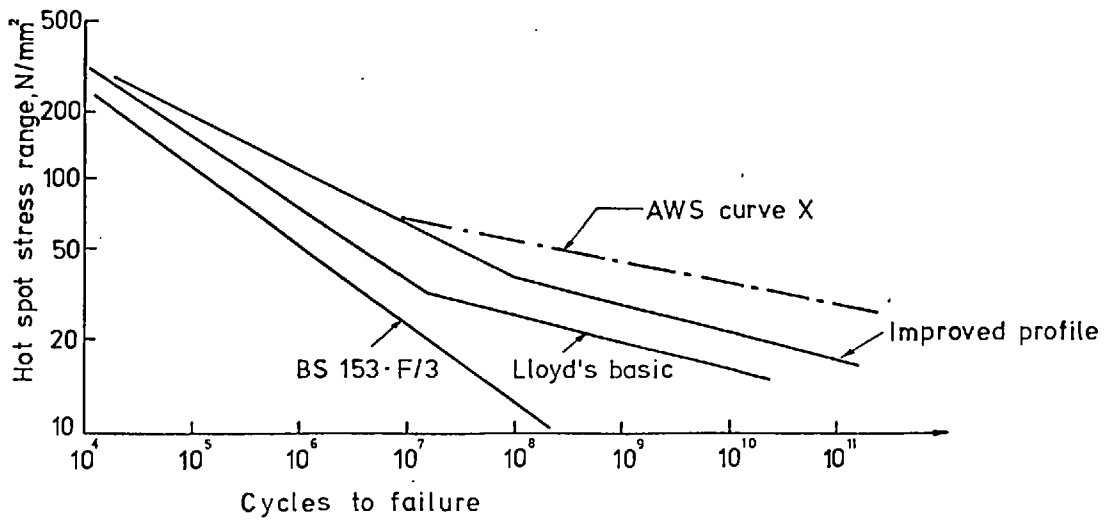
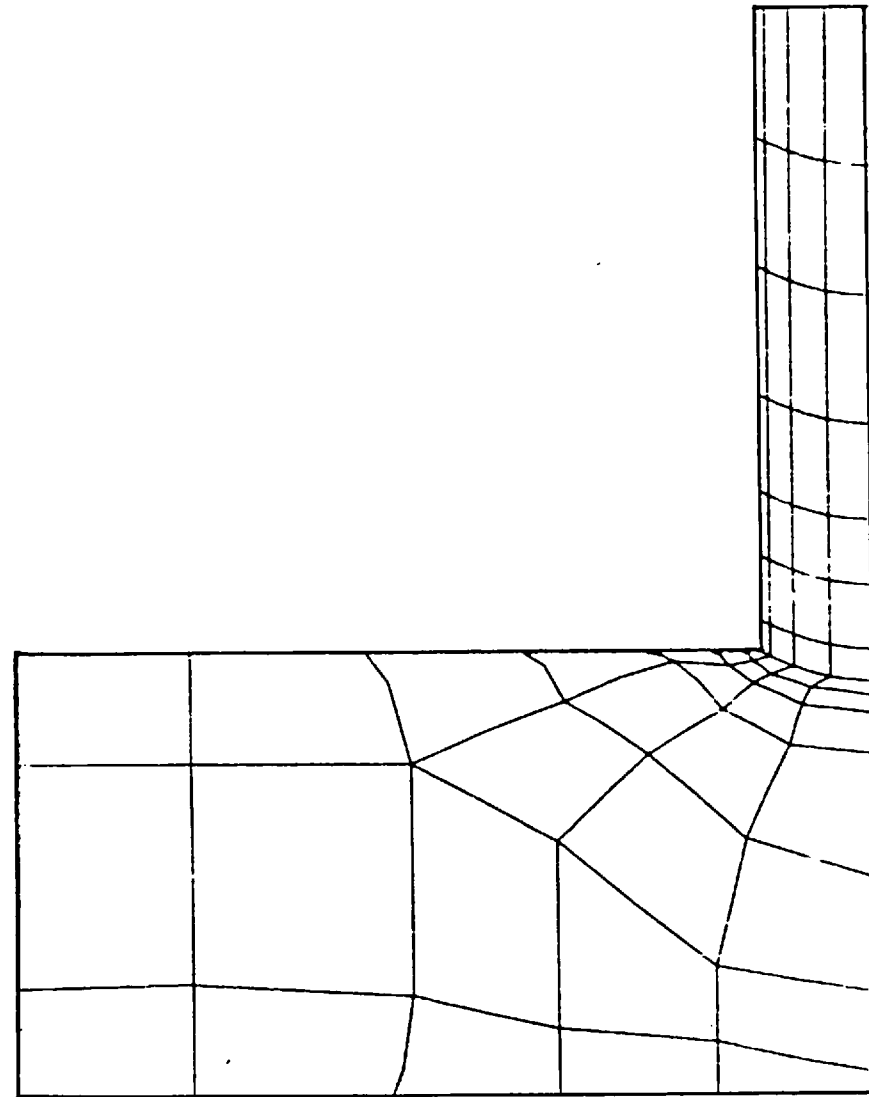
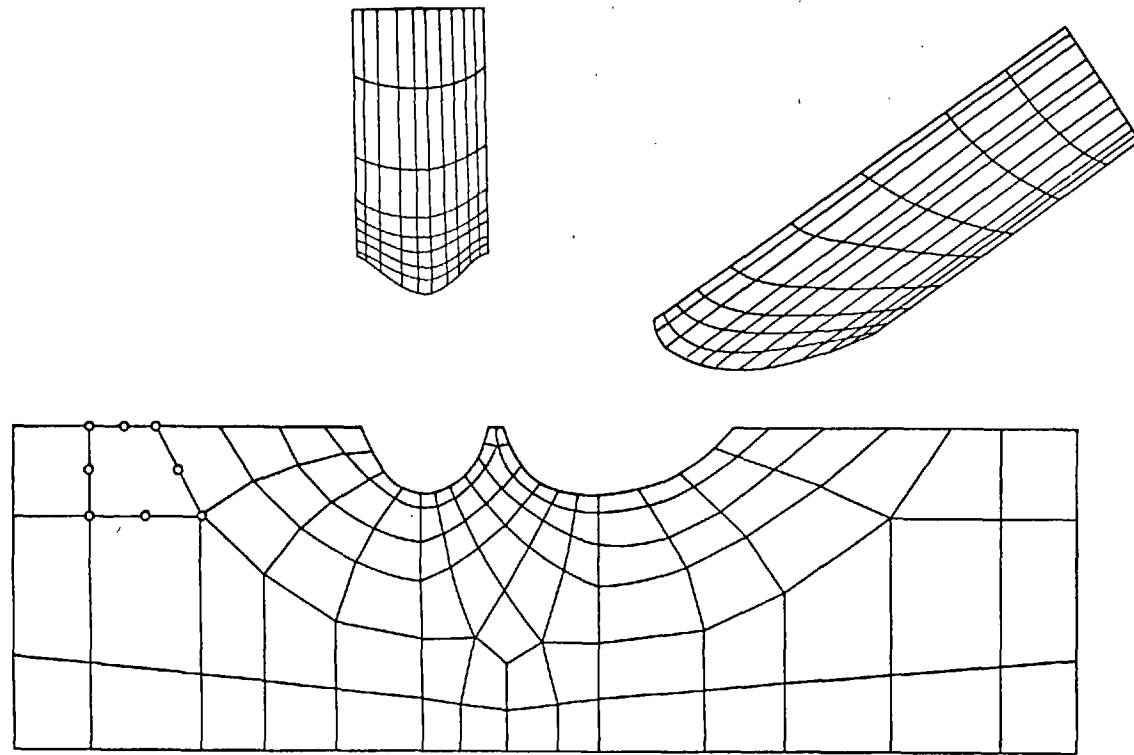


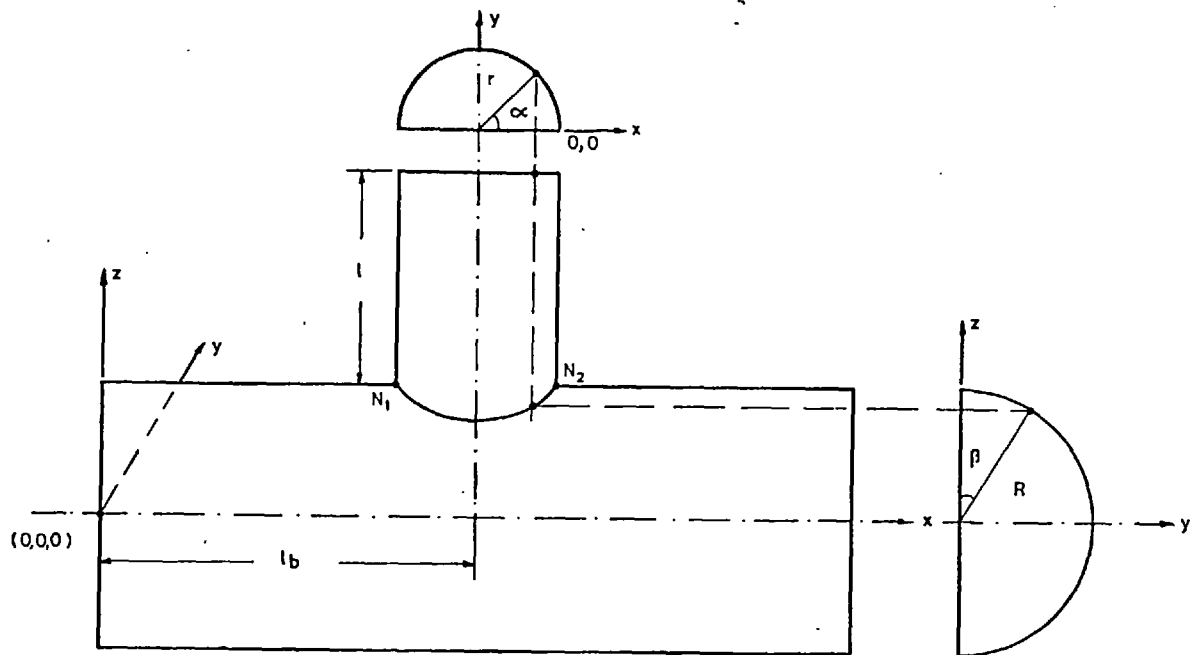
Fig (1,2) Stress range versus cycles at failure load



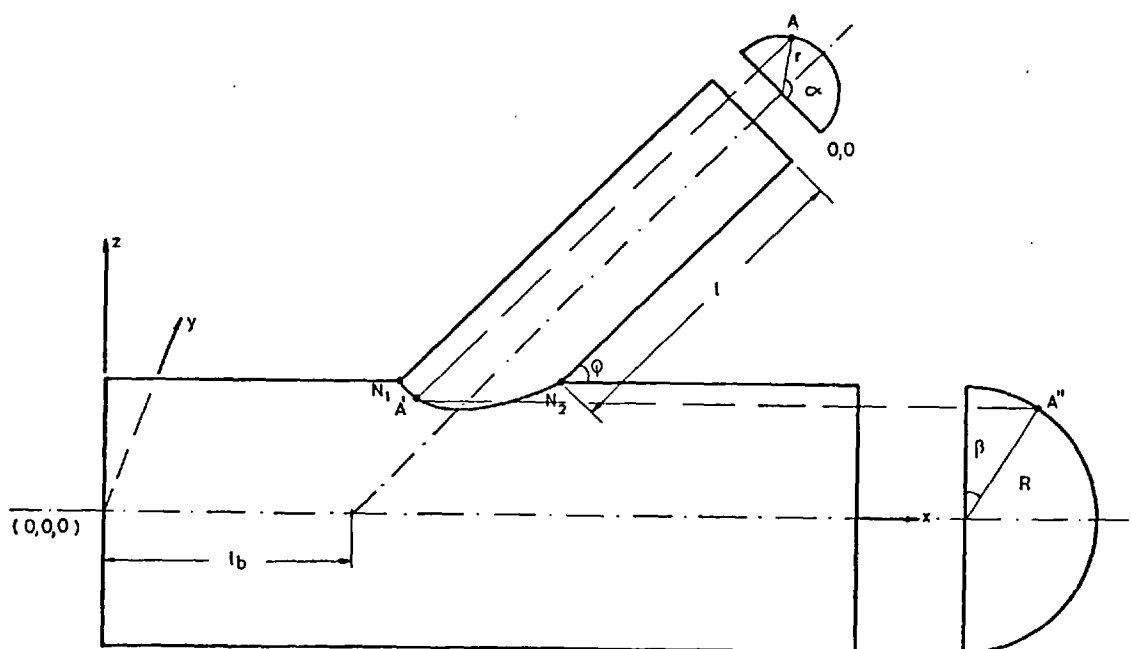
Fig(2,1) Finite Element Model  
of Tee Joint



Fig(2,2) Finite element model of K joint



Fig(2,3) Tee joint



Fig(2,4) y-Joint

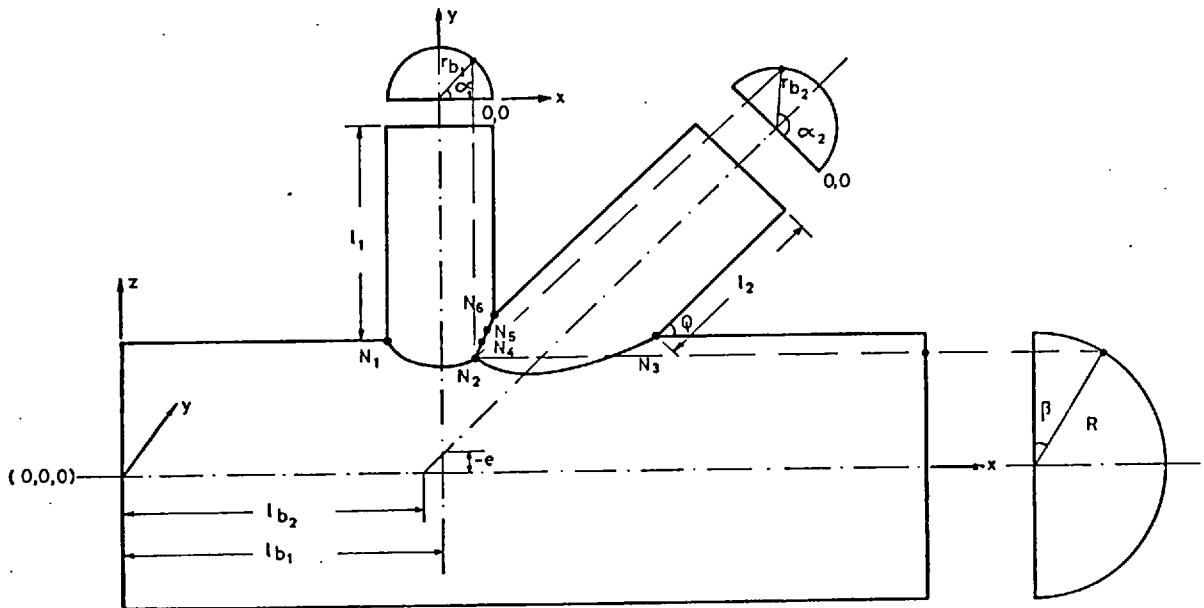
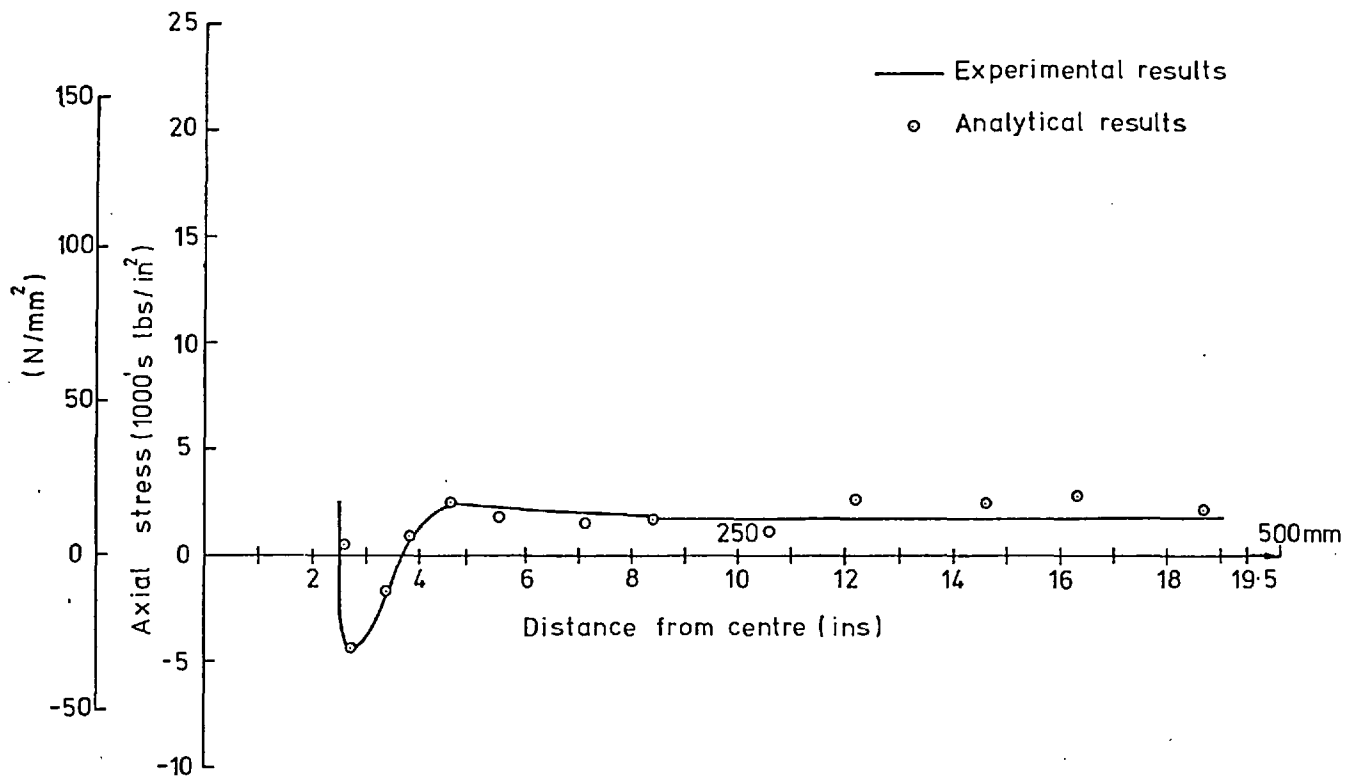
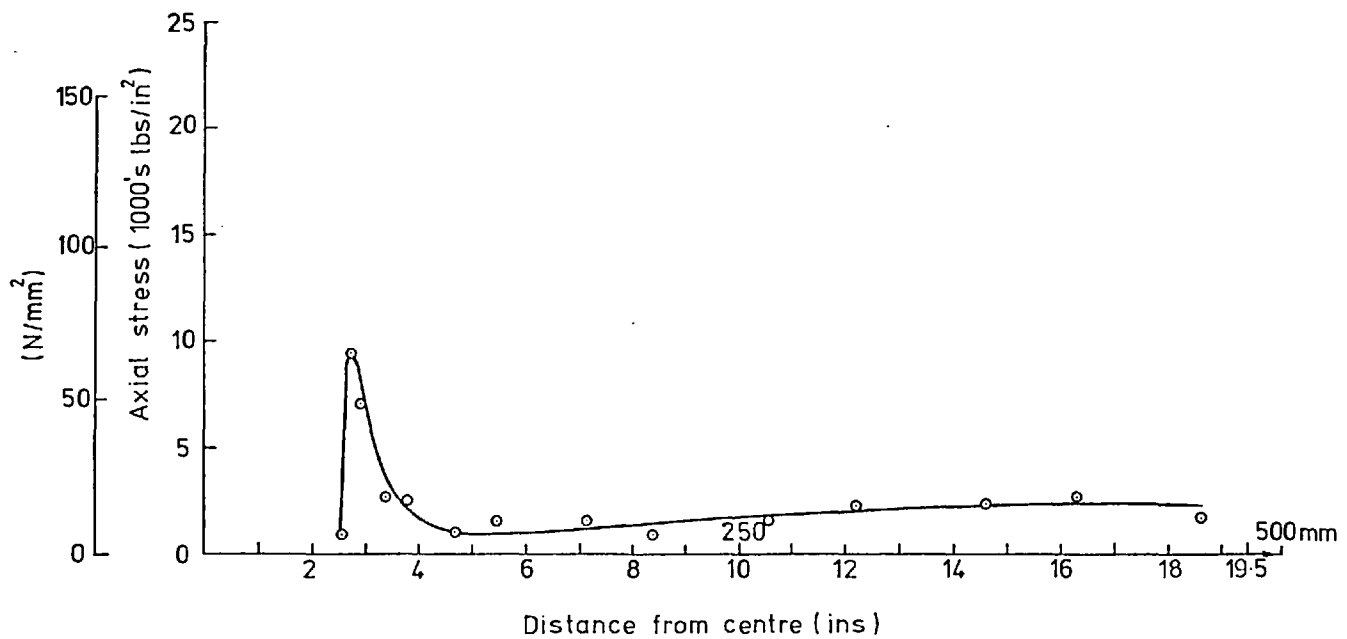


Fig (2,5) K - Joint ( Two branches joint with negative eccentricity)

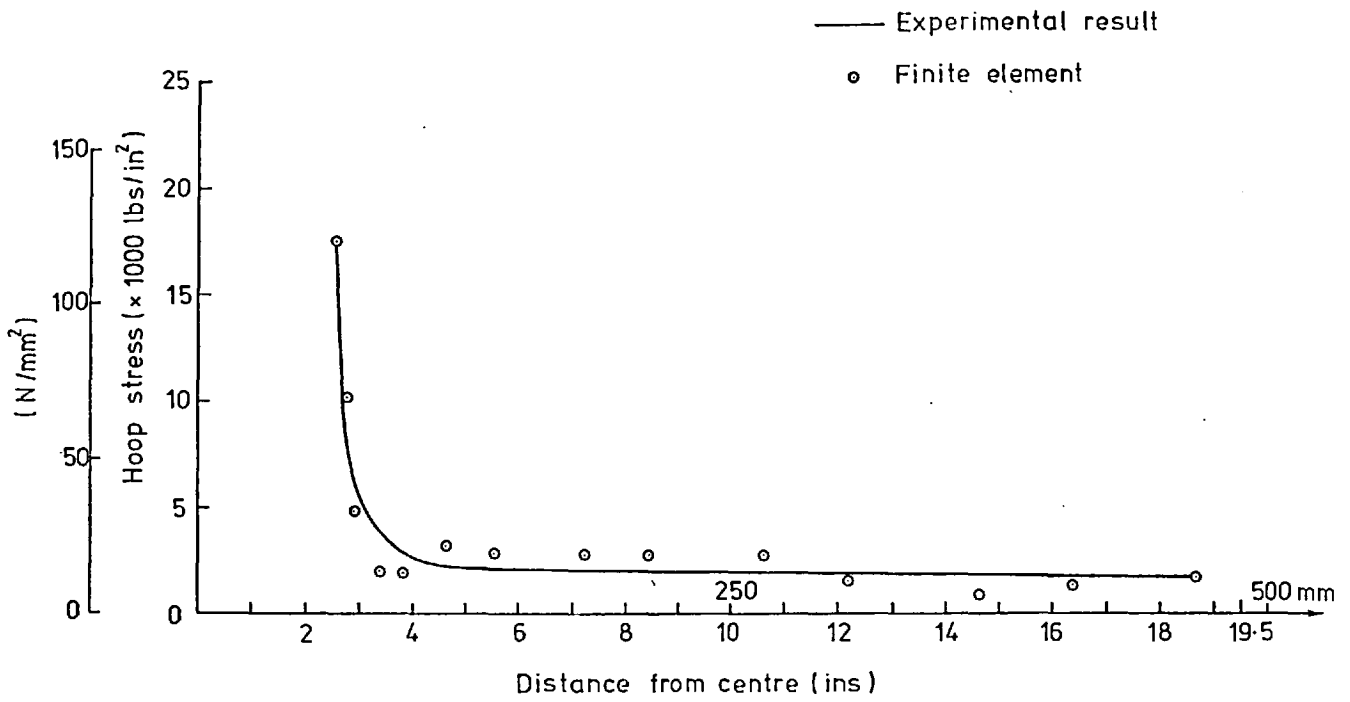


OUT-SIDE SURFACE CYLINDER 0° LINE

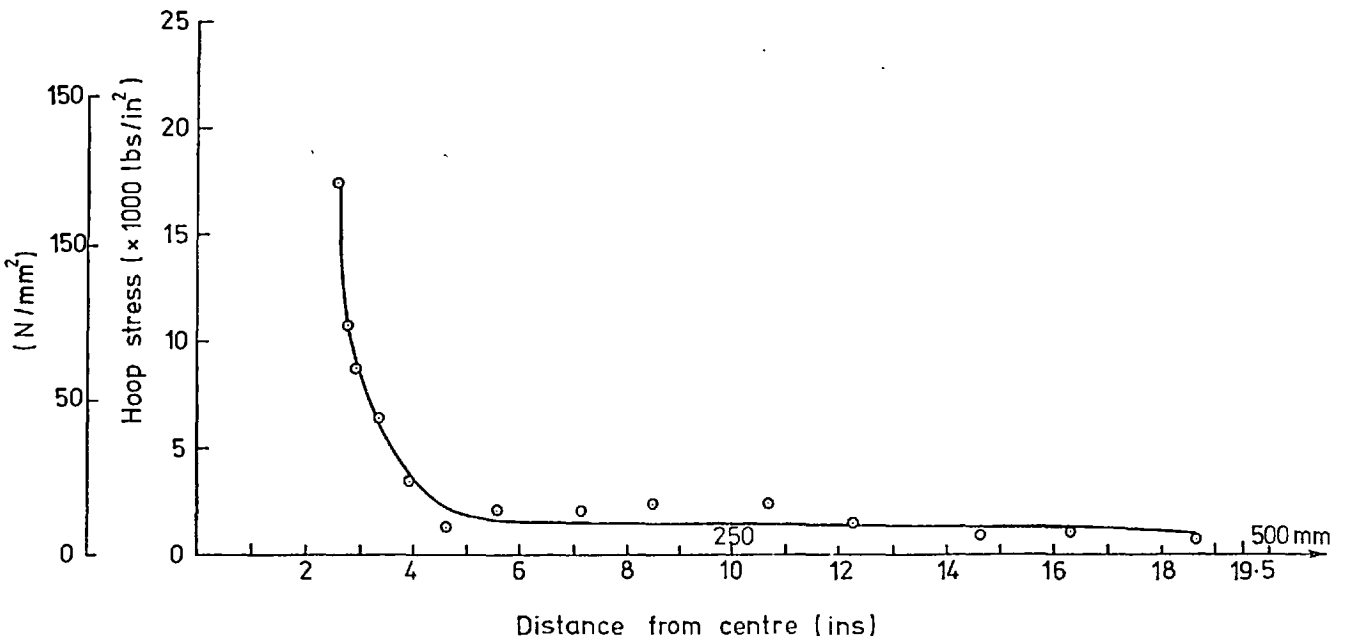


IN-SIDE SURFACE CYLINDER 0° LINE

Fig(2,6) Axial stresses

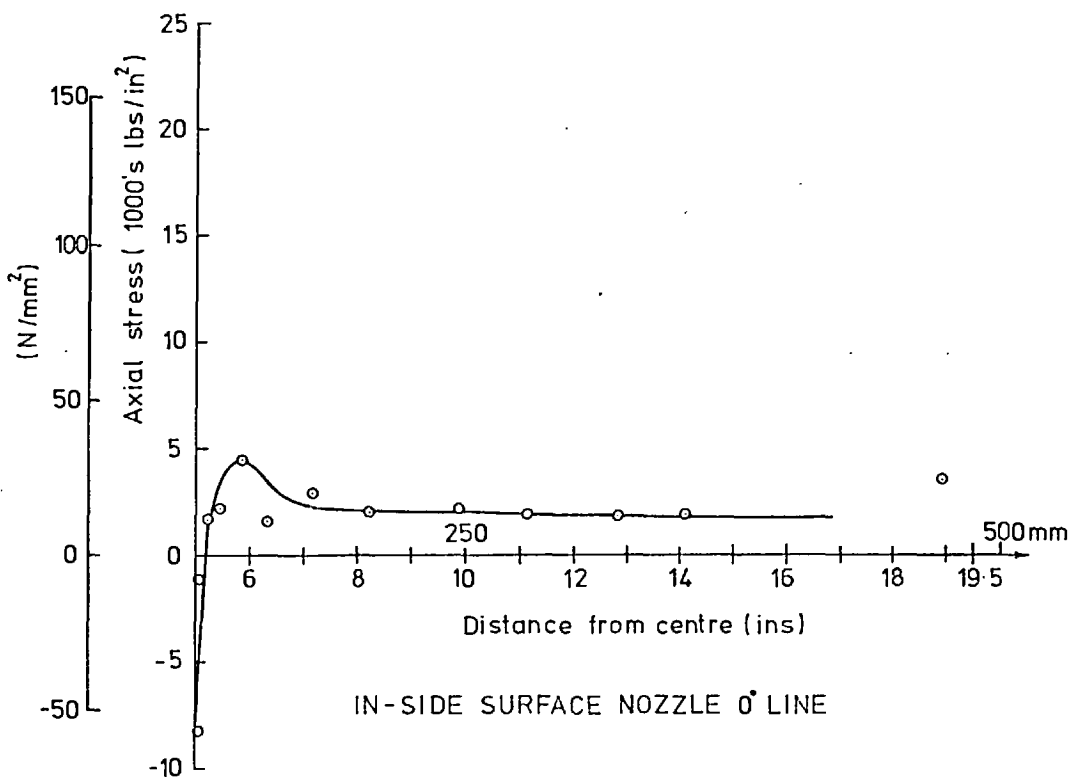
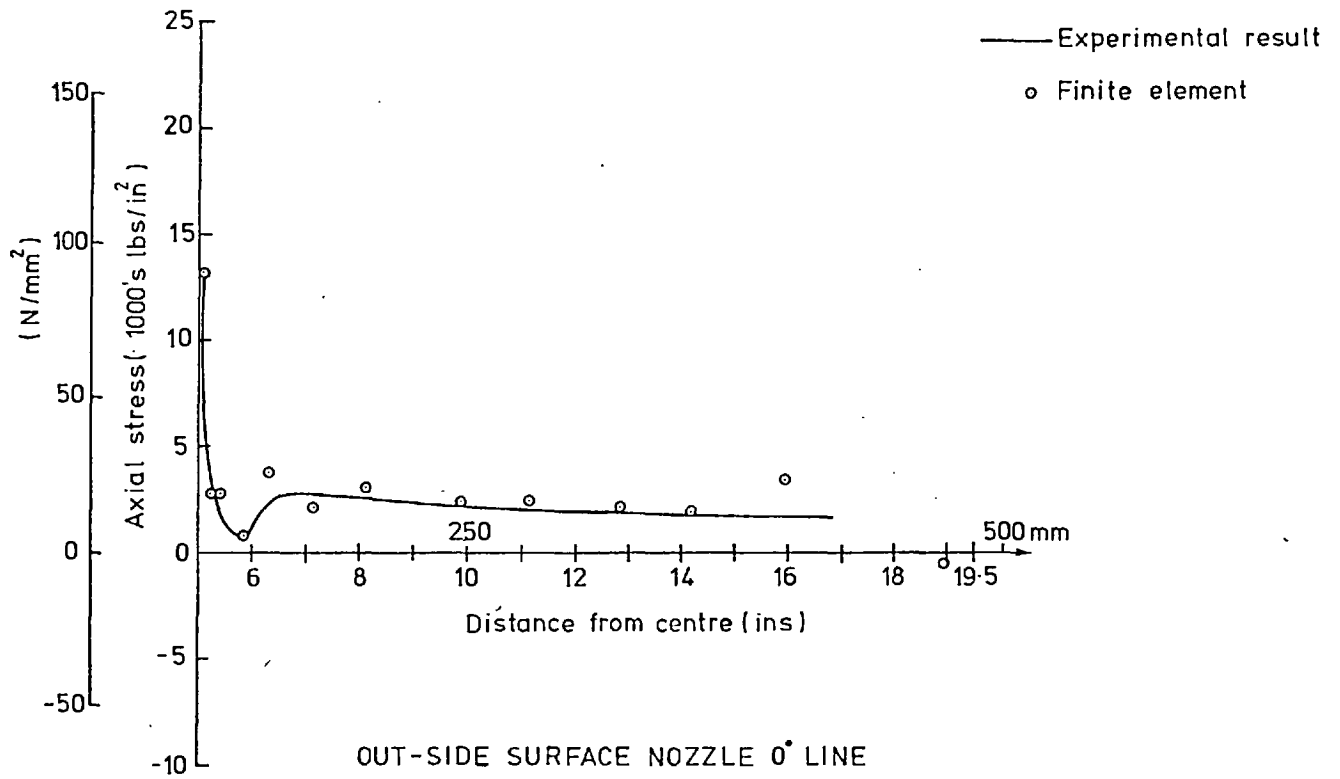


OUT-SIDE SURFACE CYLINDER 0° LINE



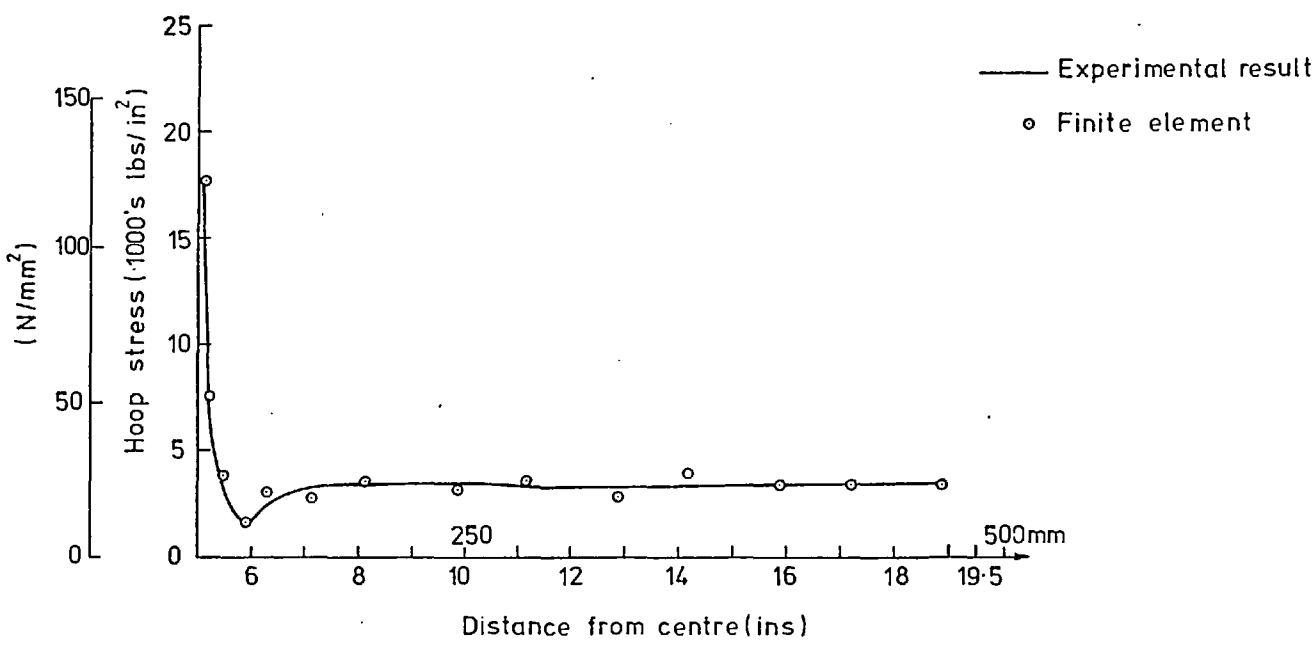
IN-SIDE SURFACE CYLINDER 0° LINE

Fig(2,7) Hoop stresses

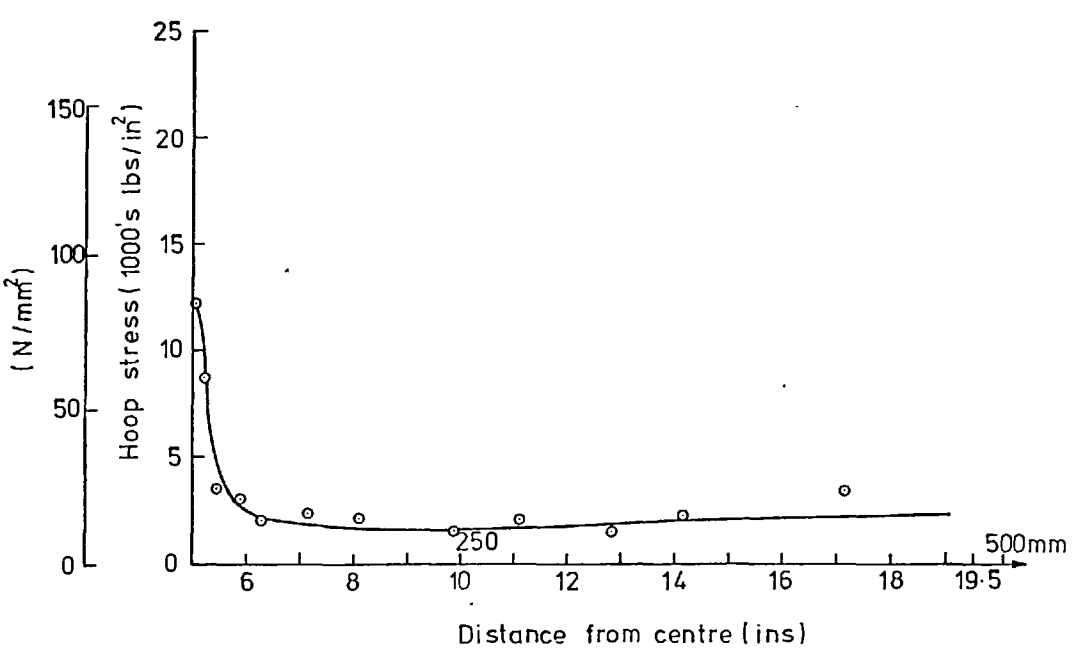


Fig(2,8) Axial stresses



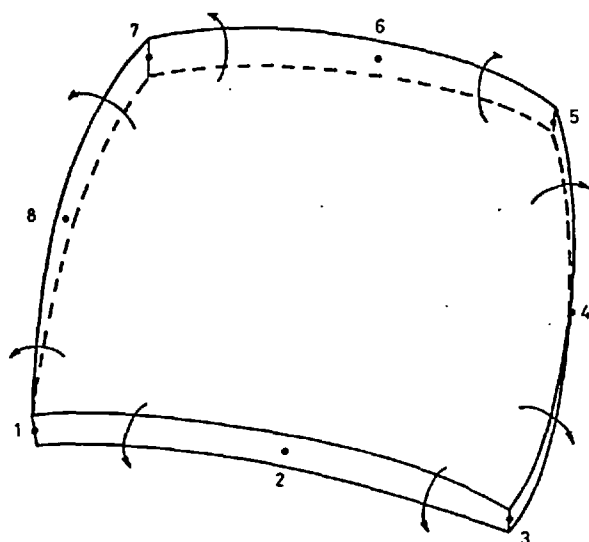


OUT-SIDE SURFACE NOZZLE 0° LINE



IN-SIDE SURFACE NOZZLE 0° LINE

Fig (2,9) Hoop stresses



Description Curved thin shell quadrilateral element

Number of nodes 8  
(vertices and mid sides)

Degrees of freedom

(a) At corner nodes:  $x, y, z$   
(b) At midsides:  $x, y, z, \theta_x, \theta_y$   
Total d.o.f = 32

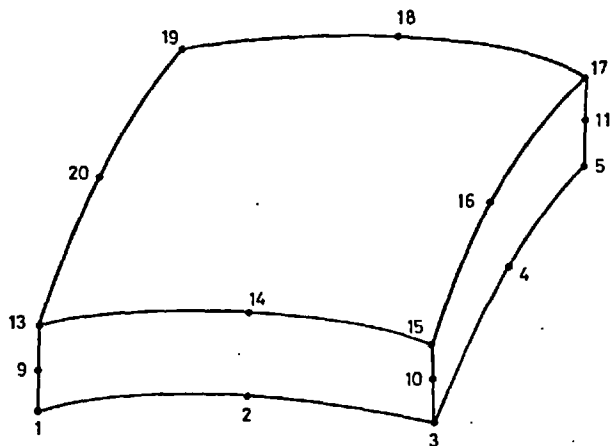
Geometric properties

$t_1, t_2, t_3, t_4, t_5, t_6, t_7, t_8$   
(thickness at the nodes)

Material properties

$E$  - Young's modulus  
 $\nu$  - Poisson's ratio

Fig(3,1) Semi loof shell nodal configuration

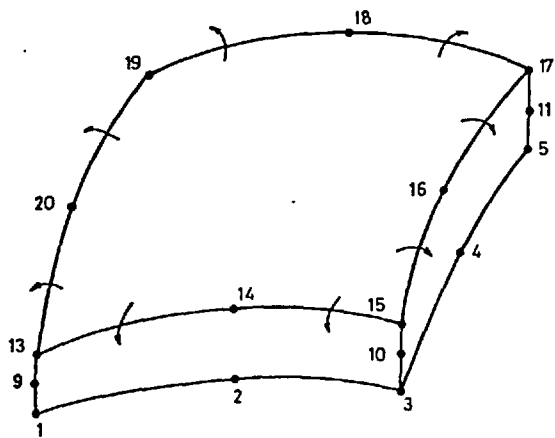


### Iso-parametric solid

Description Curved thick brick quadrilateral element

Number of nodes 20  
(vertices and midsides)

Degrees of freedom  
At corner and midside nodes:  $x, y, z$   
Total d.o.f = 60



### Semi-loof solid

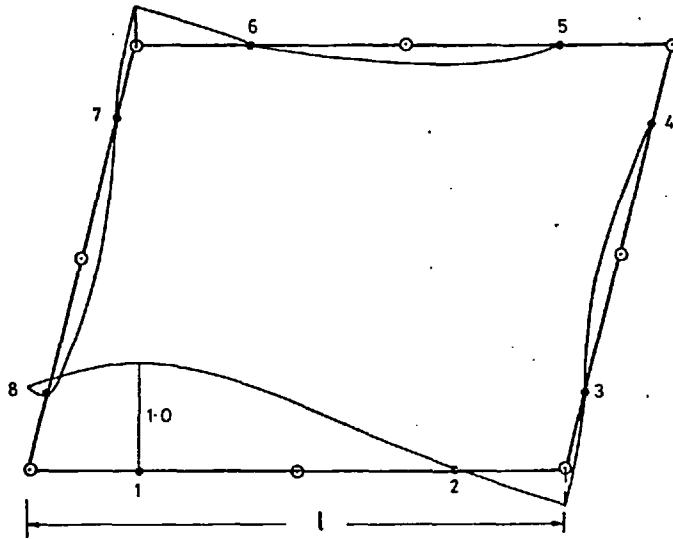
Description Curved thick brick quadrilateral element

Number of nodes 20  
(vertices and midside)

Degrees of freedom  
a) At corner and midside nodes:  $x, y, z$   
b) At top surface midside nodes:  $x, y, z, \theta_x, \theta_y$   
Total d.o.f = 68

Material properties  
E Youngs modulus  
 $\nu$  Poissons ratio

Fig(3,2) 20 Node solid and semi loof solid elements. Nodal configuration



- Loof points  $\frac{1}{2\sqrt{3}} l$  from centre
- Corner and midside nodes

Fig (3,3) Shape function L for the first loof points

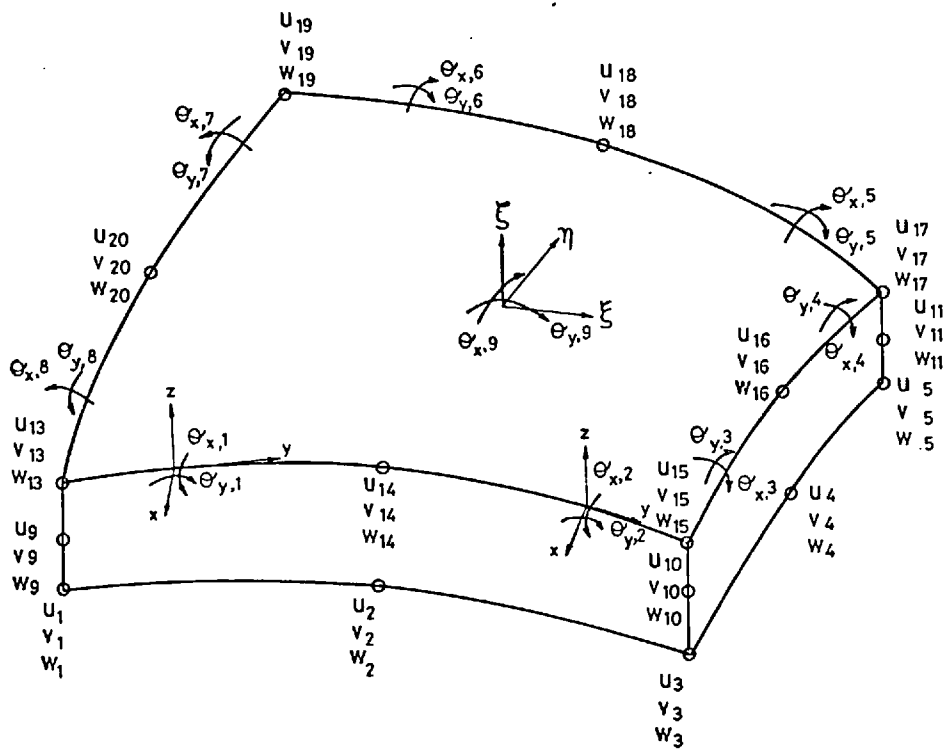
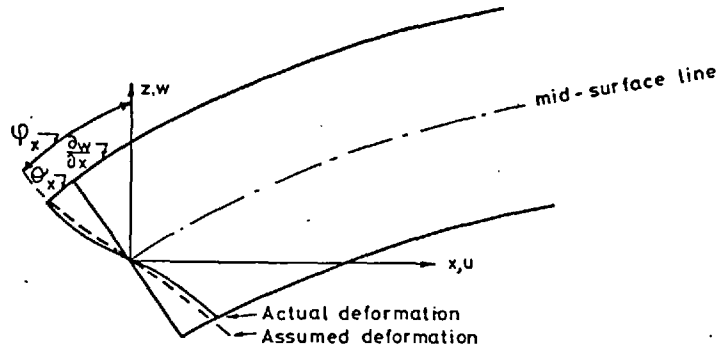
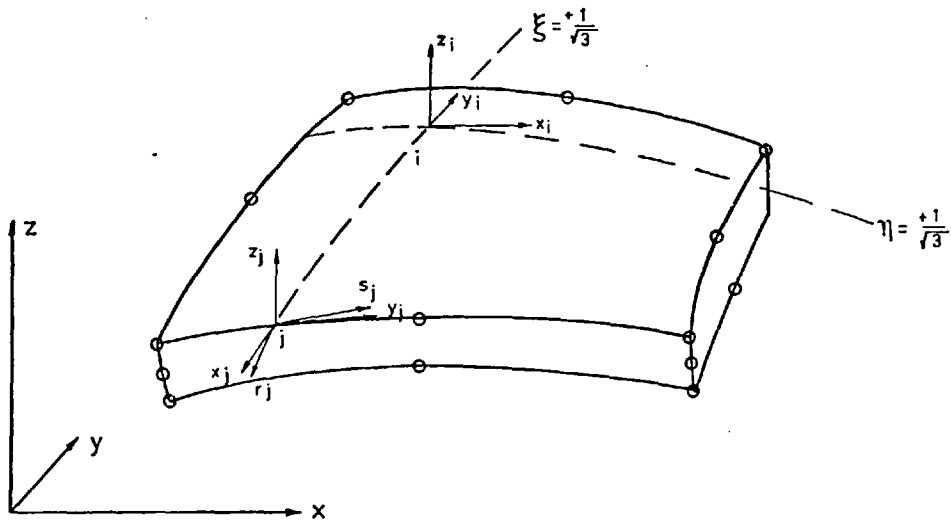


Fig (3,4) Unconstrained variables of semi loof solid

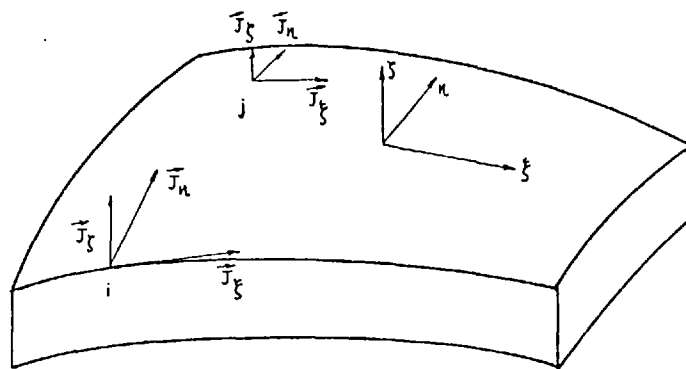


Fig(3,5) Actual deformation for thick shells



- $x, y, z$  are global cartesian system
- $z_j, y_j, z_j$  are loof local coordinate system
- $x_i, y_i, z_i$  are gauss local coordinate system

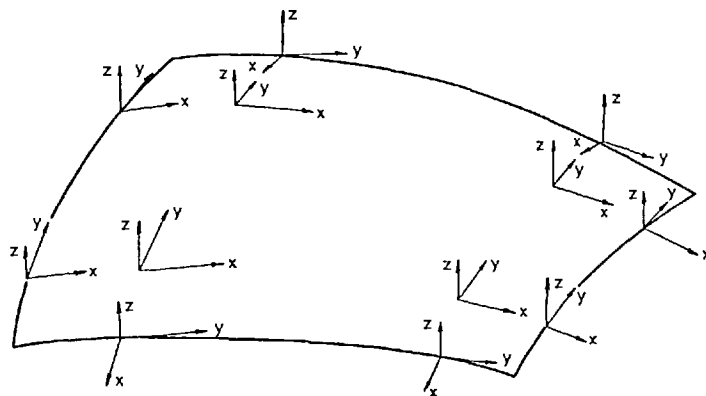
Fig (3,6) Semi loof solid co-ordinate system



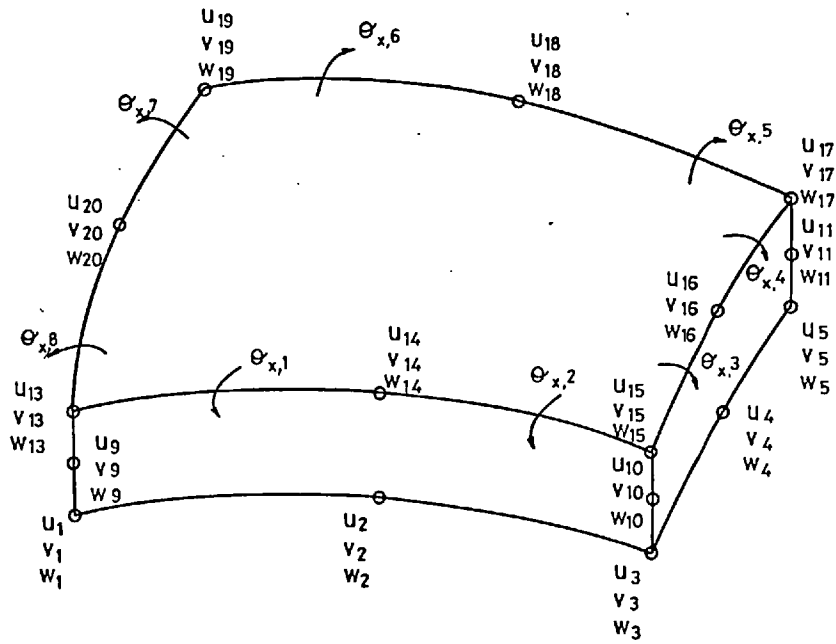
$\xi \eta \zeta$  are base vectors

$\bar{J}_\xi \bar{J}_\eta \bar{J}_\zeta$  are co-variant base vectors

Fig(3,7) Non cartesian system

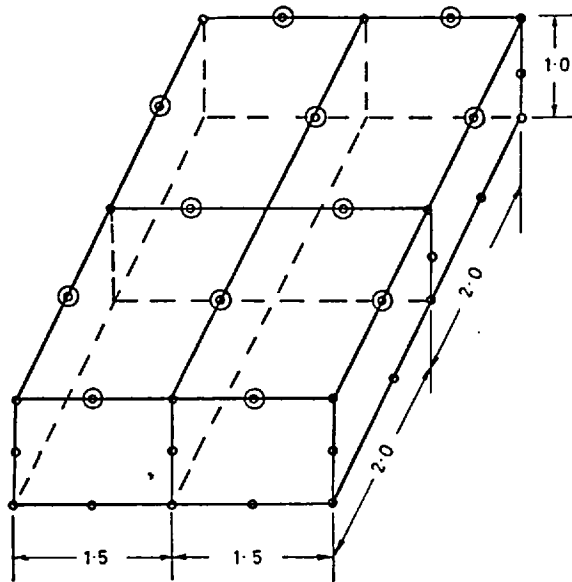


Fig(3,8) Loof nodes and gauss points  
local co-ordinate vectors



Fig(3,9) Constrained variables of semi loof solid element





- mid side and corner nodes 3 d.o.f
- ⊙ mid side nodes 5 d.o.f

Assumed displacement field :

$$u = 1 + 2x + 3y$$

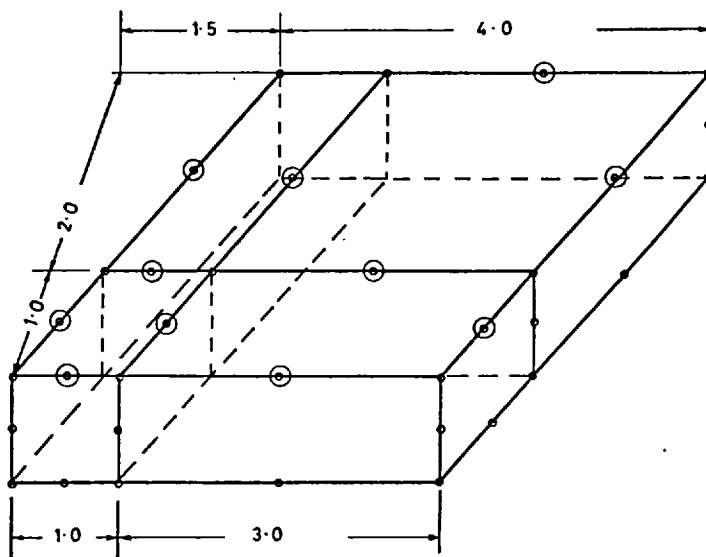
$$v = 2 + 3x + 4y$$

Constant strain state :  $\epsilon_x = 2$ ,  $\epsilon_y = 4$ ,  $\epsilon_z = 0$ ,  $\epsilon_{xy} = 6$ ,  $\epsilon_{yz} = 0$ ,  $\epsilon_{xz} = 0$

Finite element results:

$$\begin{Bmatrix} \sigma_x \\ \sigma_y \\ \sigma_z \\ \sigma_{xy} \\ \sigma_{yz} \\ \sigma_{xz} \end{Bmatrix} = \begin{Bmatrix} 10549.5 \\ 15164.8 \\ 0 \\ 6923.08 \\ 0 \\ 0 \end{Bmatrix}$$

Fig (3,10) General rectangular (u, v patch test)



• mid side and corner nodes 3 d.o.f

⊙ mid side nodes 5 d.o.f

Assumed displacement field :

$$u = 1 + 2x + 3y$$

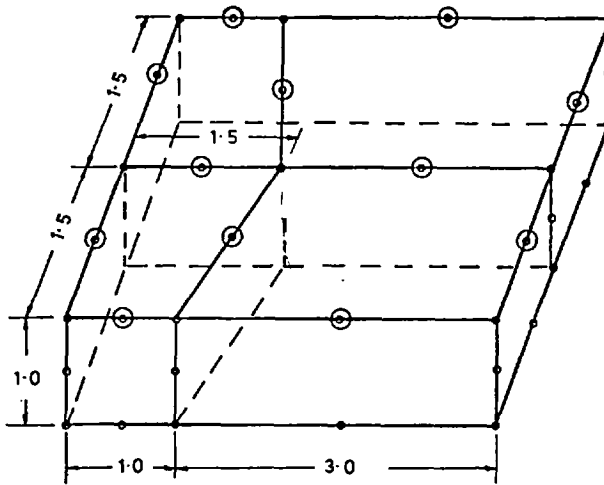
$$v = 2 + 3x + 4y$$

Constant strain state :  $\epsilon_x = 2$ ,  $\epsilon_y = 4$ ,  $\epsilon_z = 0$ ,  $\epsilon_{xy} = 6$ ,  $\epsilon_{yz} = 0$ ,  $\epsilon_{xz} = 0$

Finite element results:

$$\begin{Bmatrix} \sigma_x \\ \sigma_y \\ \sigma_z \\ \sigma_{xy} \\ \sigma_{yz} \\ \sigma_{xz} \end{Bmatrix} = \begin{Bmatrix} 10549.5 \\ 15164.8 \\ 0 \\ 6923.08 \\ 0 \\ 0 \end{Bmatrix}$$

Fig(3,11) Parallelogram patch test



- mid side and corner nodes 3 d.o.f
- ⊙ mid side nodes 5 d.o.f

Assumed displacement field :

$$u = 1 + 2x + 3y$$

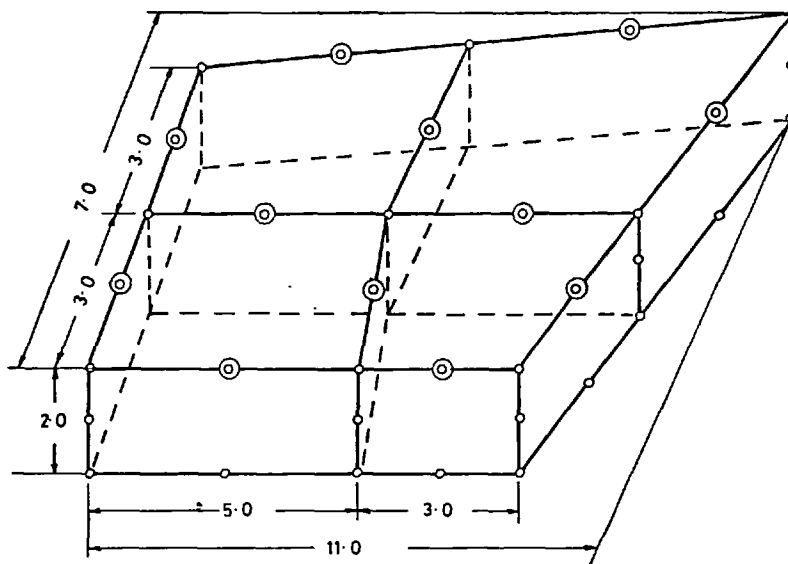
$$v = 2 + 3x + 4y$$

Constant strain state :  $\epsilon_x = 2$ ,  $\epsilon_y = 4$ ,  $\epsilon_z = 0$ ,  $\epsilon_{xy} = 6$ ,  $\epsilon_{yz} = 0$ ,  $\epsilon_{xz} = 0$

Finite element results:

$$\begin{Bmatrix} \sigma_x \\ \sigma_y \\ \sigma_z \\ \sigma_{xy} \\ \sigma_{yz} \\ \sigma_{xz} \end{Bmatrix} = \begin{Bmatrix} 10549.5 \\ 15164.8 \\ 0 \\ 6923.08 \\ 0 \\ 0 \end{Bmatrix}$$

Fig(3,12) Trapezoidal patch test



- mid side and corner nodes 3 d.o.f
- ⊙ mid side nodes 5 d.o.f

Assumed displacement field :

$$u = 1 + x + 2y$$

$$v = 1 + x + y$$

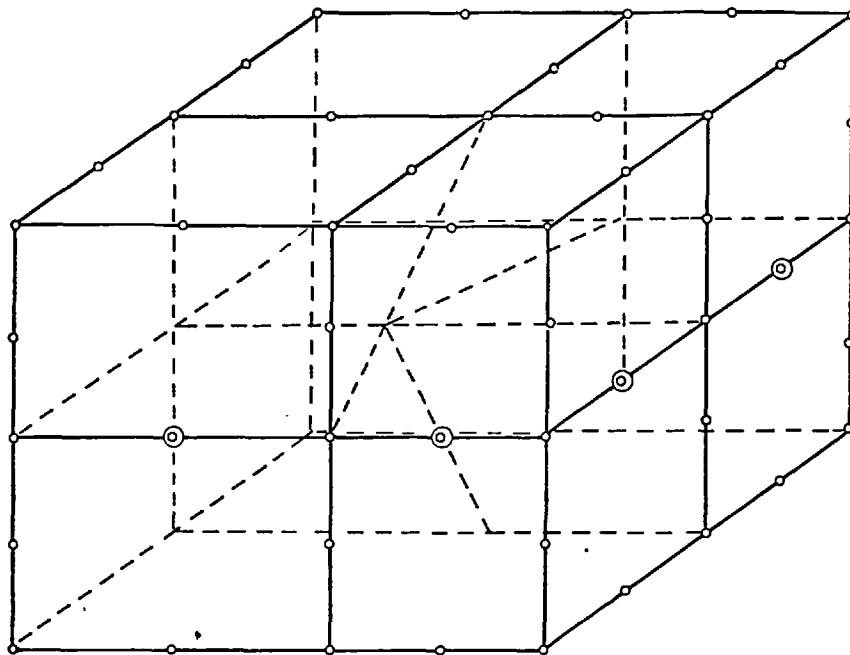
$$w = 1 + 2x + y$$

Constant strain state :  $\epsilon_x = 1$ ,  $\epsilon_y = 1$ ,  $\epsilon_z = 0$ ,  $\epsilon_{xy} = 3$ ,  $\epsilon_{yz} = 1$ ,  $\epsilon_{xz} = 2$

Finite element results:

$$\begin{Bmatrix} \sigma_x \\ \sigma_y \\ \sigma_z \\ \sigma_{xy} \\ \sigma_{yz} \\ \sigma_{xz} \end{Bmatrix} = \frac{3000}{0.52} \begin{bmatrix} 0.7 & 0.3 & 0.3 \\ 0.3 & 0.7 & 0.3 \\ 0.3 & 0.3 & 0.7 \\ & & & 0.2 \\ & & & & 0.2 \\ & & & & & 0.2 \end{bmatrix} \begin{Bmatrix} 1 \\ 1 \\ 0 \\ 3 \\ 1 \\ 2 \end{Bmatrix} = \begin{Bmatrix} 5769.23 \\ 5769.23 \\ 0 \\ 3461.54 \\ 1153.846 \\ 2307.692 \end{Bmatrix}$$

Fig(3,13) Arbitrary hexagonal patch test



- mid side and corner nodes 3 d.o.f
- ⊙ mid side nodes 5 d.o.f

General arbitrary quadrilateral  
(w Free patch test)

Assumed displacement field:

$$w = 1 + 2x + 3y$$

Constant strain state:  $\epsilon_x = 0, \epsilon_y = 0, \epsilon_z = 0, \epsilon_{xy} = 0, \epsilon_{yz} = 3, \epsilon_{xz} = 2$

Finite element results:

$$\begin{Bmatrix} \sigma_x \\ \sigma_y \\ \sigma_z \\ \sigma_{xy} \\ \sigma_{yz} \\ \sigma_{xz} \end{Bmatrix} = \frac{3000}{0.52} \begin{bmatrix} 0.7 & 0.3 & 0.3 \\ 0.3 & 0.7 & 0.3 \\ 0.3 & 0.3 & 0.7 \\ & & & 0.2 \\ & & & & 0.2 \\ & & & & & 0.2 \end{bmatrix} \begin{Bmatrix} 0 \\ 0 \\ 0 \\ 0 \\ 3 \\ 2 \end{Bmatrix} = \begin{Bmatrix} 0 \\ 0 \\ 0 \\ 0 \\ 3461.54 \\ 2307.69 \end{Bmatrix}$$

Fig (3,14) Arbitrary hexagonal  
(w free patch test)

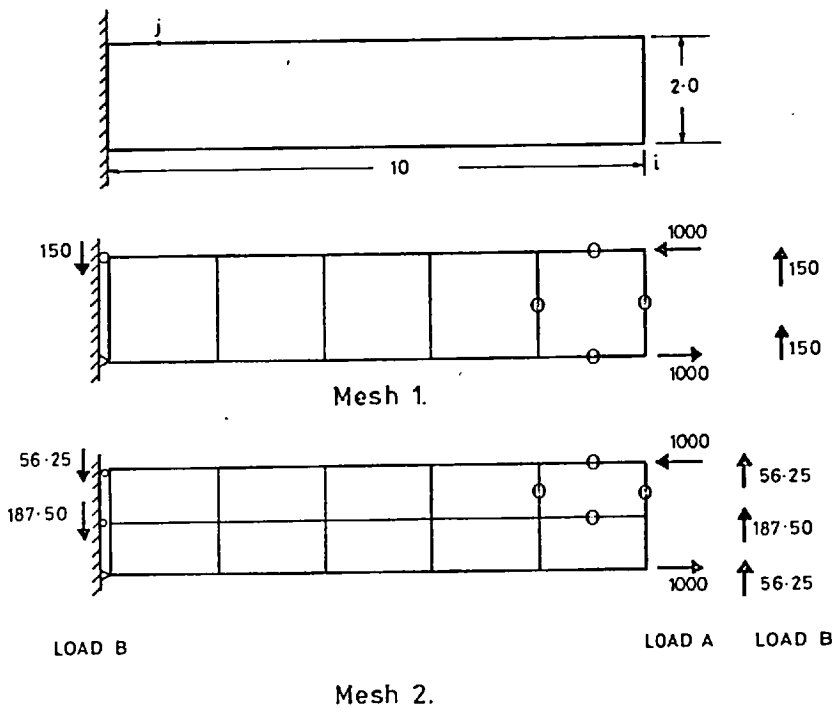
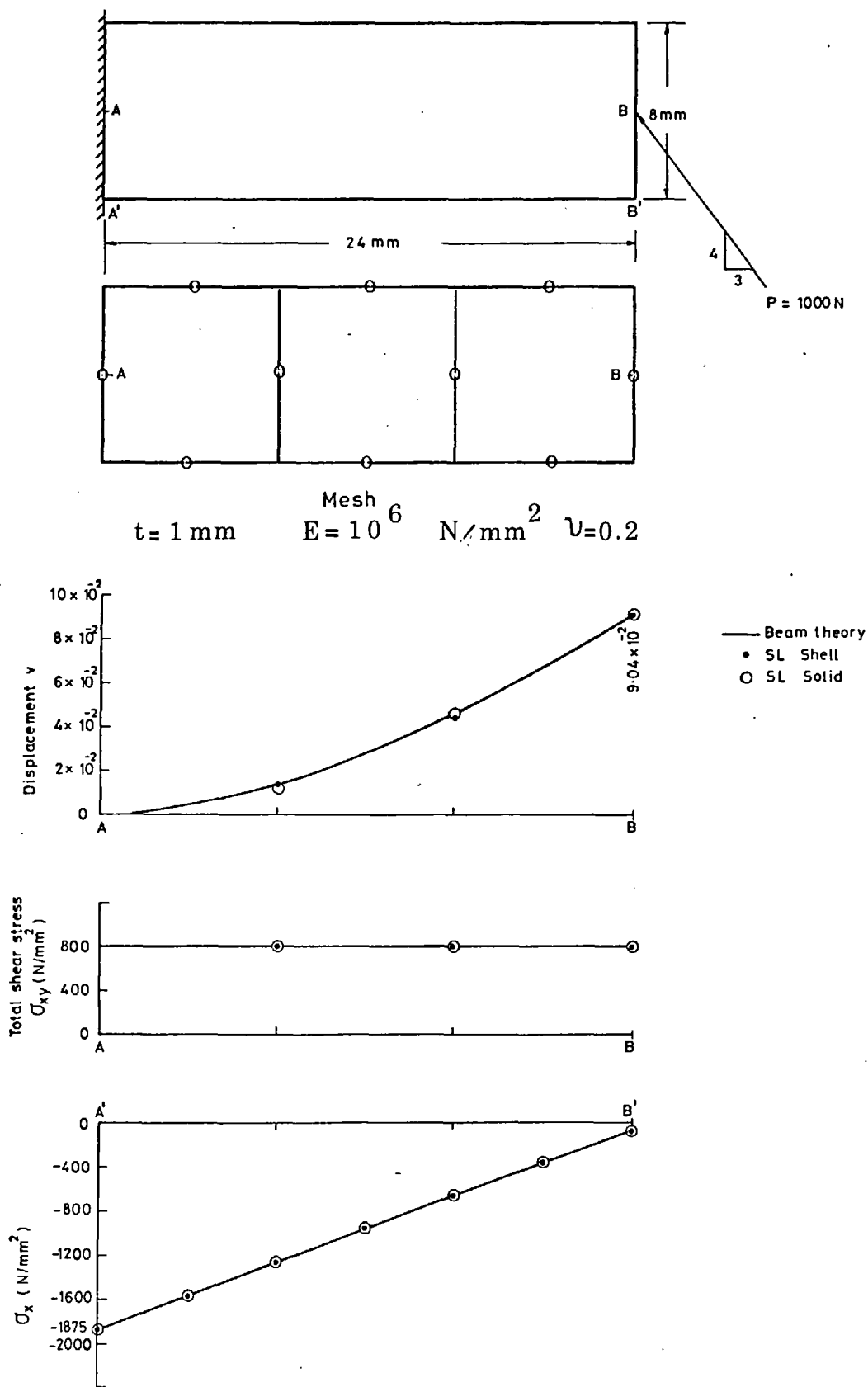
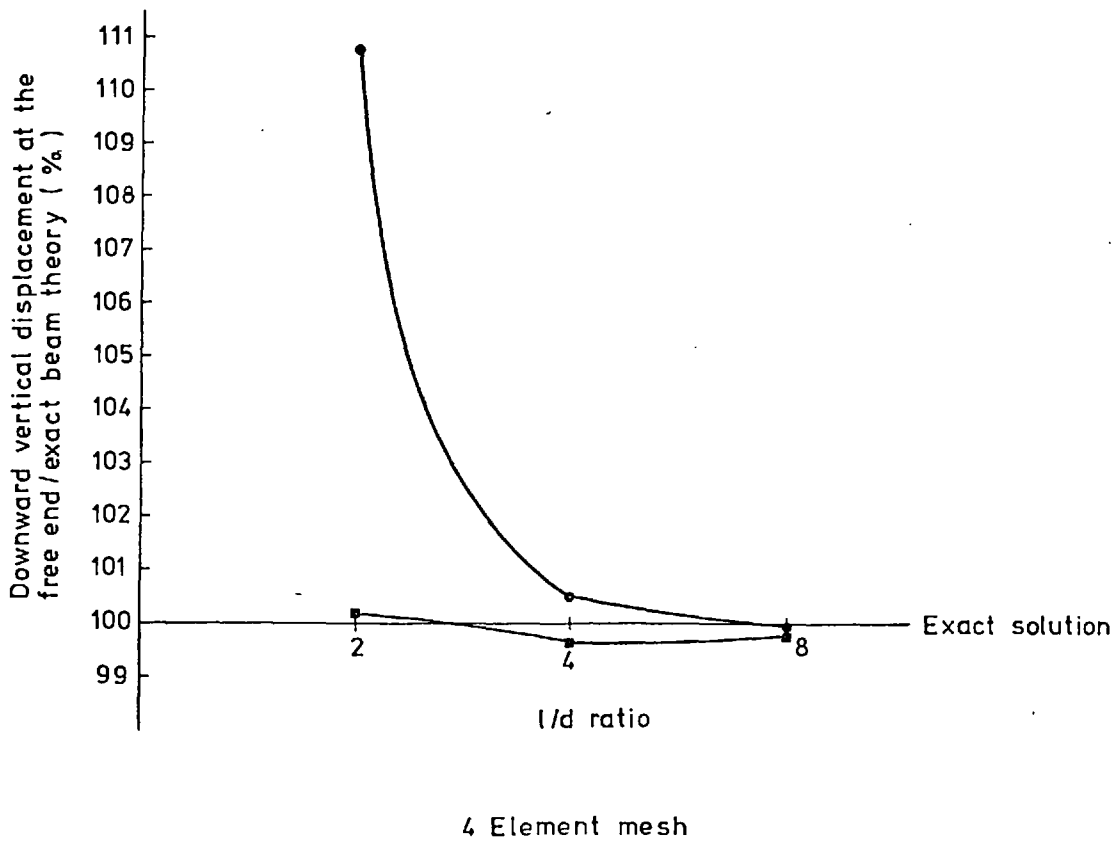
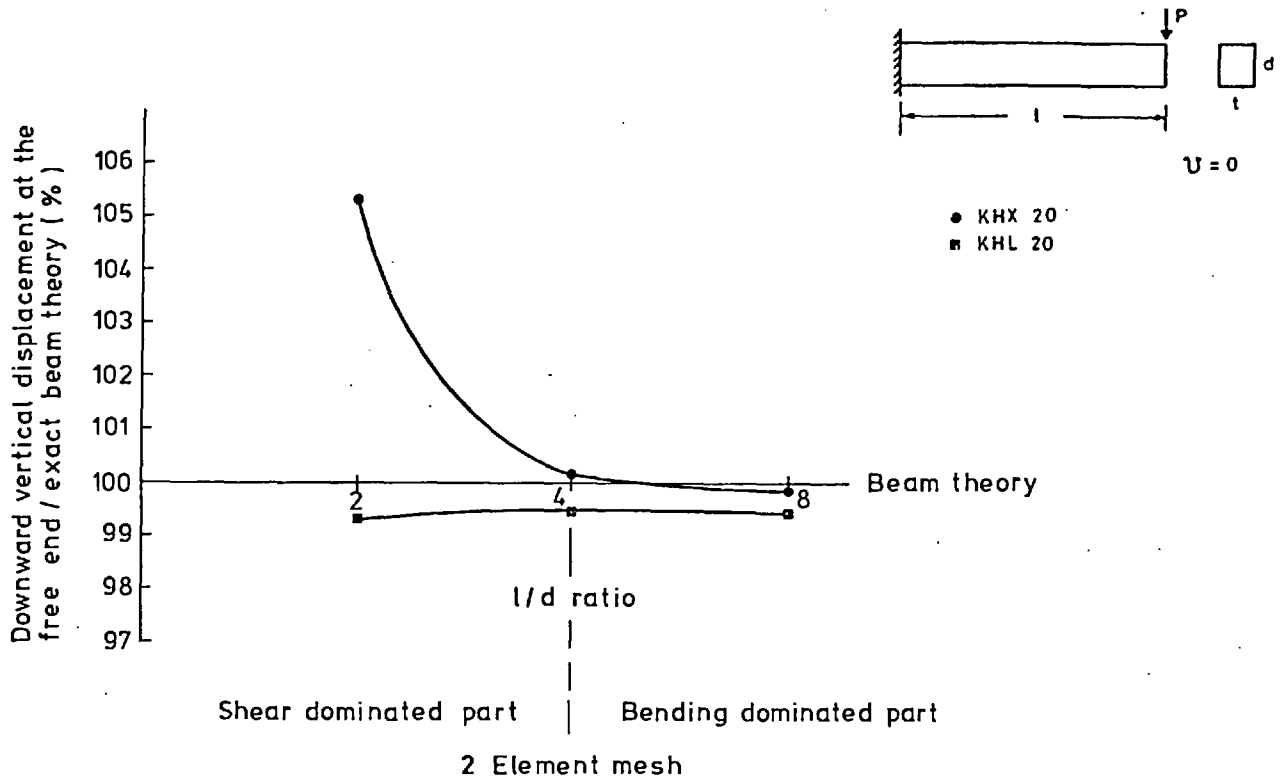


Fig (3,15) Cantilever beam



Fig(3.16) Cantilever mesh idealization and results comparison with beam theory



Fig(3,17) Cantilever beam



Mesh in symmetric quarter no. of elements		1 * 1	2 * 2	4 * 4	6 * 6	Theory	
Concentrated load P	KHL 20	Central deflection $w_c$ $0.01160 \frac{Pa^2}{D} + w_s$	999.214	1001.85	1099.15	1189.02	1203.258
		Percentage of exact deflection	930	823	913	988	
	KHX 20	Central deflection $w_c + w_s$	1194.65	1280.85	1320.79	1342.15	1203.258
		Percentage	992	1056	1097	1115	

$$D = \frac{Et^3}{12(1-\nu^2)} = 0.09157509$$

$$P = 40 \quad Q = 12$$

- KHX 20 2\*2+2 Gaussian integration
- KHL 20 14 point rule

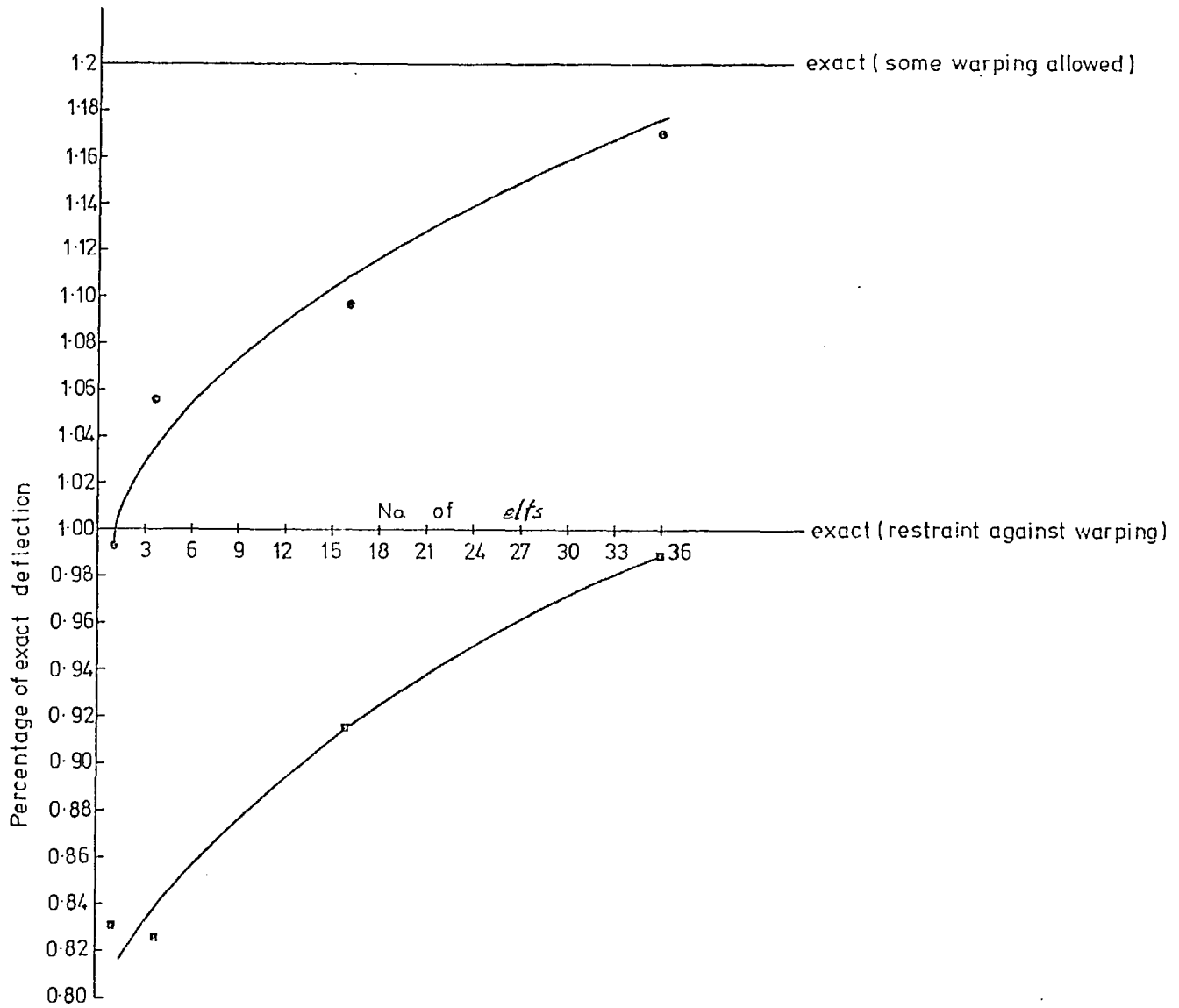


Fig (3,18) Simply supported square plate under central concentrated load

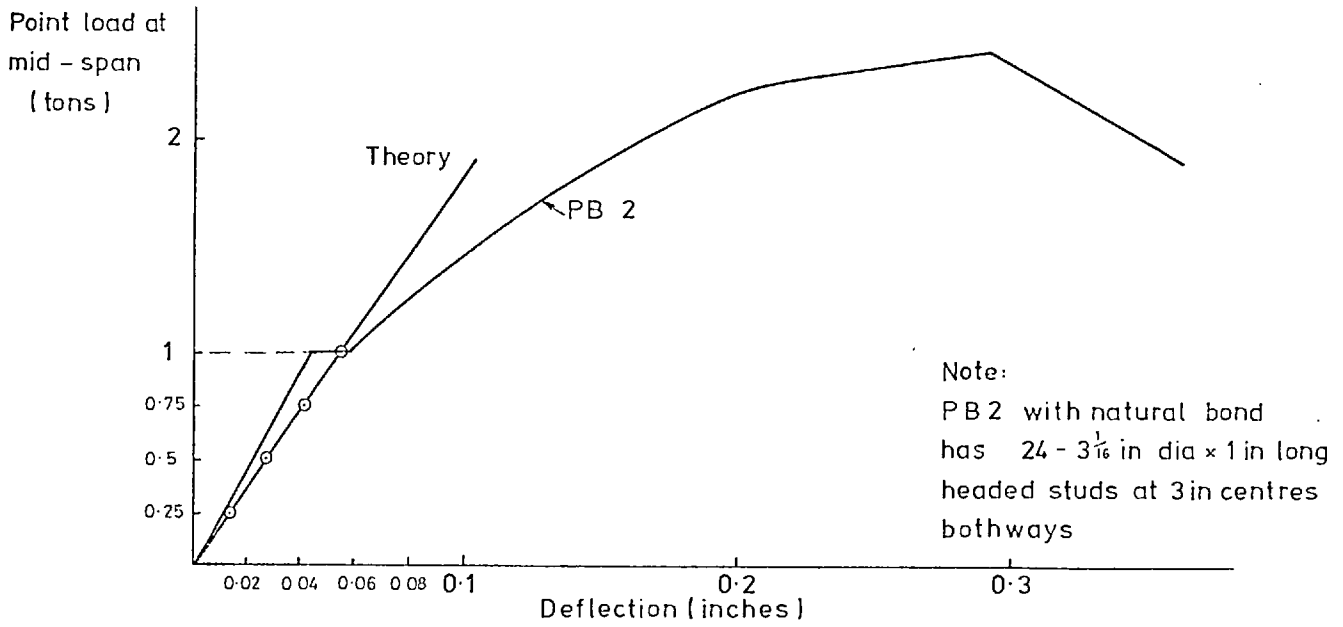
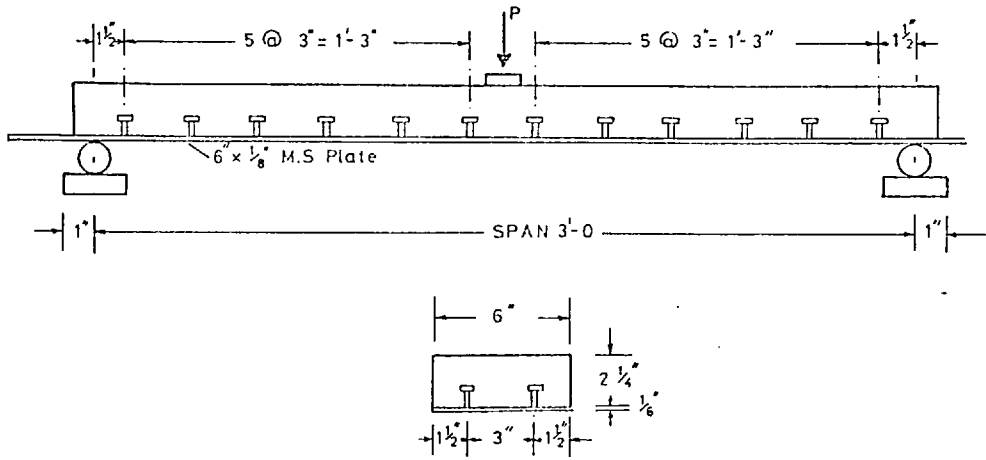
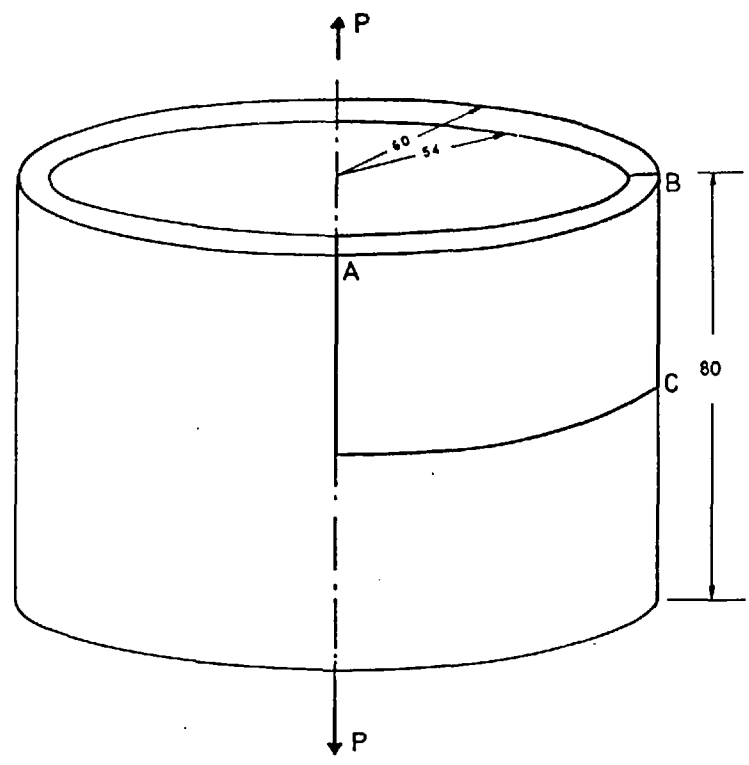
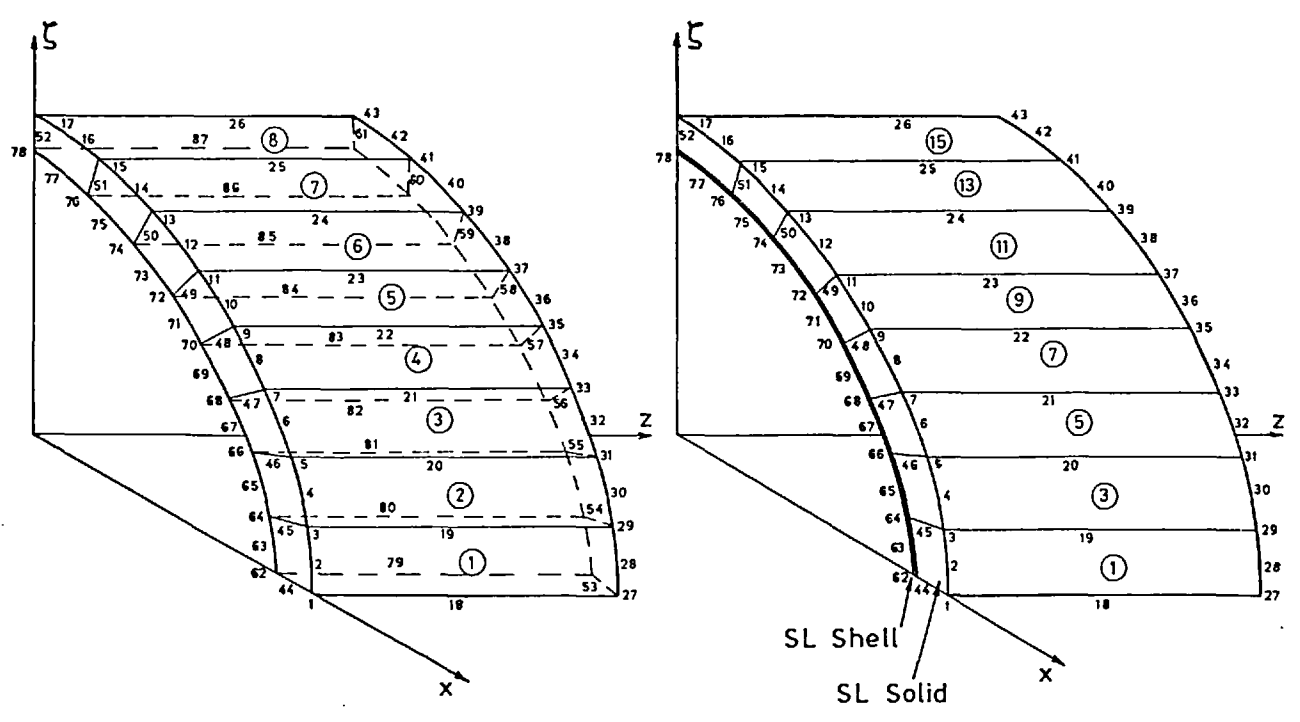


Fig (3,19) Details of plated beam.  
deflection against load curve



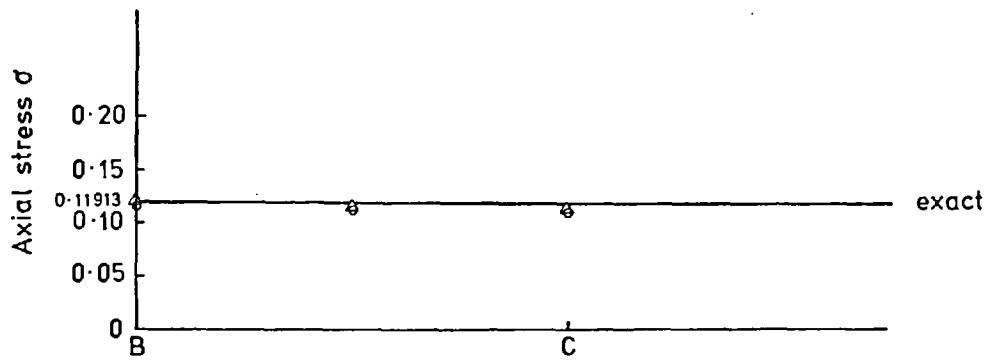
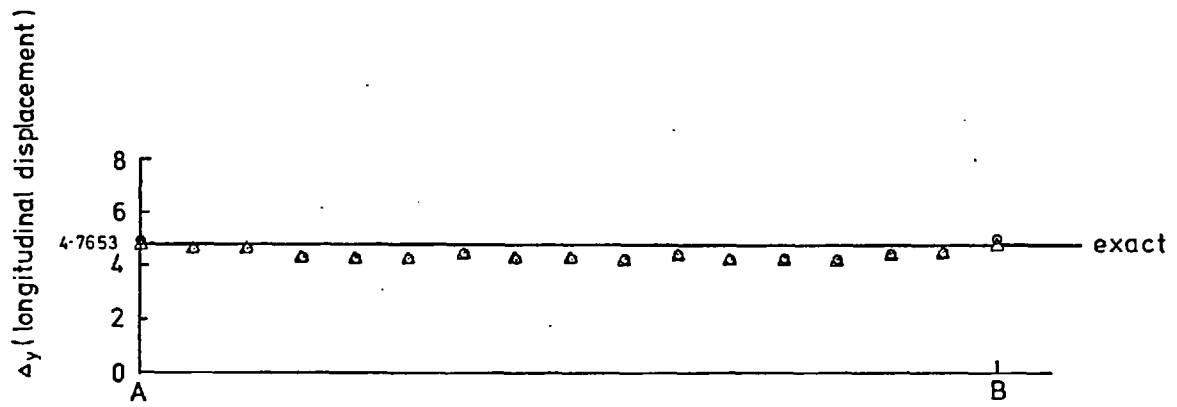
Fig(3,20) Uniform axial load acting on cylinder



Case a - 8 (20 node brick) Elements  
Mesh

Case b - 8 (SL Solid) Elements  
+ 8 (SL Shell) Elements  
Mesh

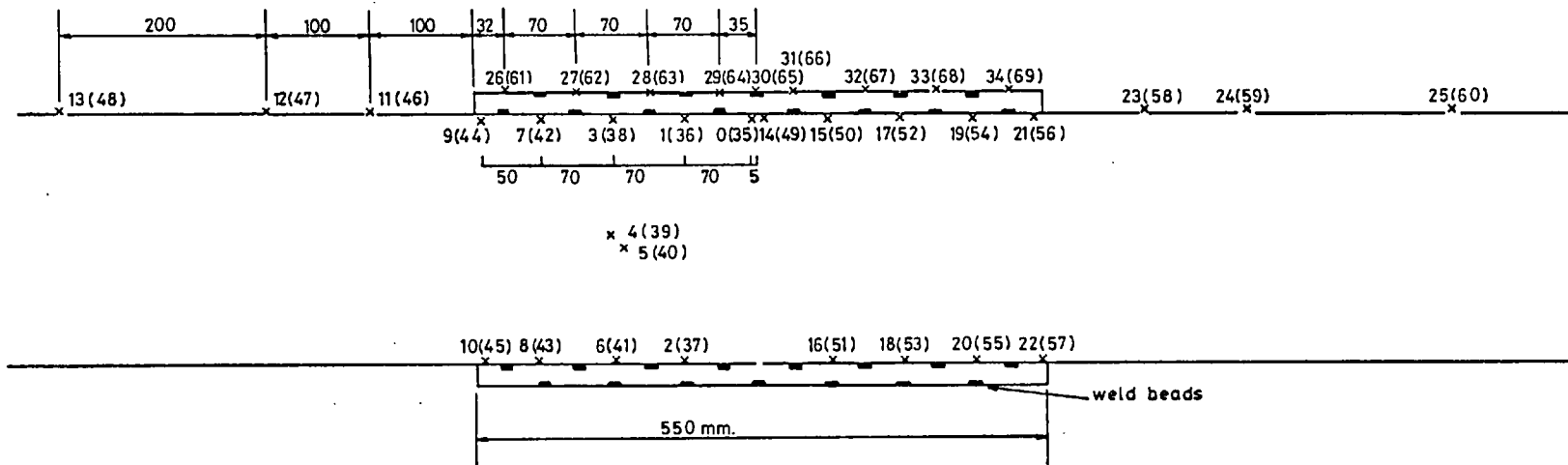
Fig(3,21) The mesh idealization



○ 20 node solid element (case a)

△ SL solid + SL shell (case b)

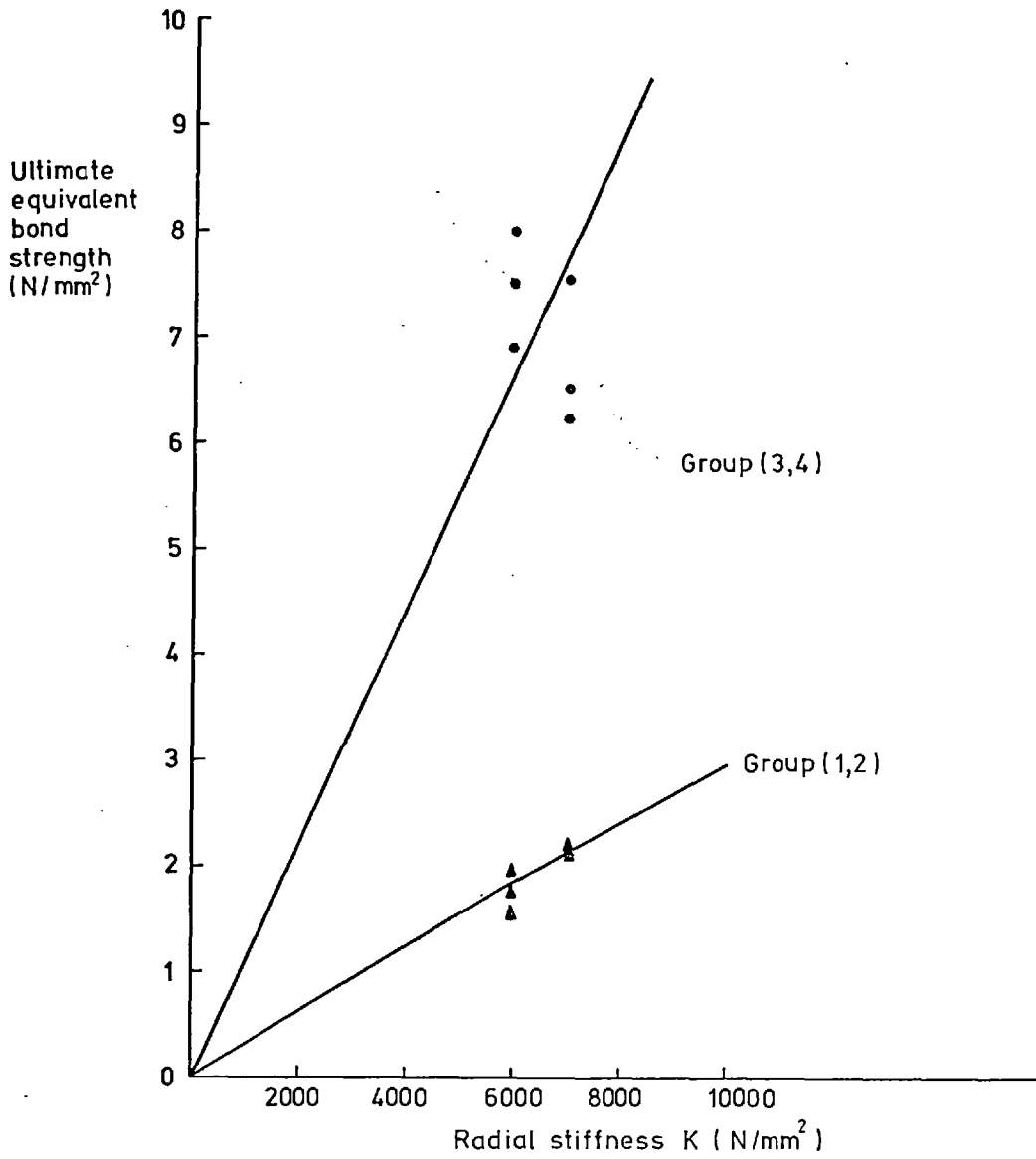
Fig (3,22) Axial stress and longitudinal displacement



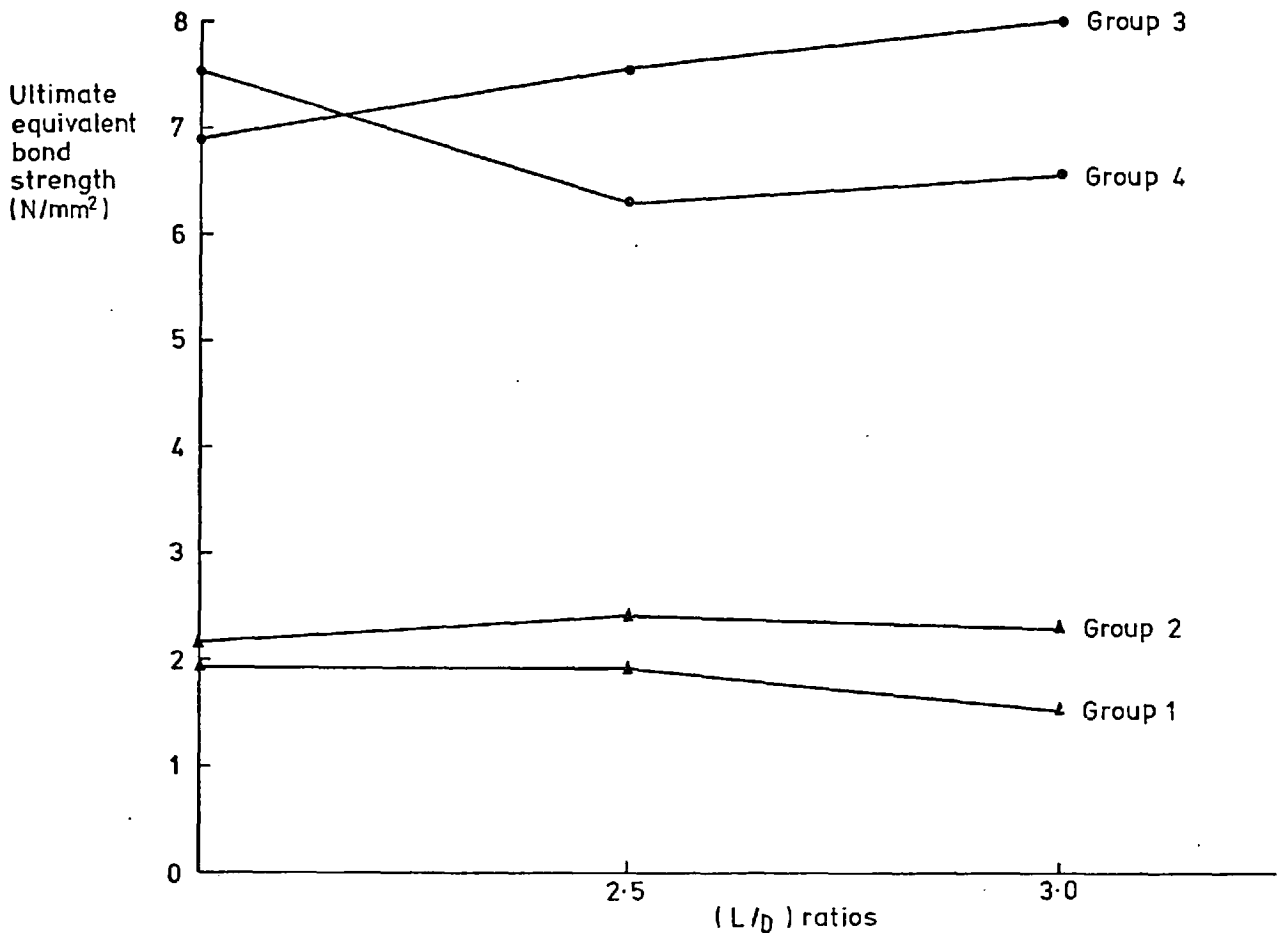
0 - 34 Axial strain gauges

(35)-(69) Circumferential strain gauges

Fig(4,1) Strain gauge layout



Fig(4.2) Effect of radial stiffness on ultimate equivalent bond strength



Fig(4,3) Effect of length /diameter ratio on bond strength

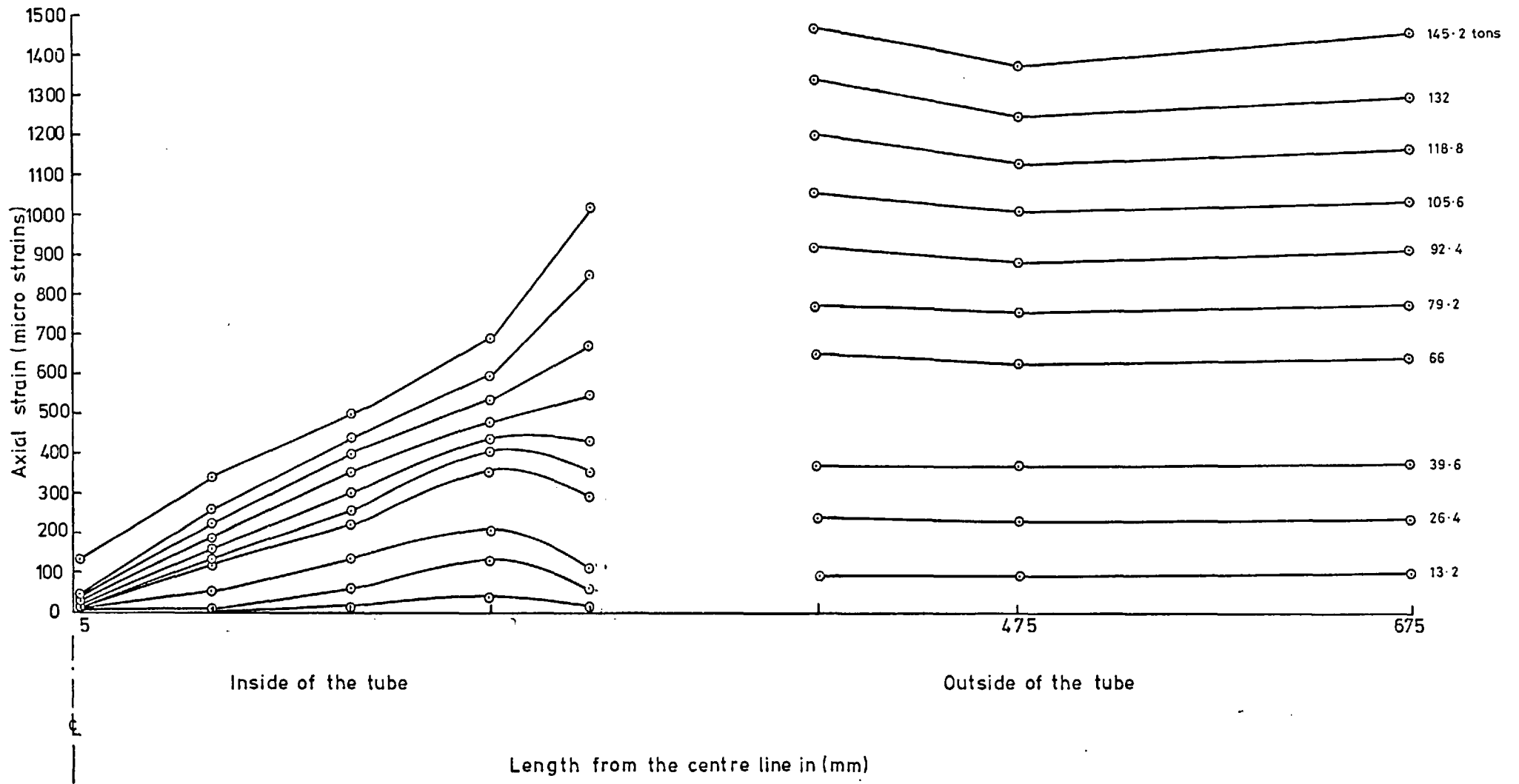
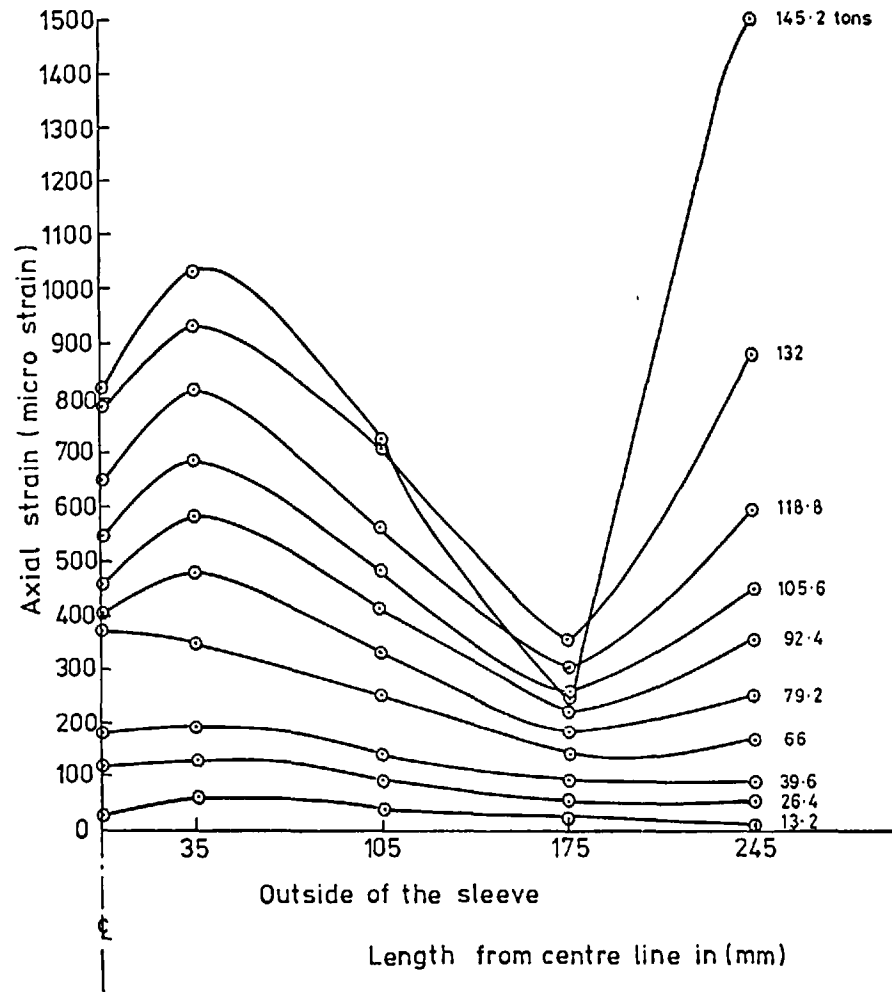
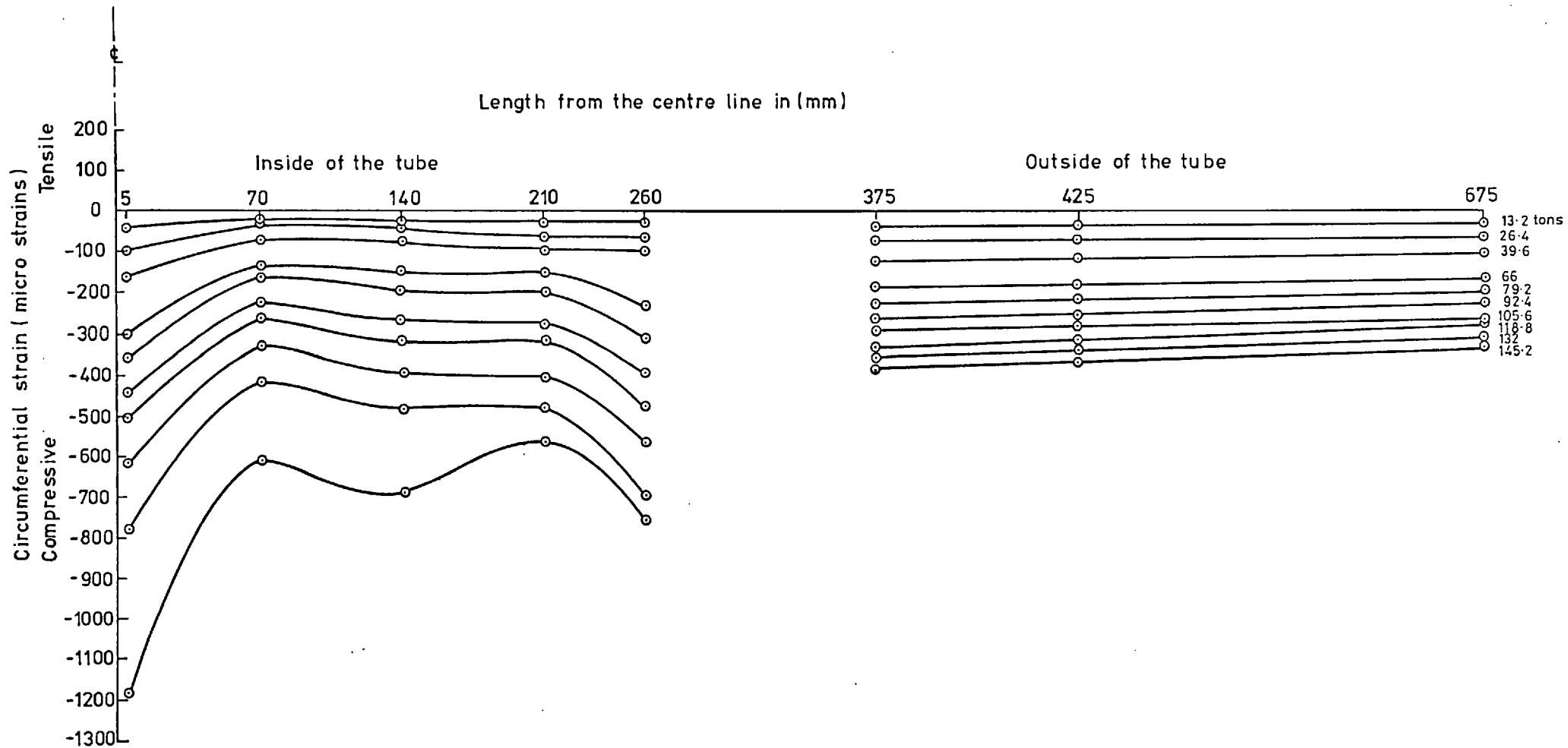


Fig (4,4) Axial strain distribution along the length of tube

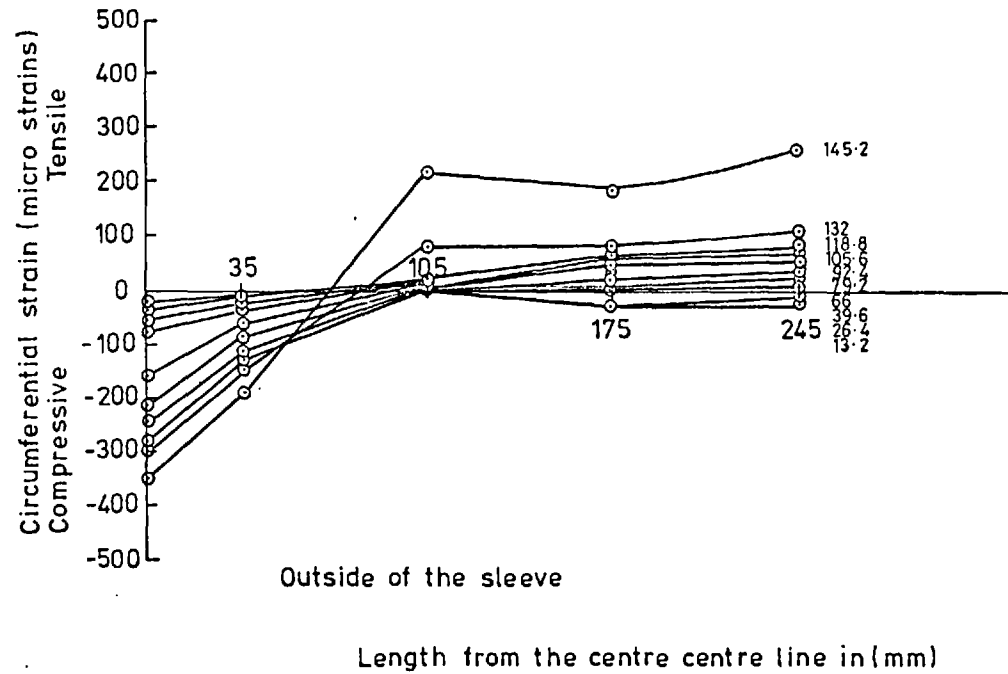




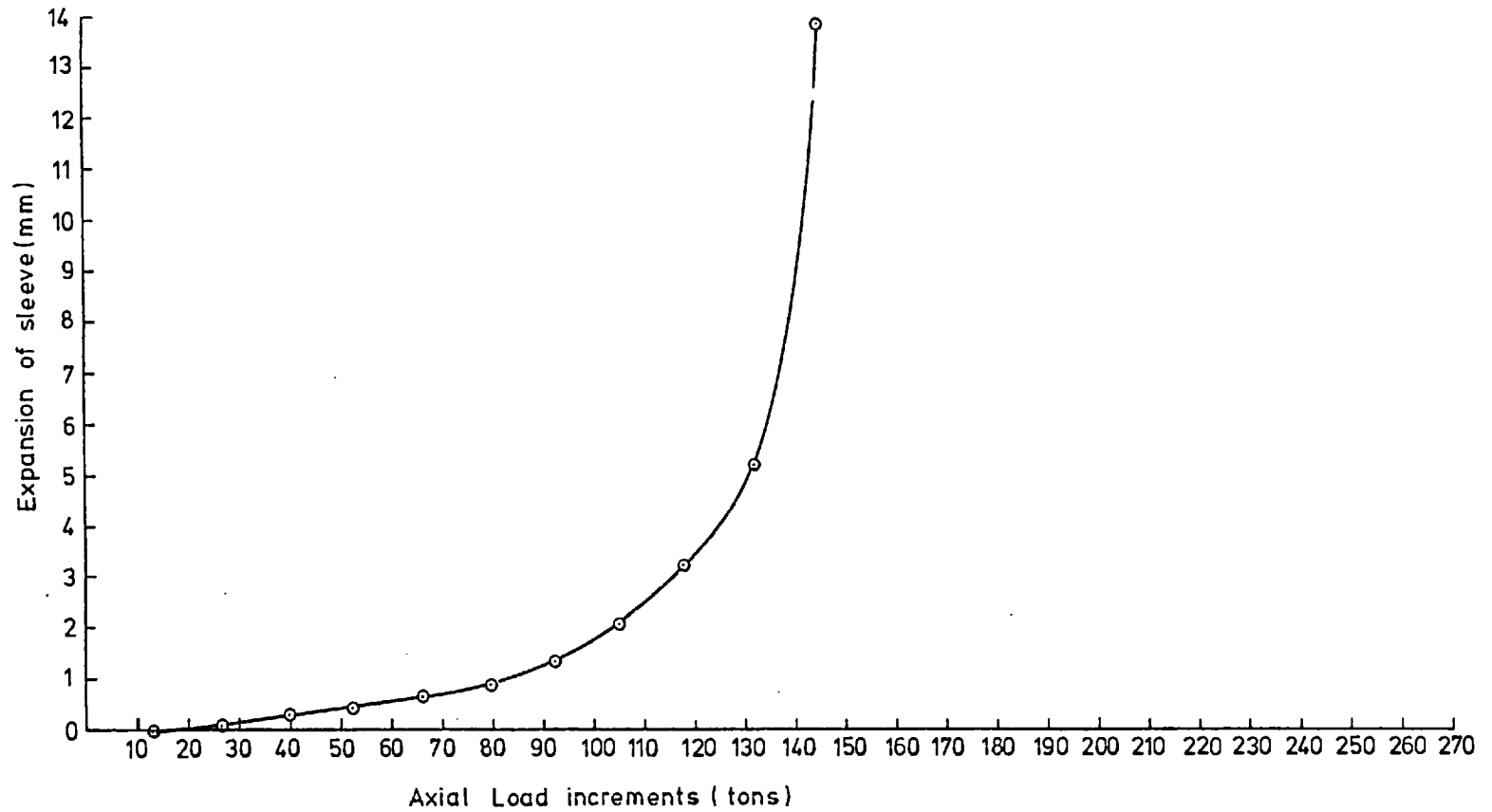
Fig(4.5) Axial strain distribution along the length of sleeve



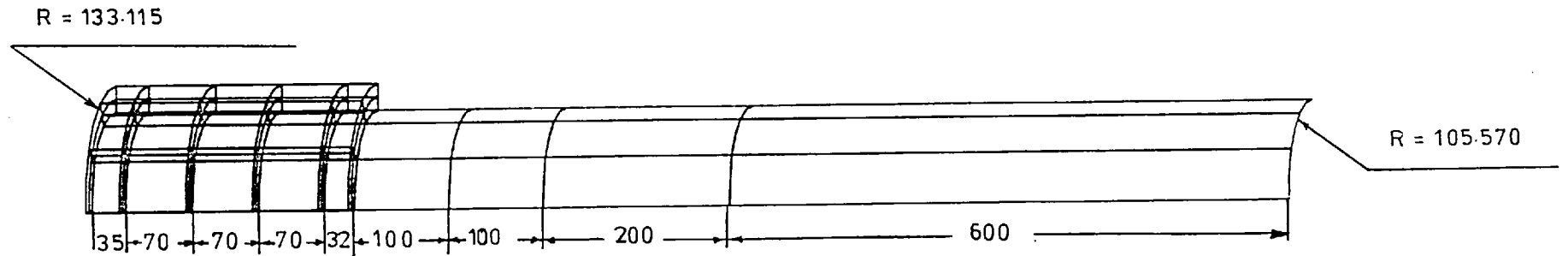
- Fig (4,6) Circumferential strain distribution along the length of tube



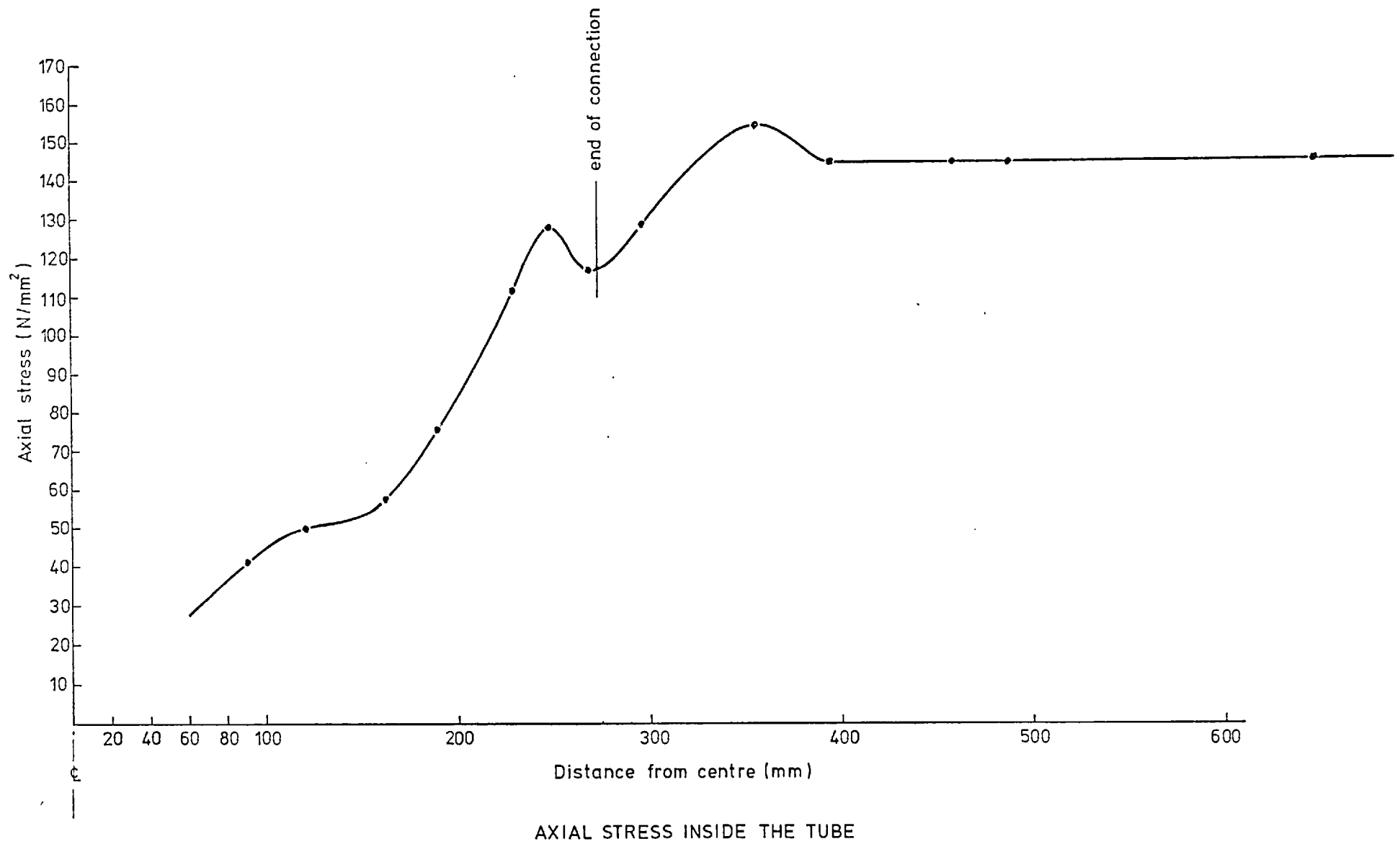
Fig(4,7) Circumferential strain distribution along the length of sleeve



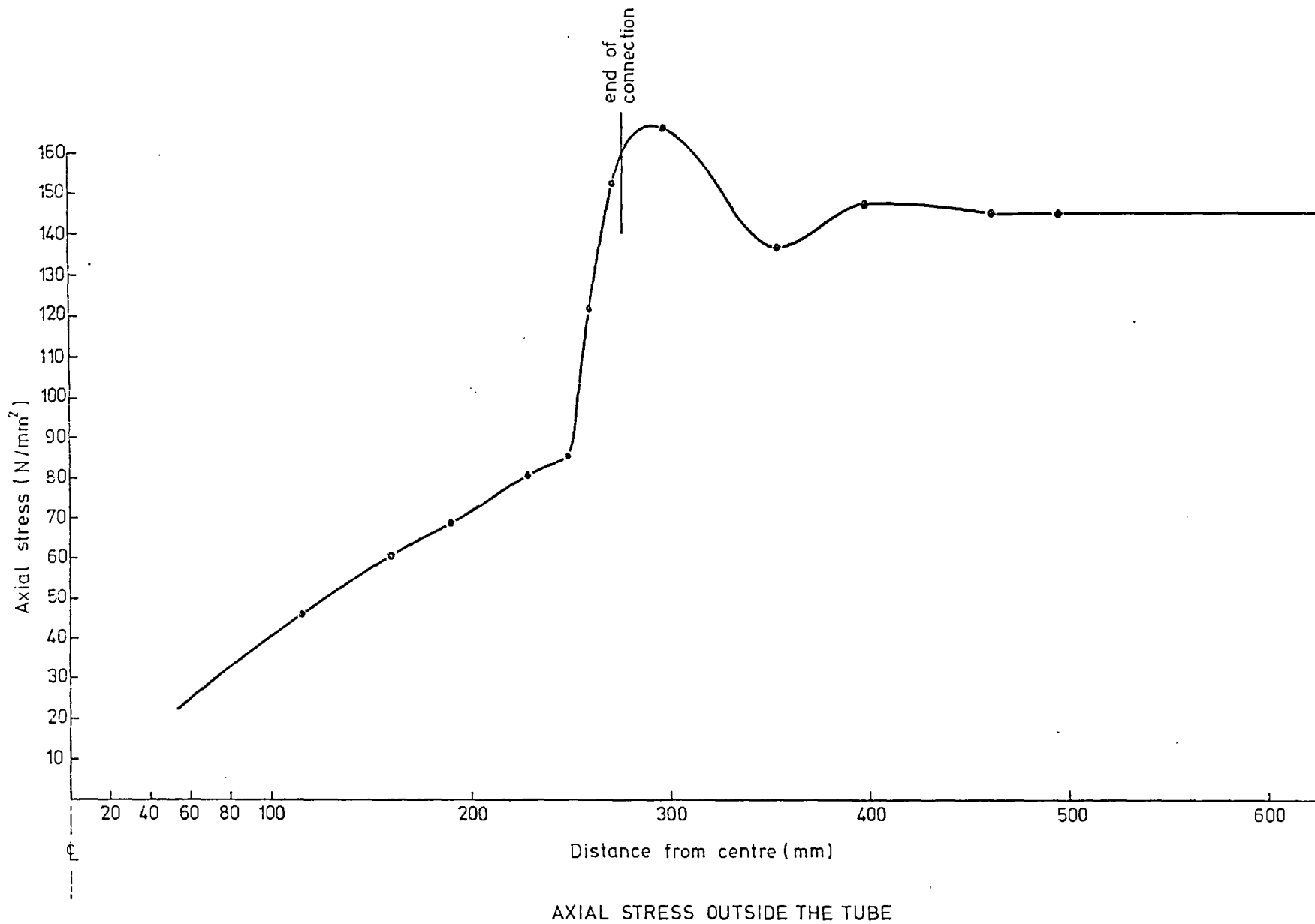
Fig(4,8) Sleeve and tube displacement curve



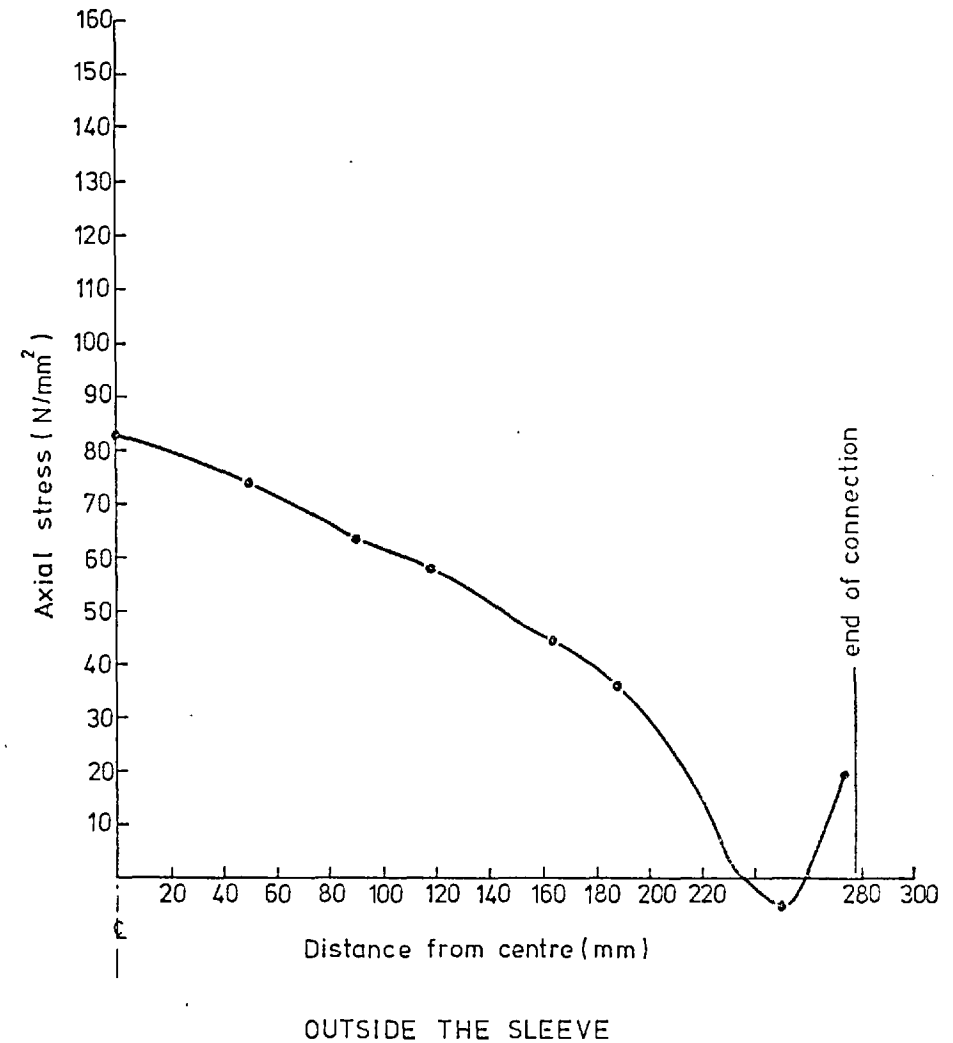
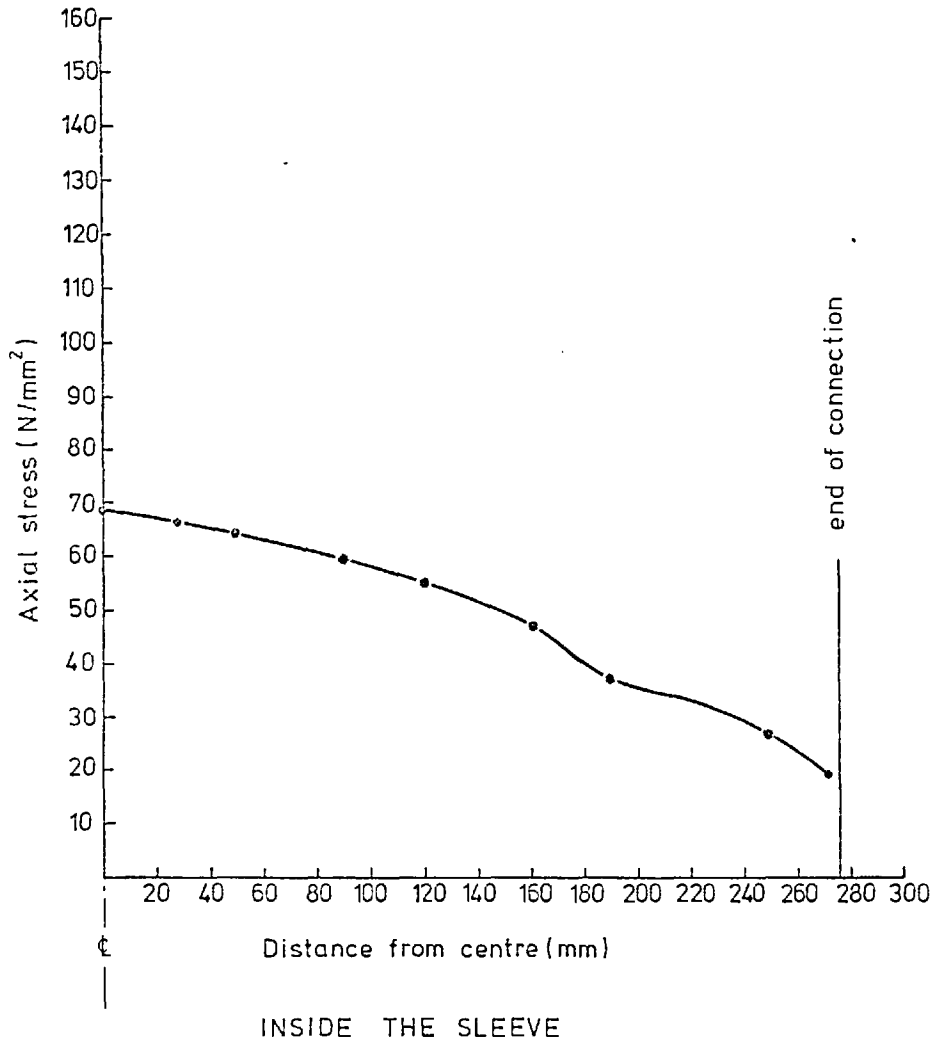
Fig(5,1) Composite connection with steel sleeve filled with concrete , mesh idealization



Fig(5,2) Steel tubes connected by a steel sleeve filled with concrete

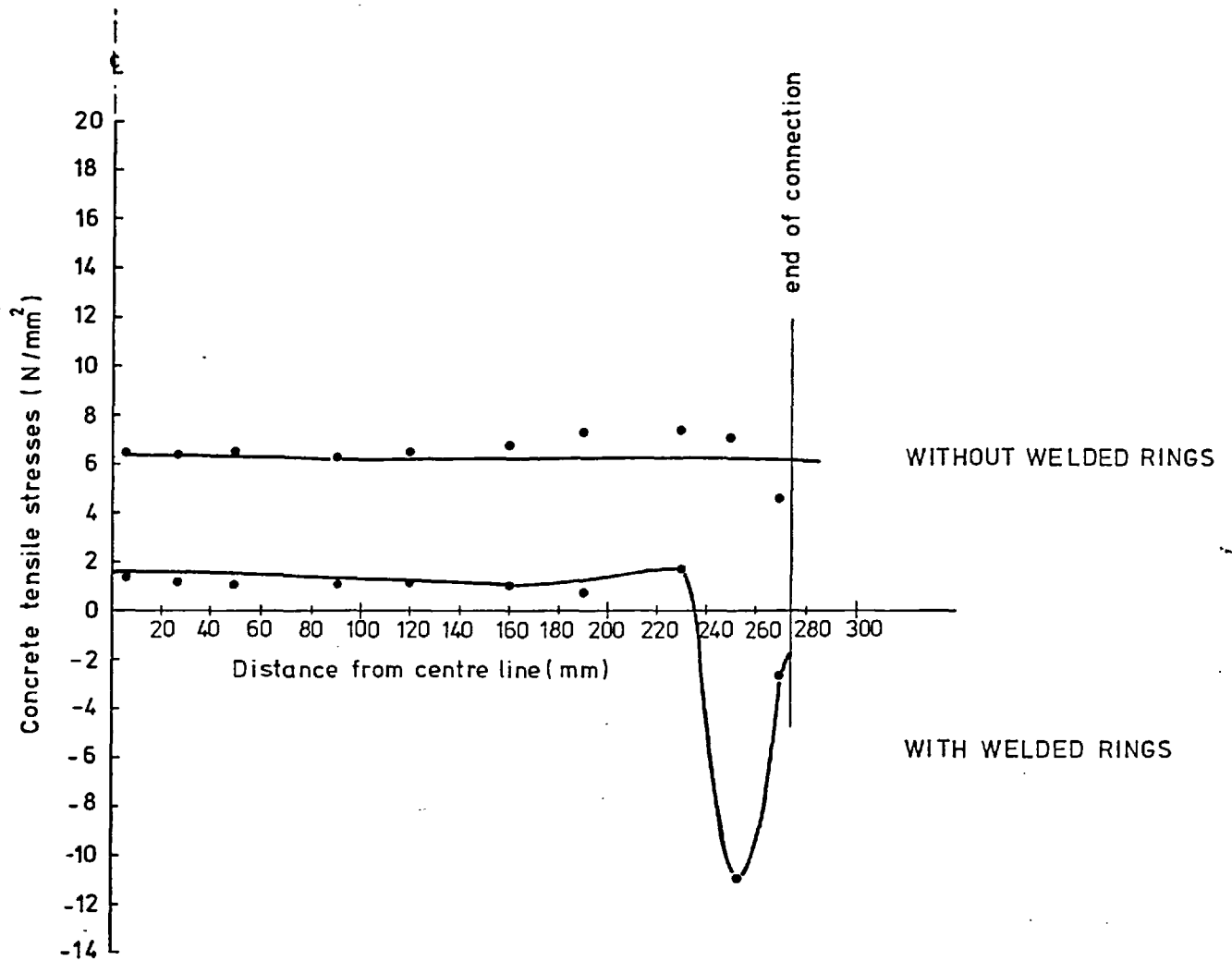


Fig(5,3) Steel tubes connected by a steel sleeve filled with concrete

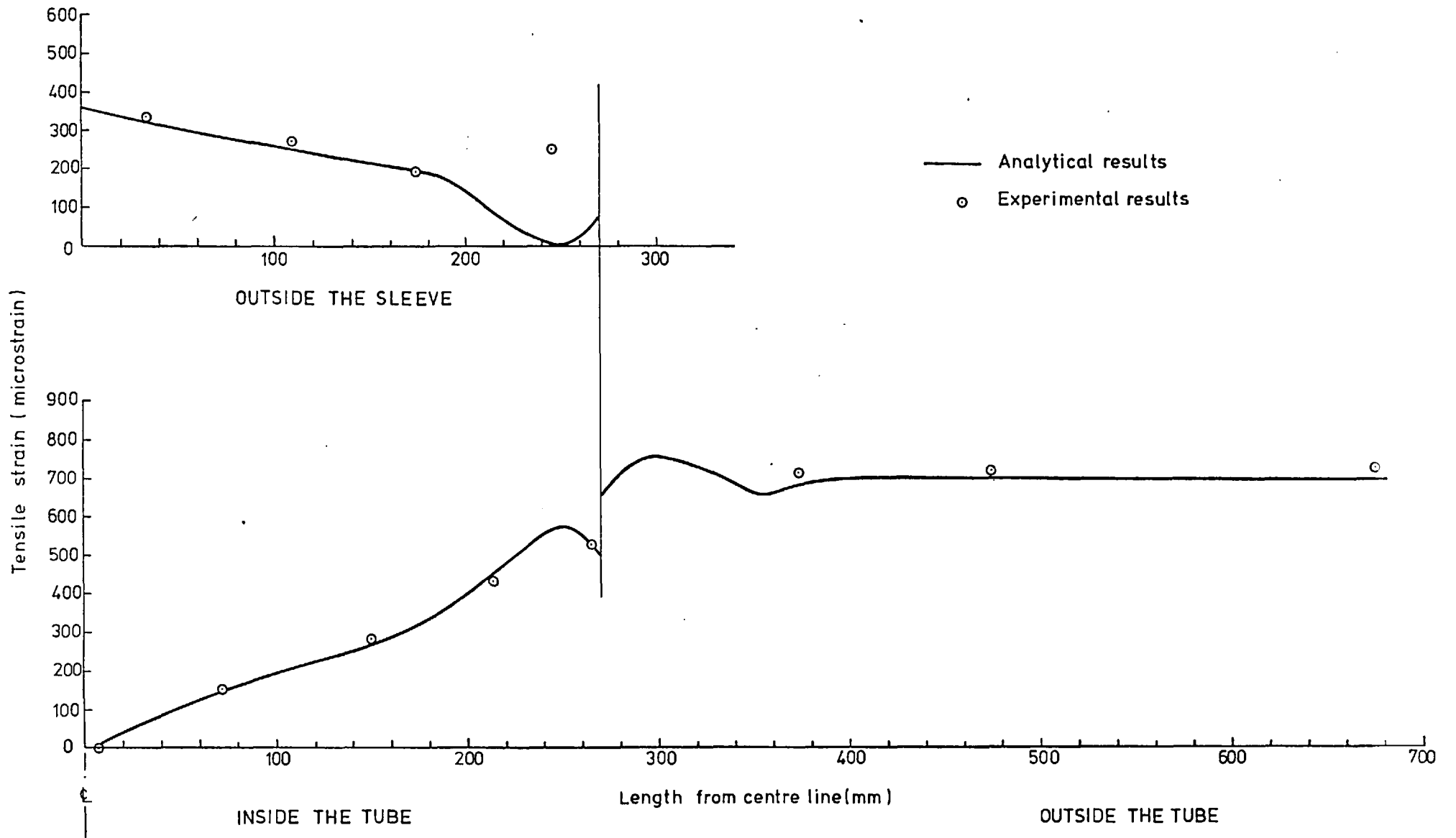


Fig(5,4) Steel tubes connected by a steel sleeve filled with concrete

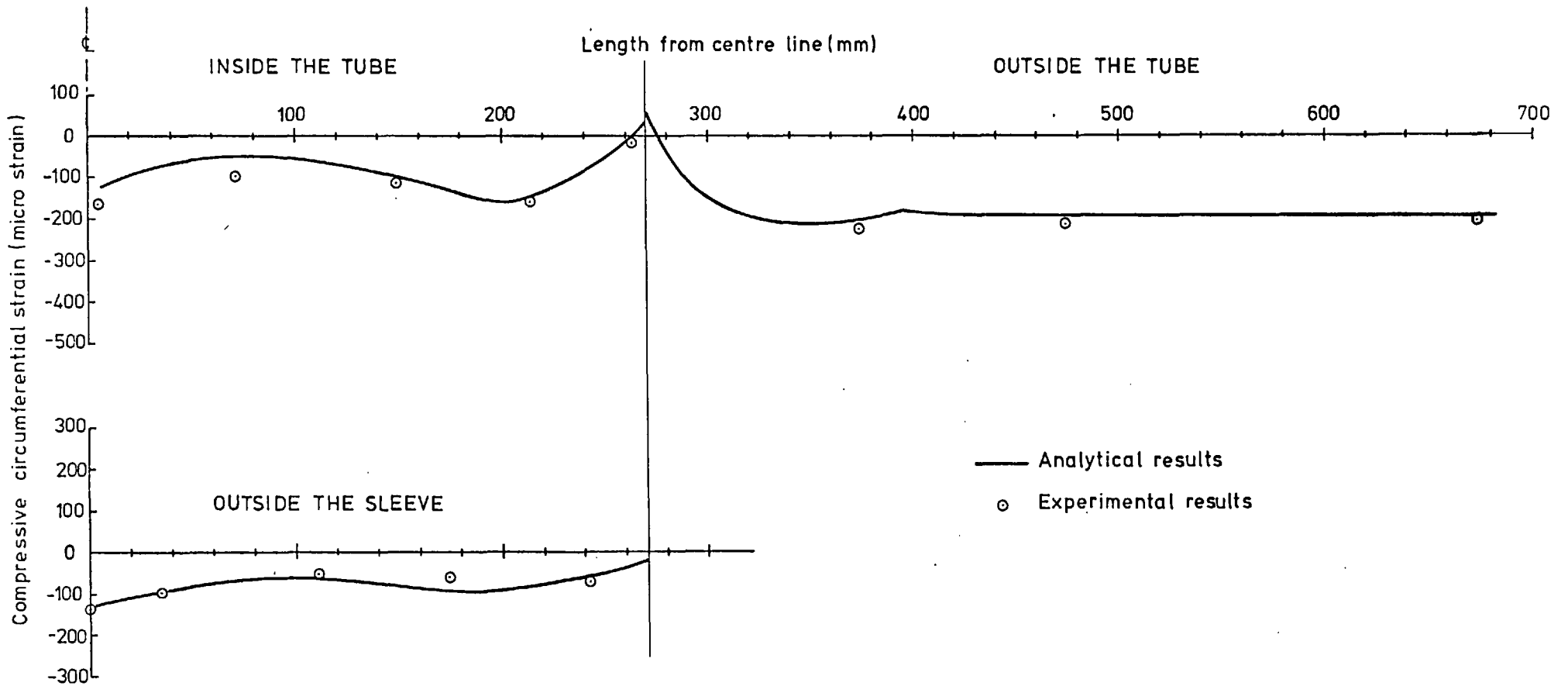




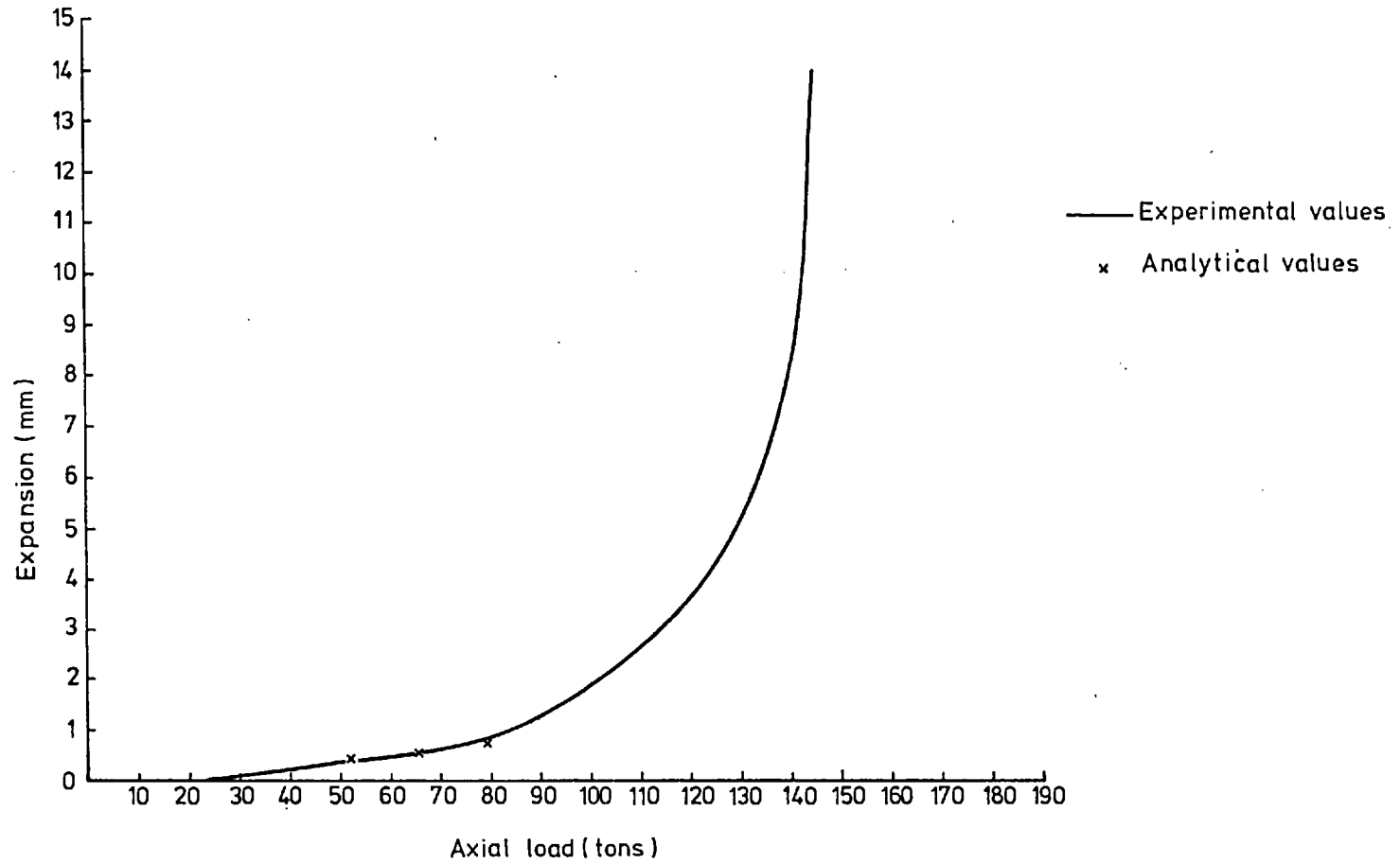
Fig(5,5) The effect of steel rings welded at both extremities on tensile stress of concrete



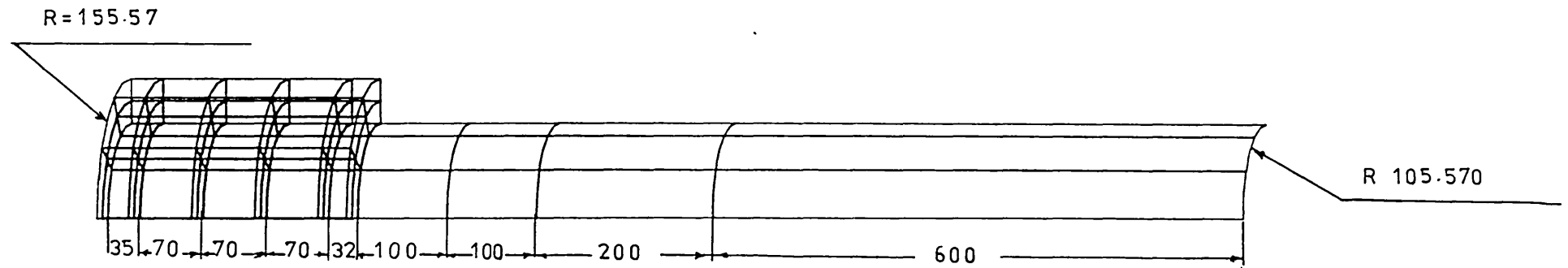
Fig(5,6) Axial strains



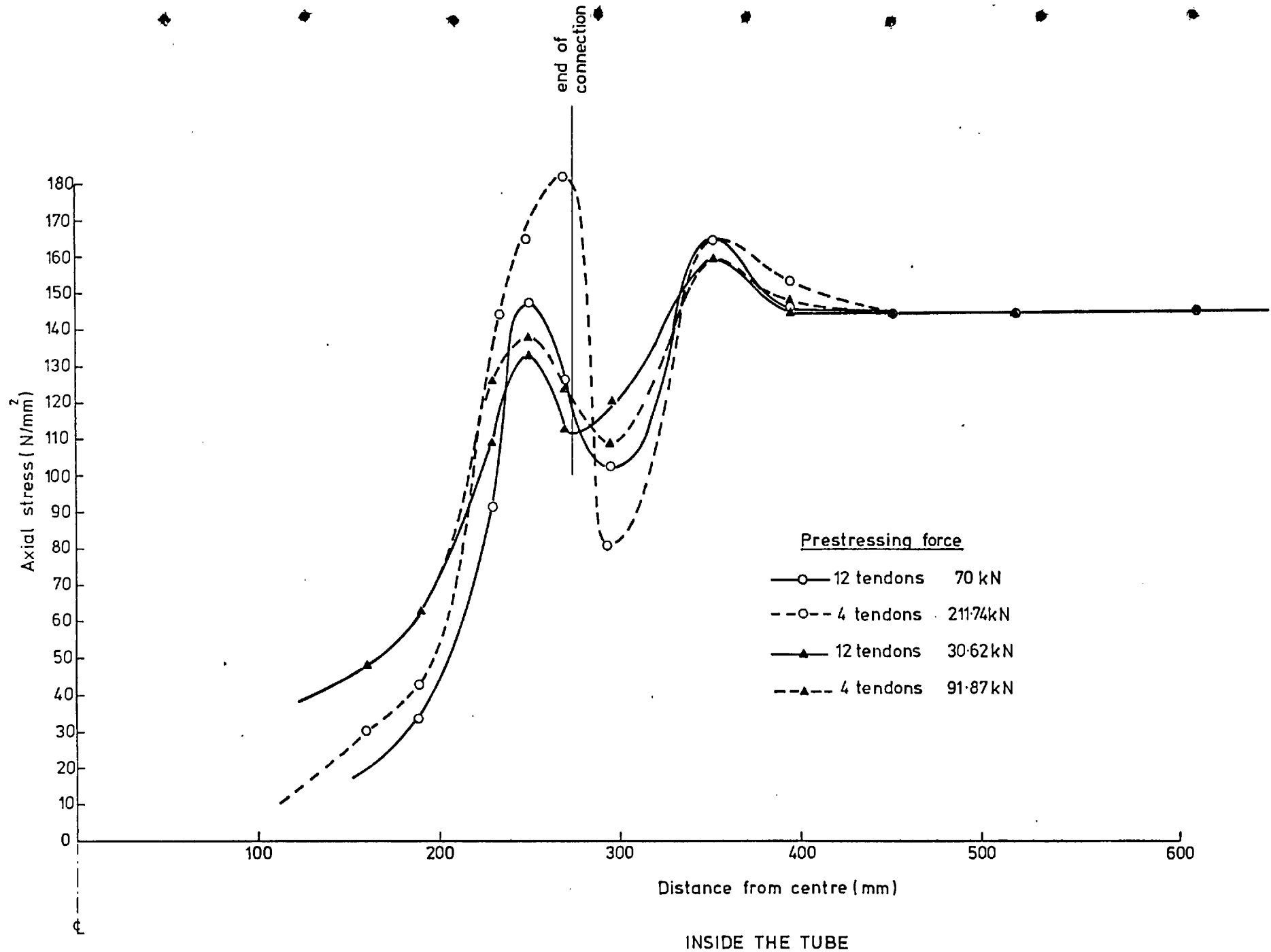
Fig(5,7) Circumferential strains



Fig(5,8) Displacement curve



Fig(5,9) Prestressed composite connection  
, mesh idealization



Fig(5,10) Axial stresses of various prestressed connections

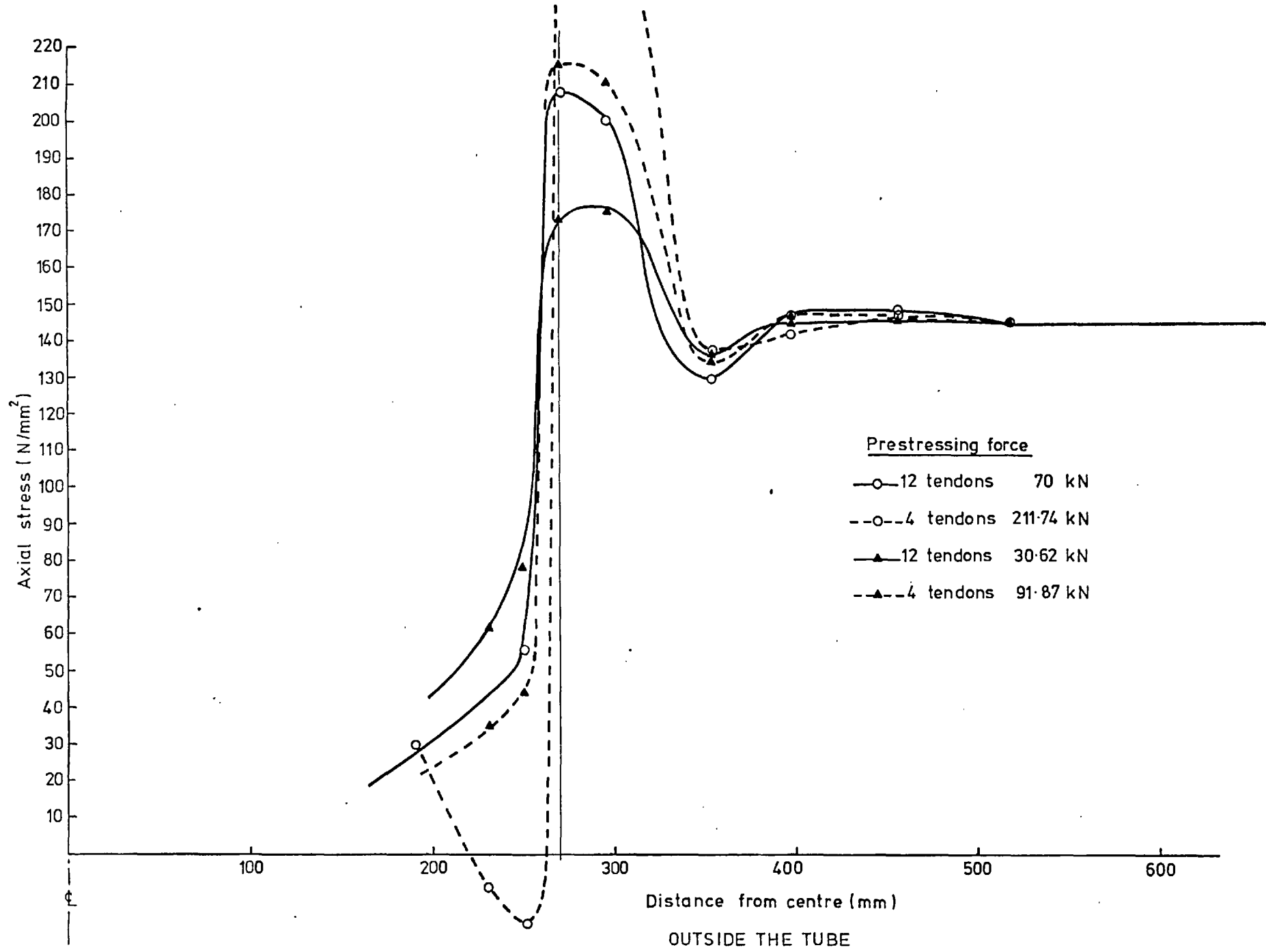


Fig (5,11) Axial stresses of various prestressed connections

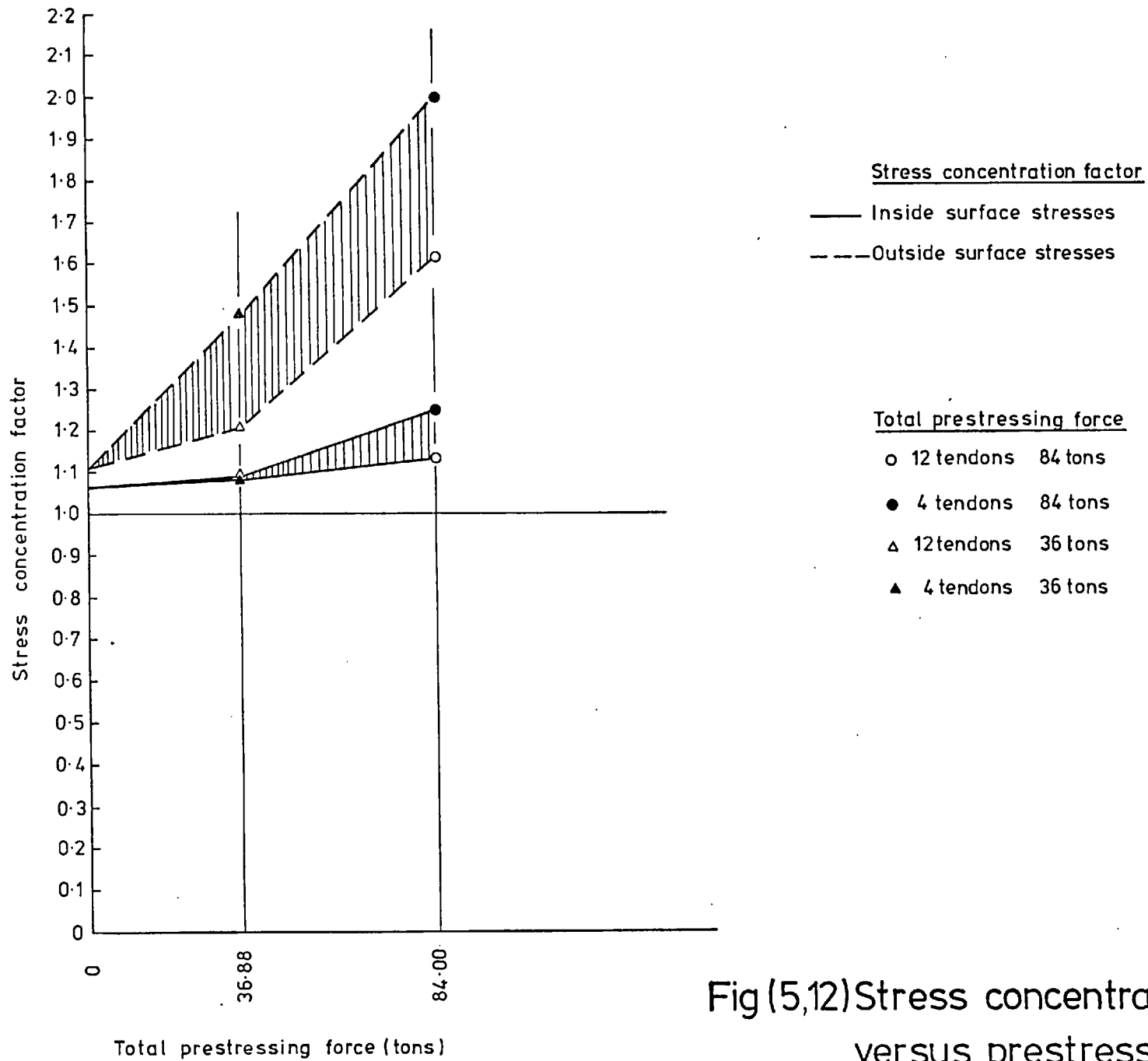
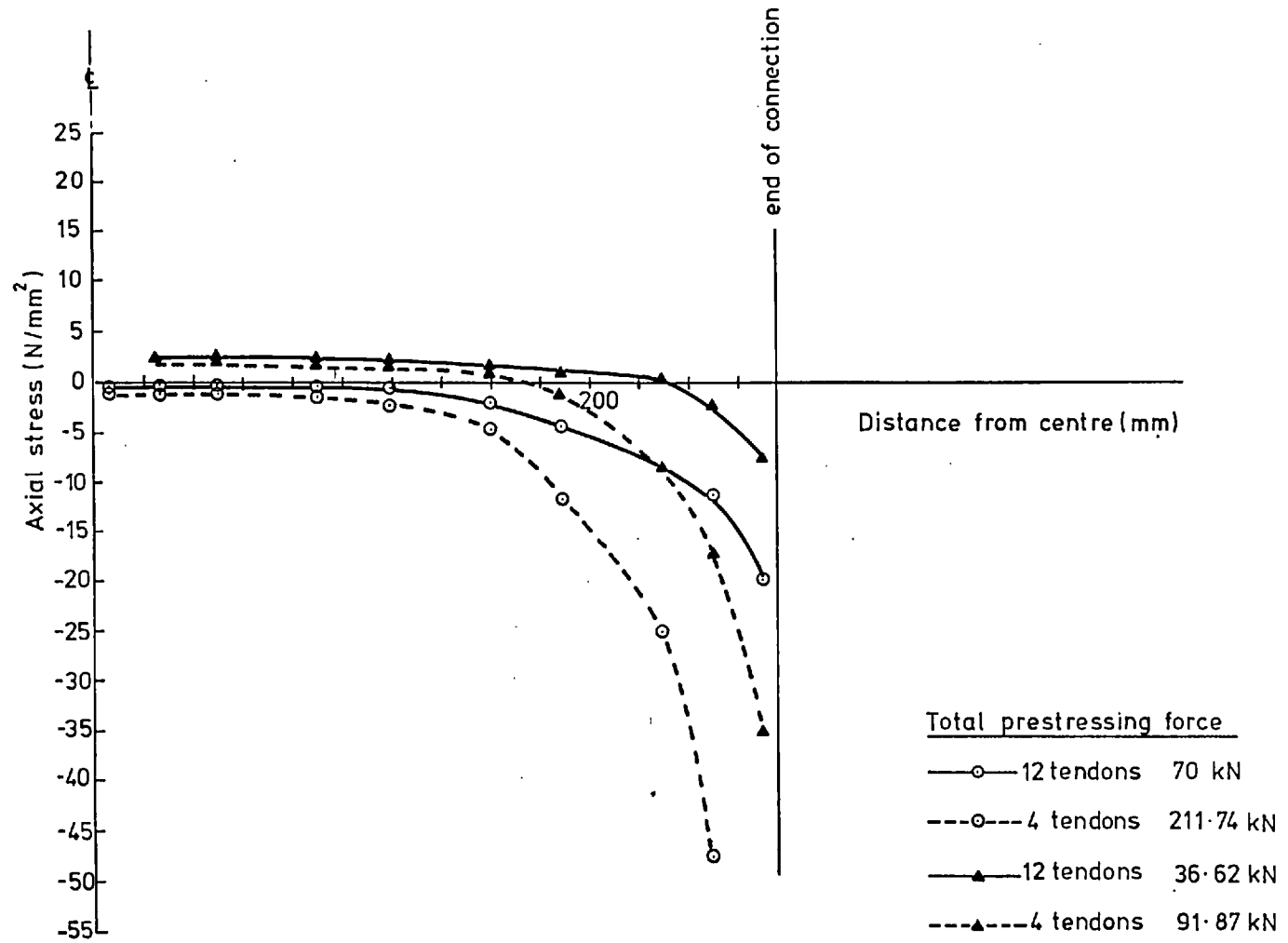
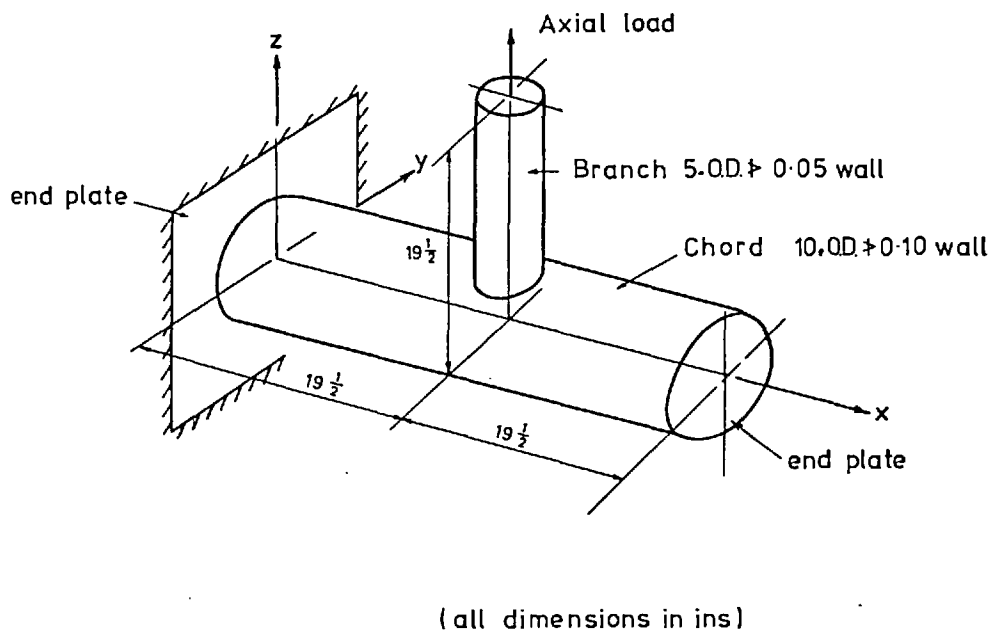


Fig (5,12) Stress concentration factor versus prestressing force

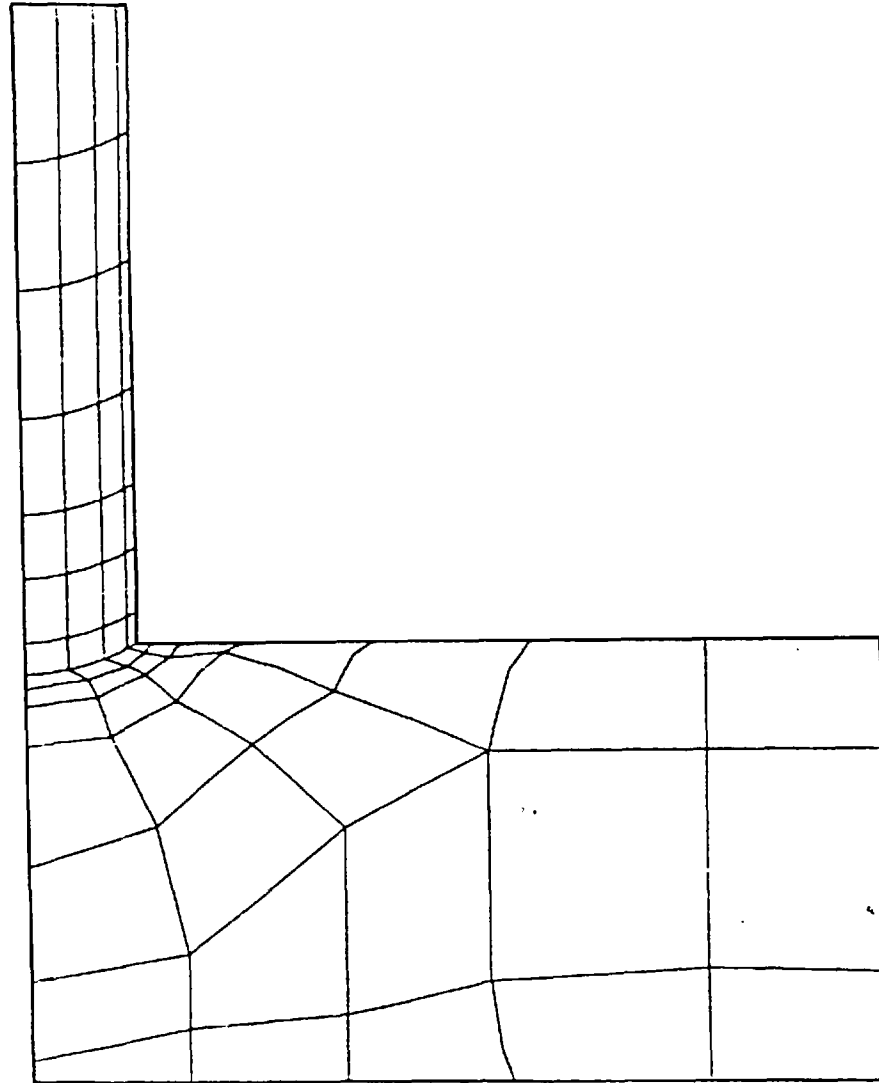




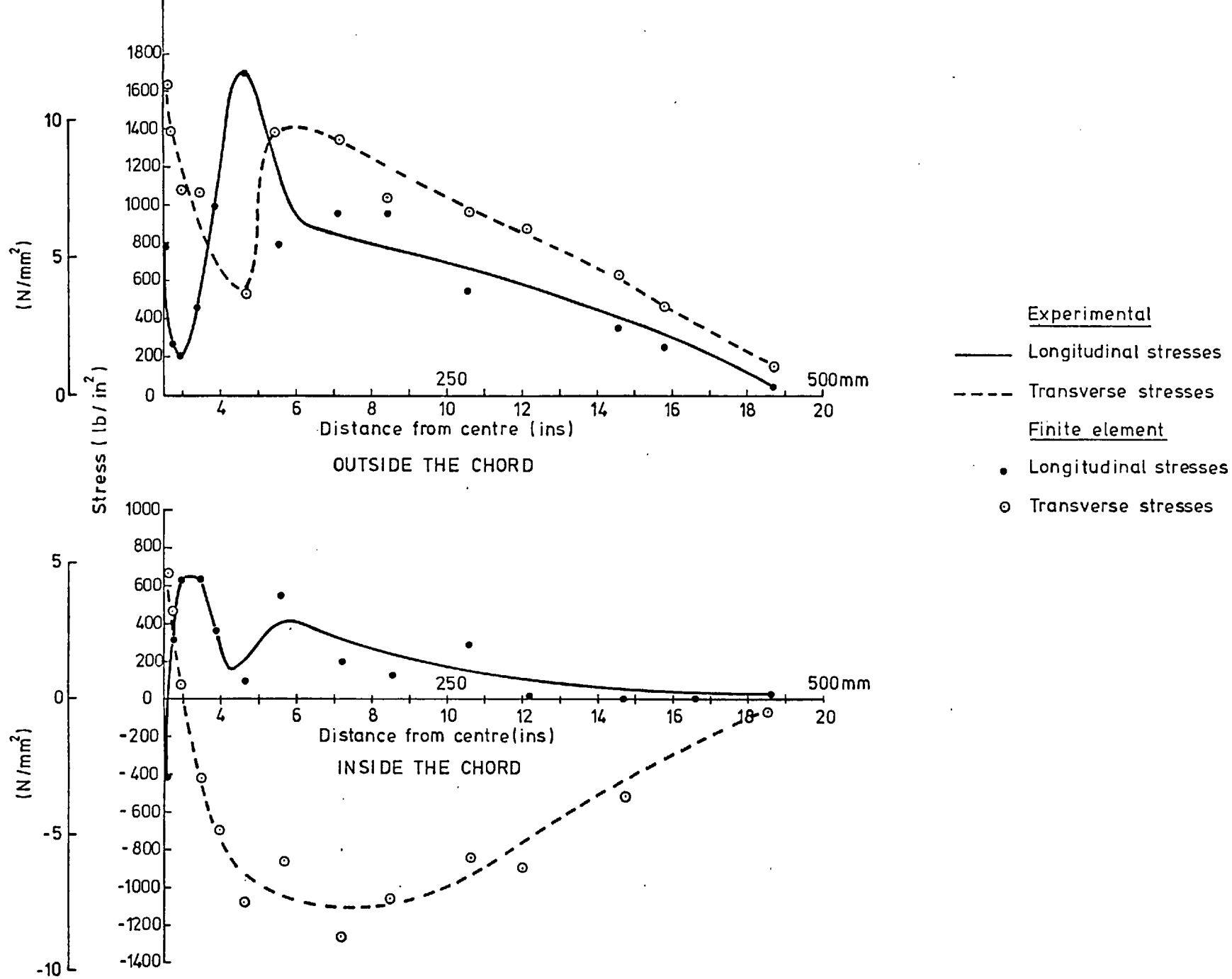
Fig(5,13) Axial stress of concrete



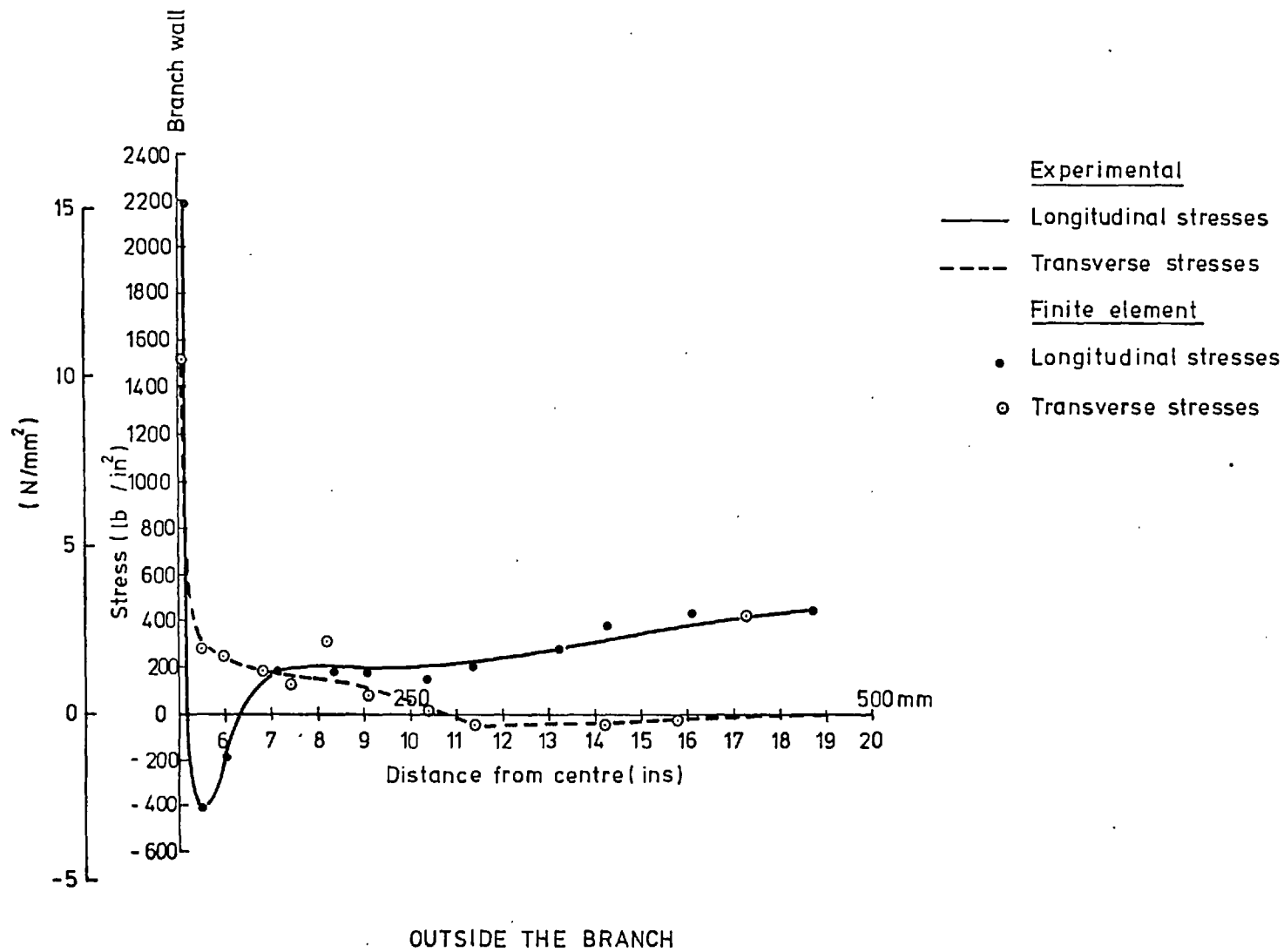
Fig(5,14)Dimensions and loading of the T- joint



Fig(5,15)Welded T-joint ,mesh idealization



Fig(5,16) Stresses for branch axial load 0° line



Fig(5,17 ) Stresses for branch axial load case in branch

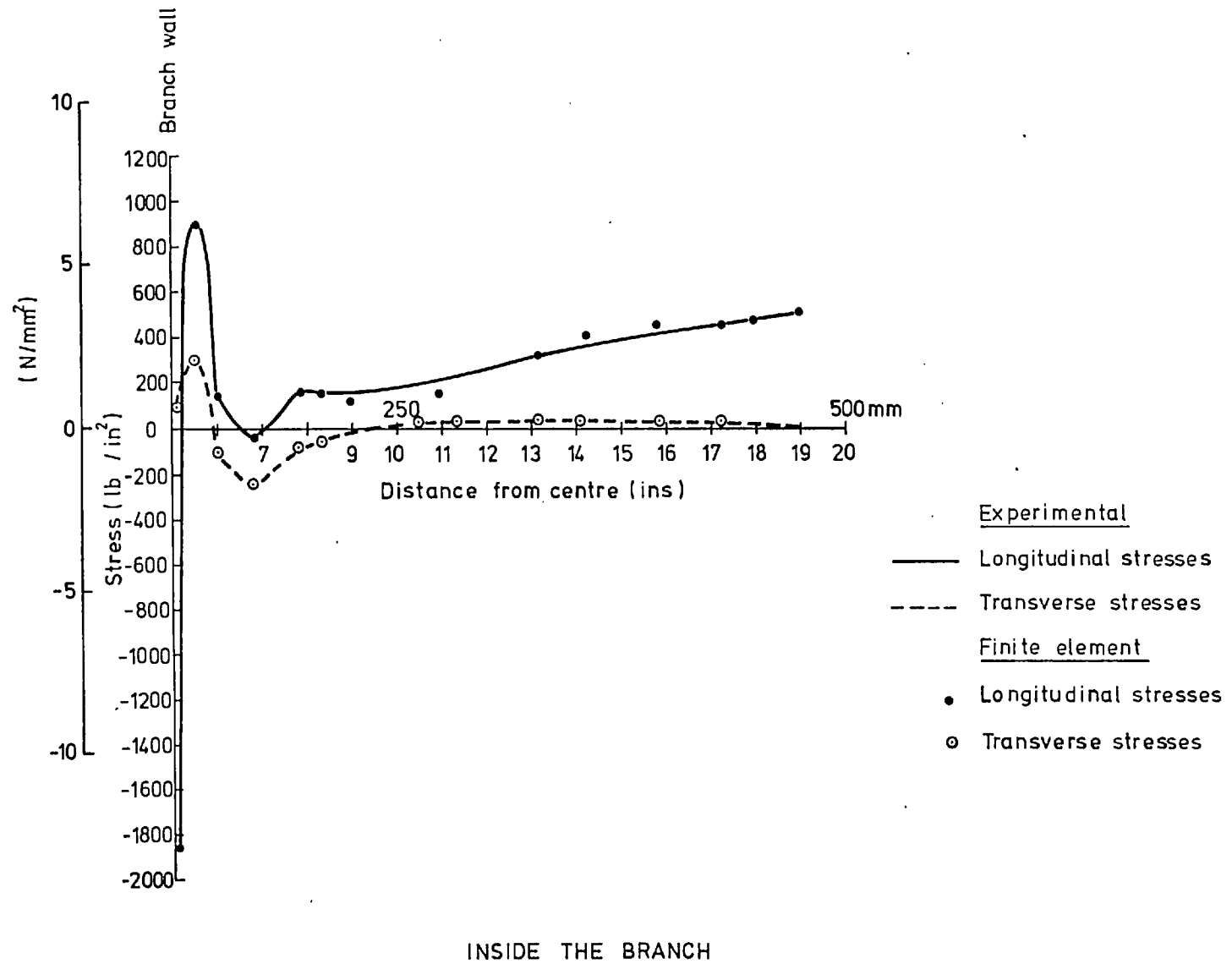
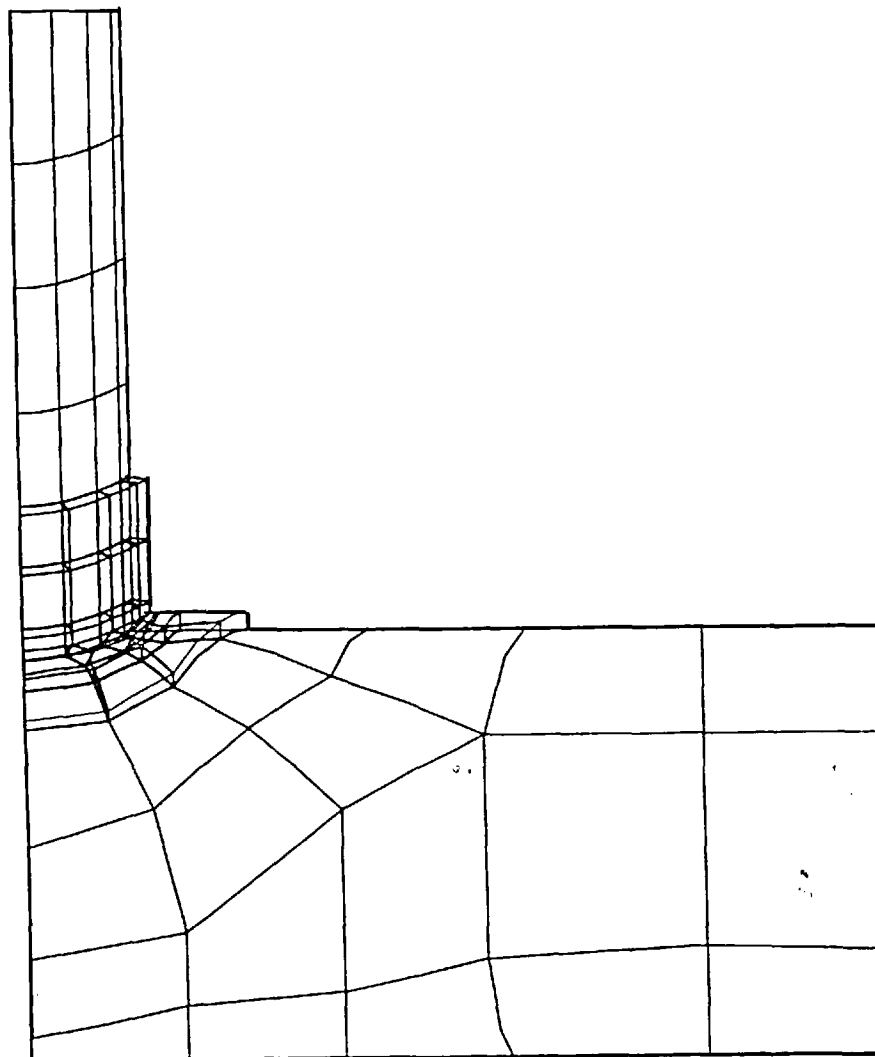
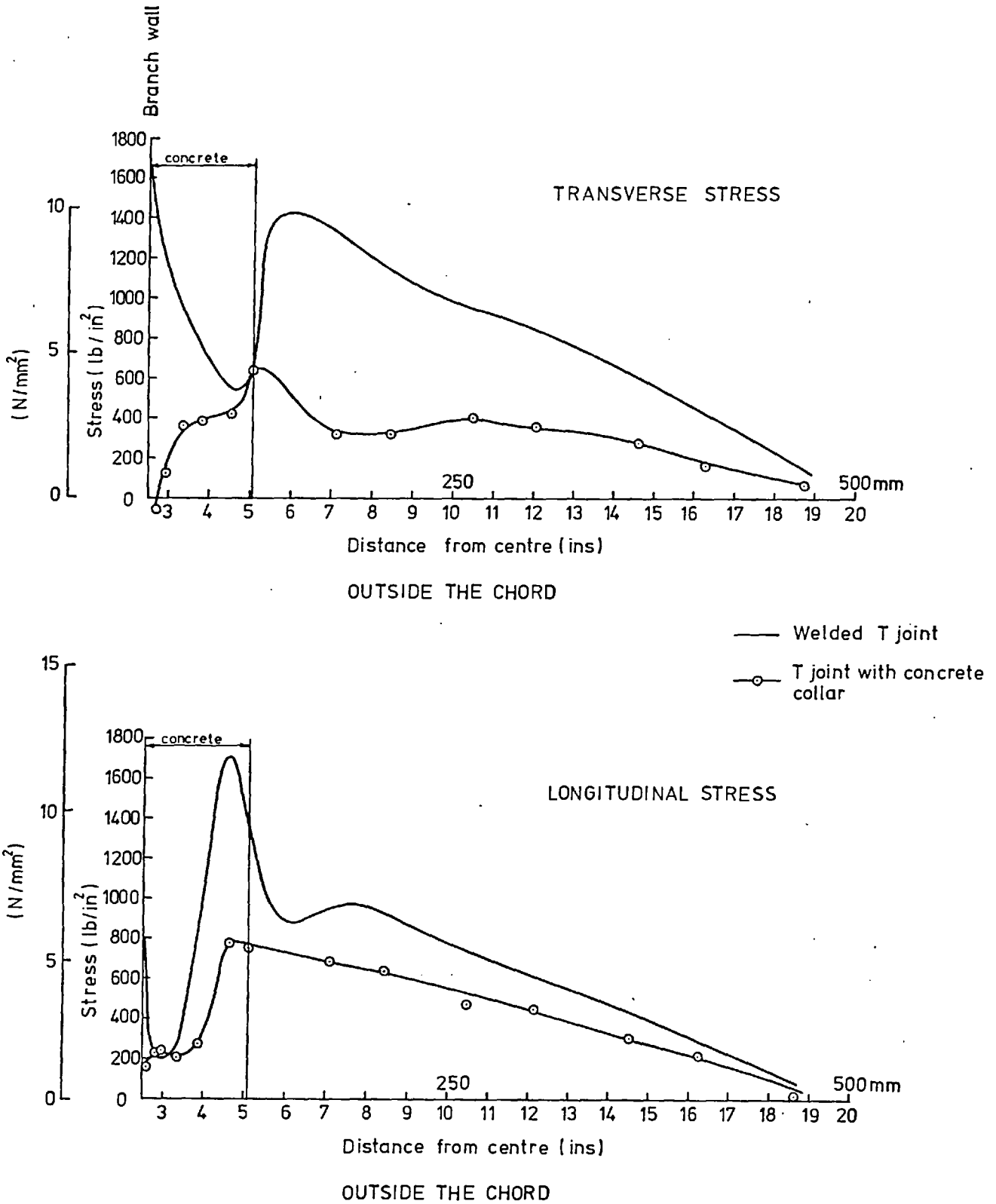


Fig (5,18) Stresses for branch axial load case in branch



Fig(5,19) T-joint with concrete collar ,mesh idealization



Fig(5,20) Chord stresses along (0 line)



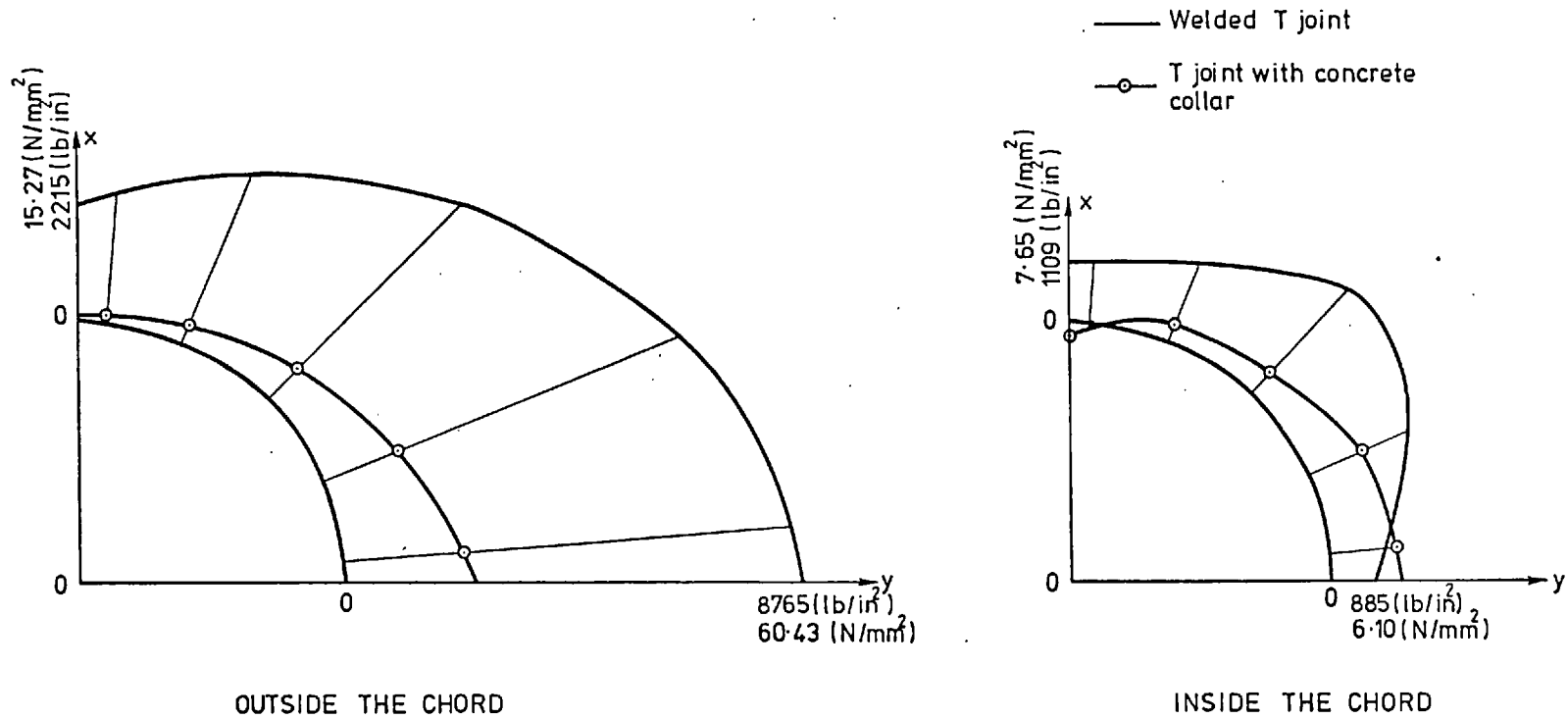
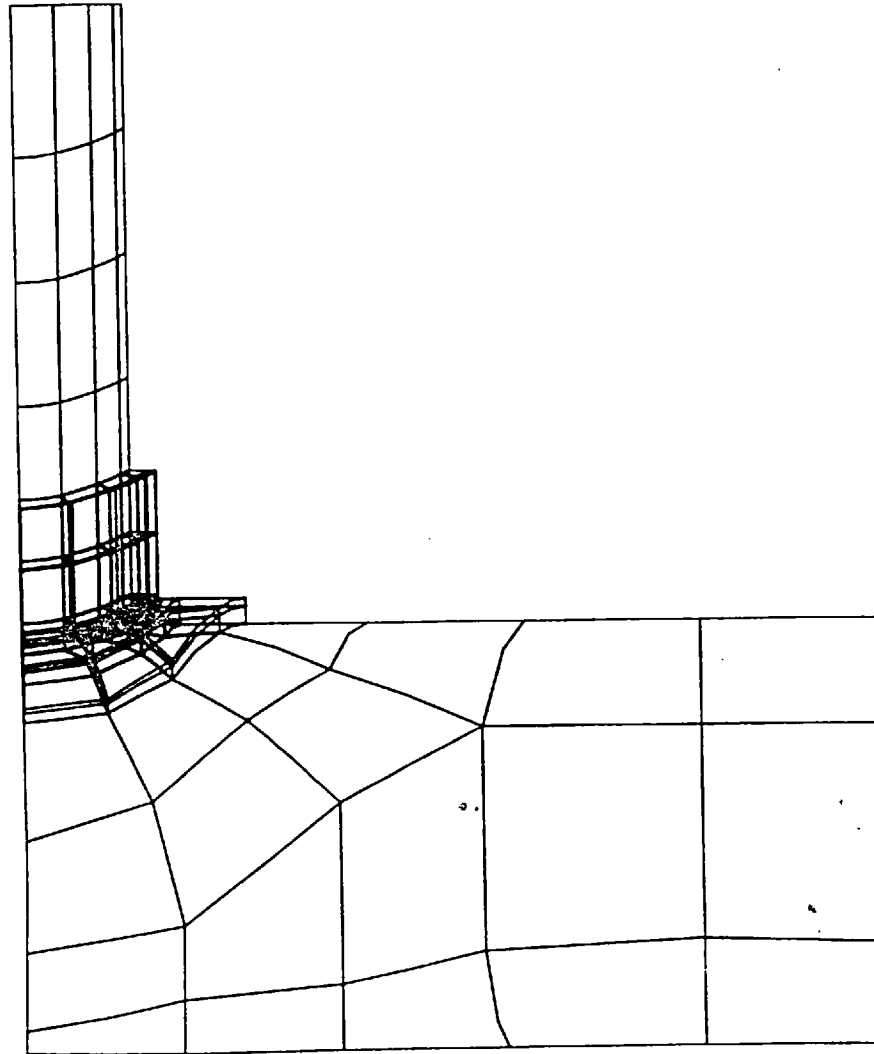
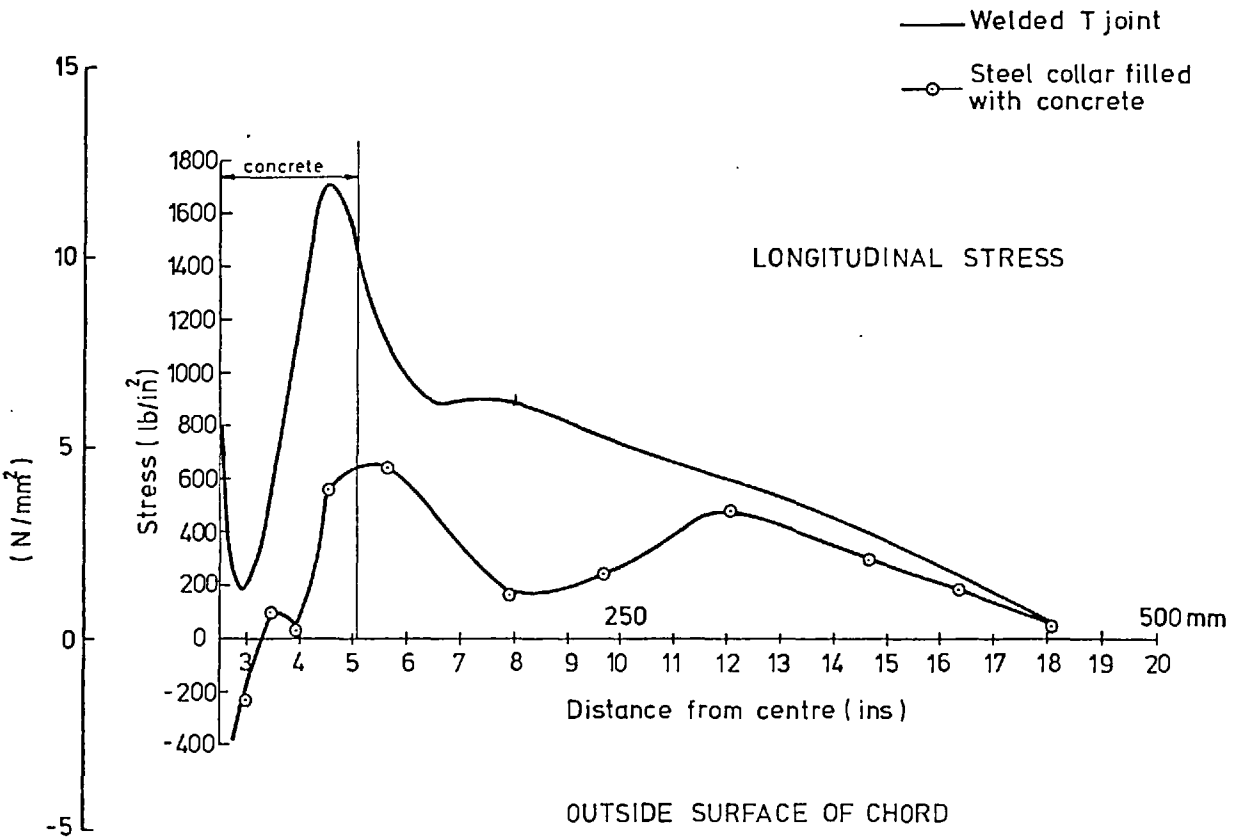
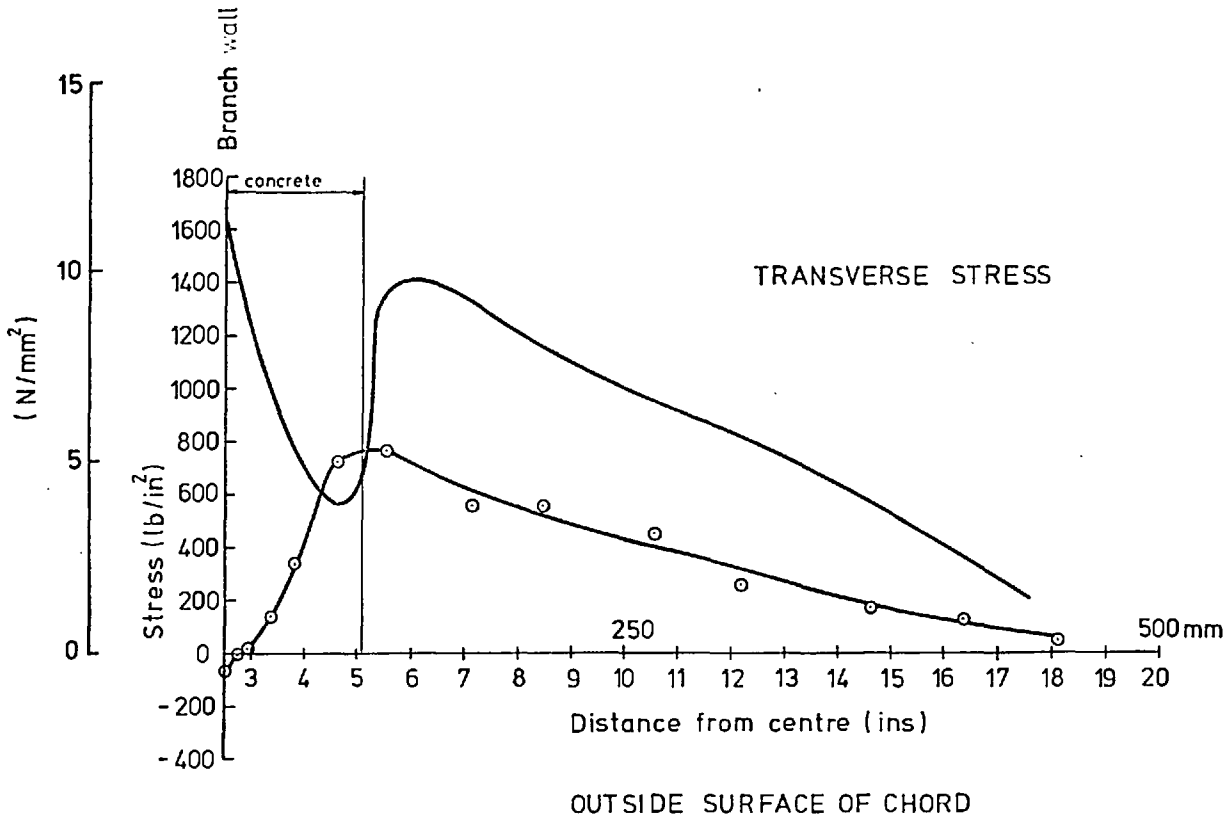


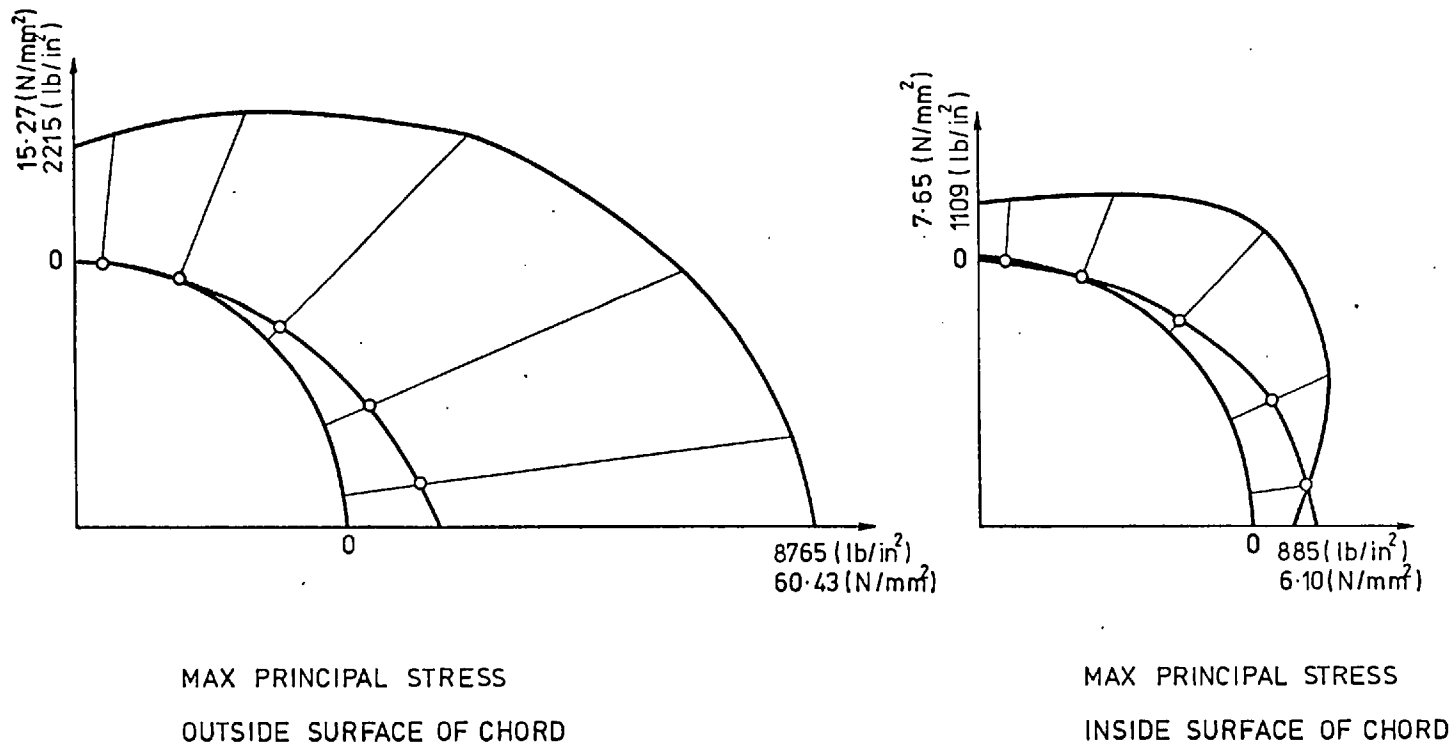
Fig (5,21) Variation of maximum principal stresses around intersection line



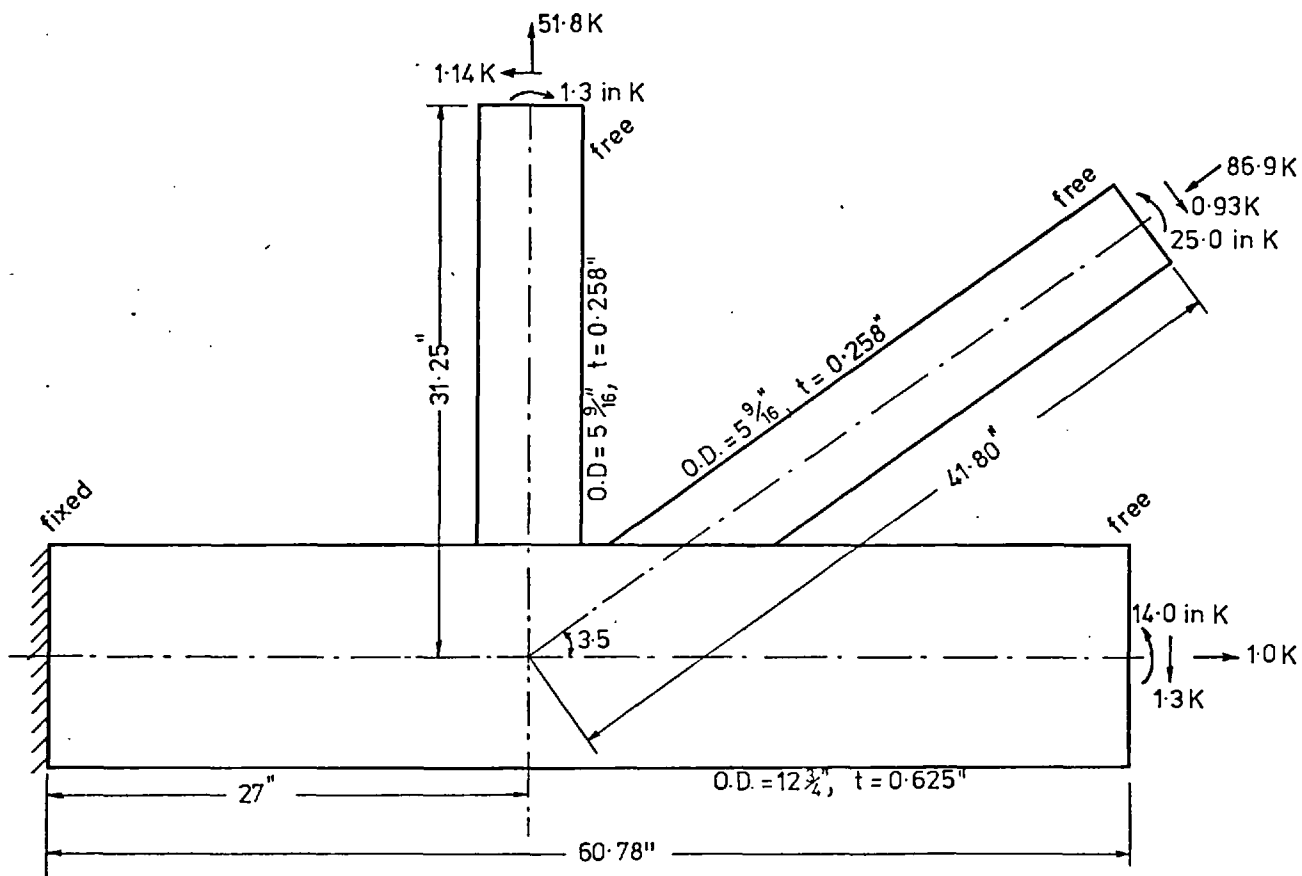
Fig(5,22)T-joint with steel collar filled with concrete  
,mesh idealization



Fig(5,23) T. Joint with steel collar filled with concrete. Stress variation along 0 line



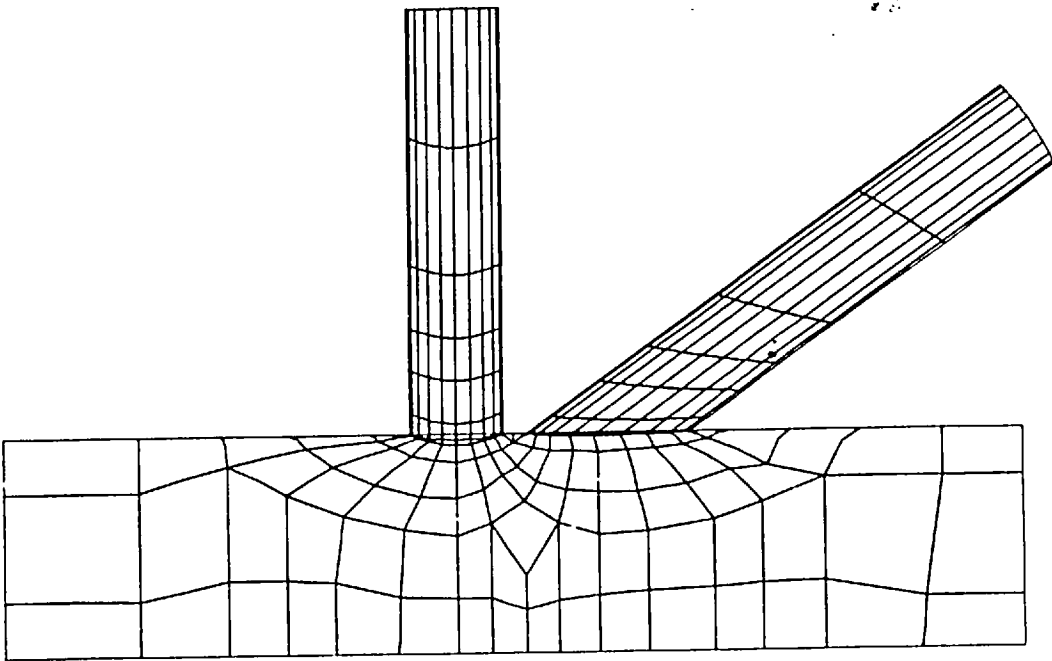
Fig(5,24) Variation of principal stresses around intersection line



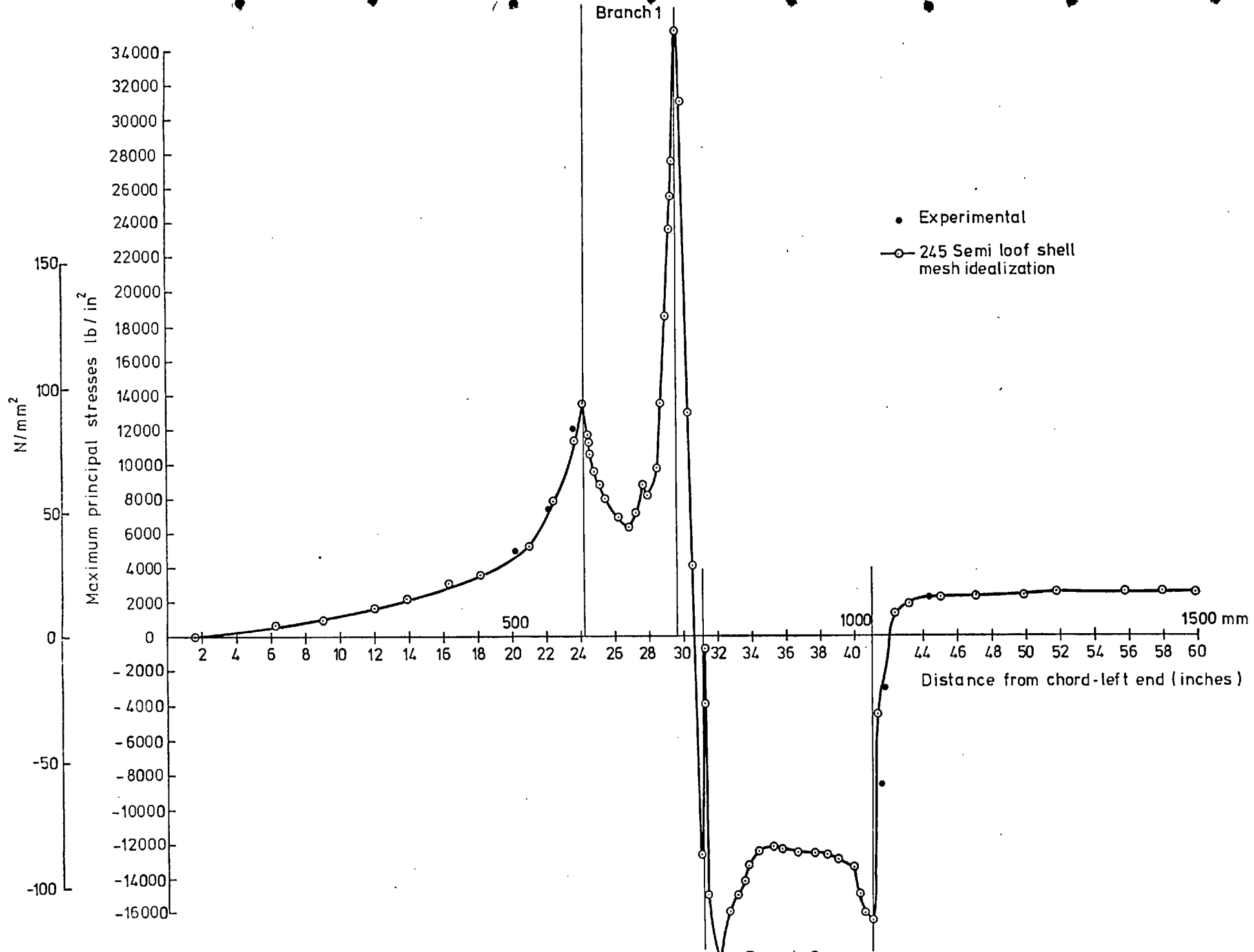
Elastic modulus 29000 Ksi

Poisson ratio 0.3

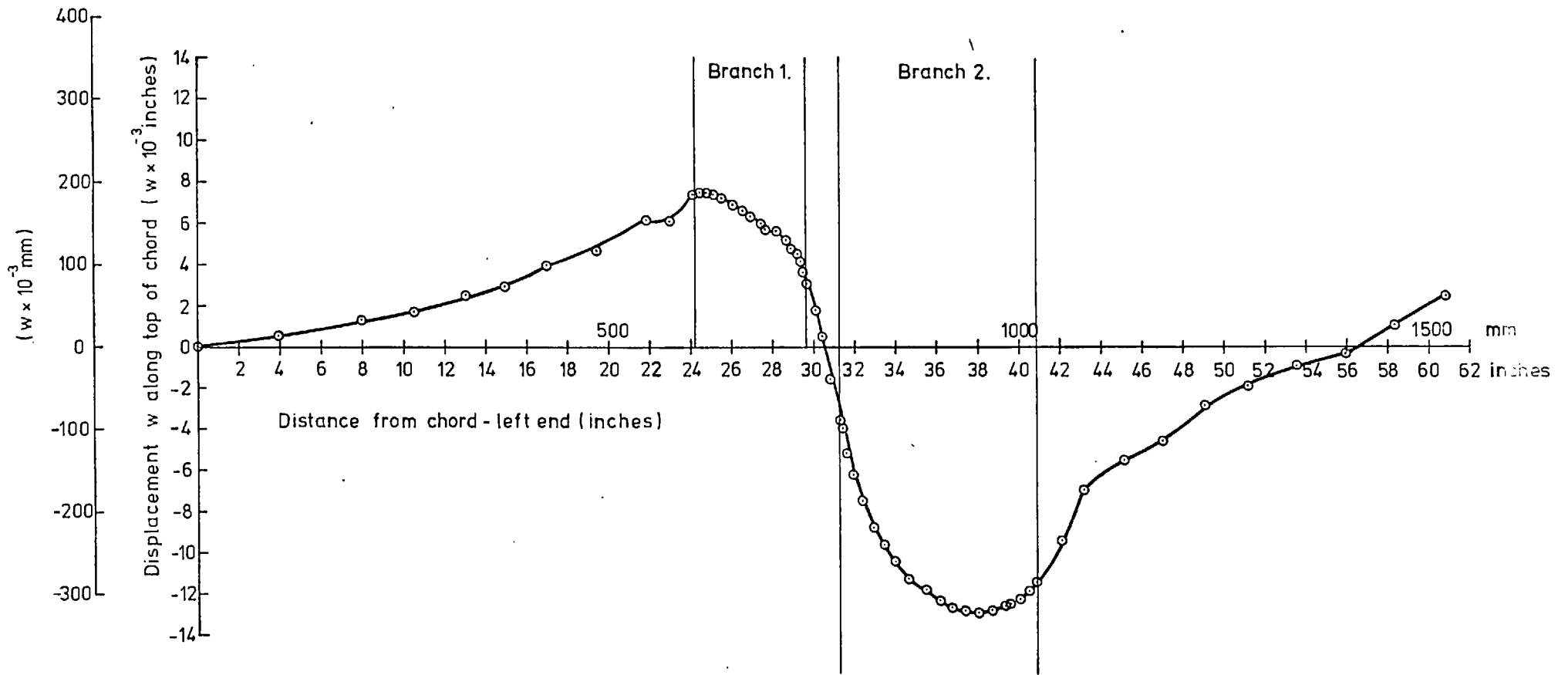
Fig(5,25) K-Joint, boundary condition and loading



Fig(5,26) K - joint , mesh idealization

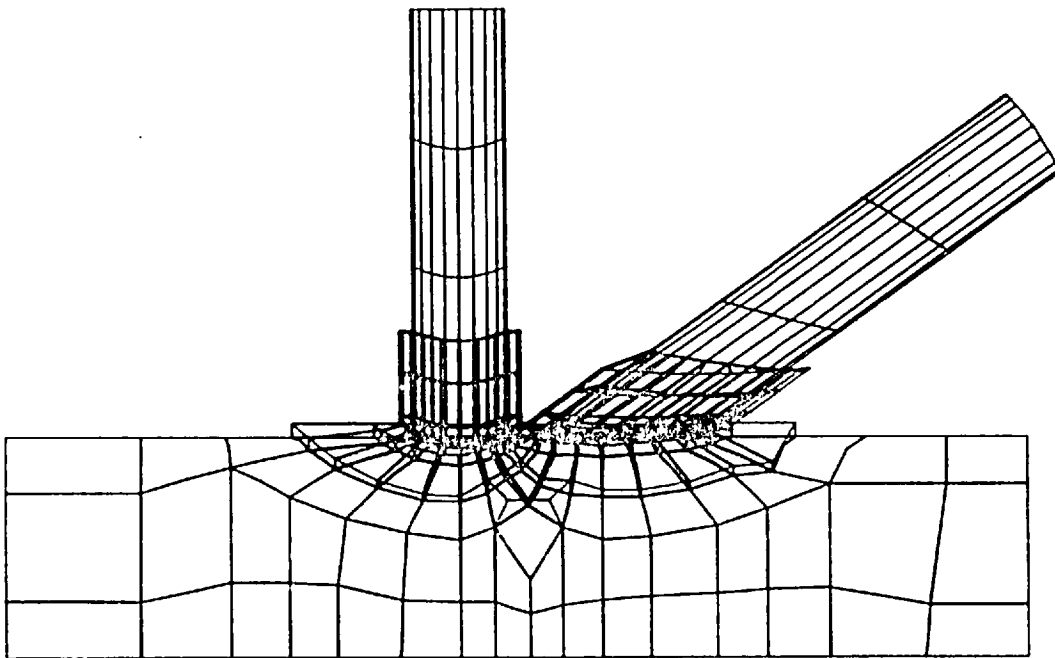


Fig(5,27) Chord surface stresses (along top of chord)



Fig(5,28) Displacements w along top of chord





Fig(5,29)Composite K-joint, mesh idealization

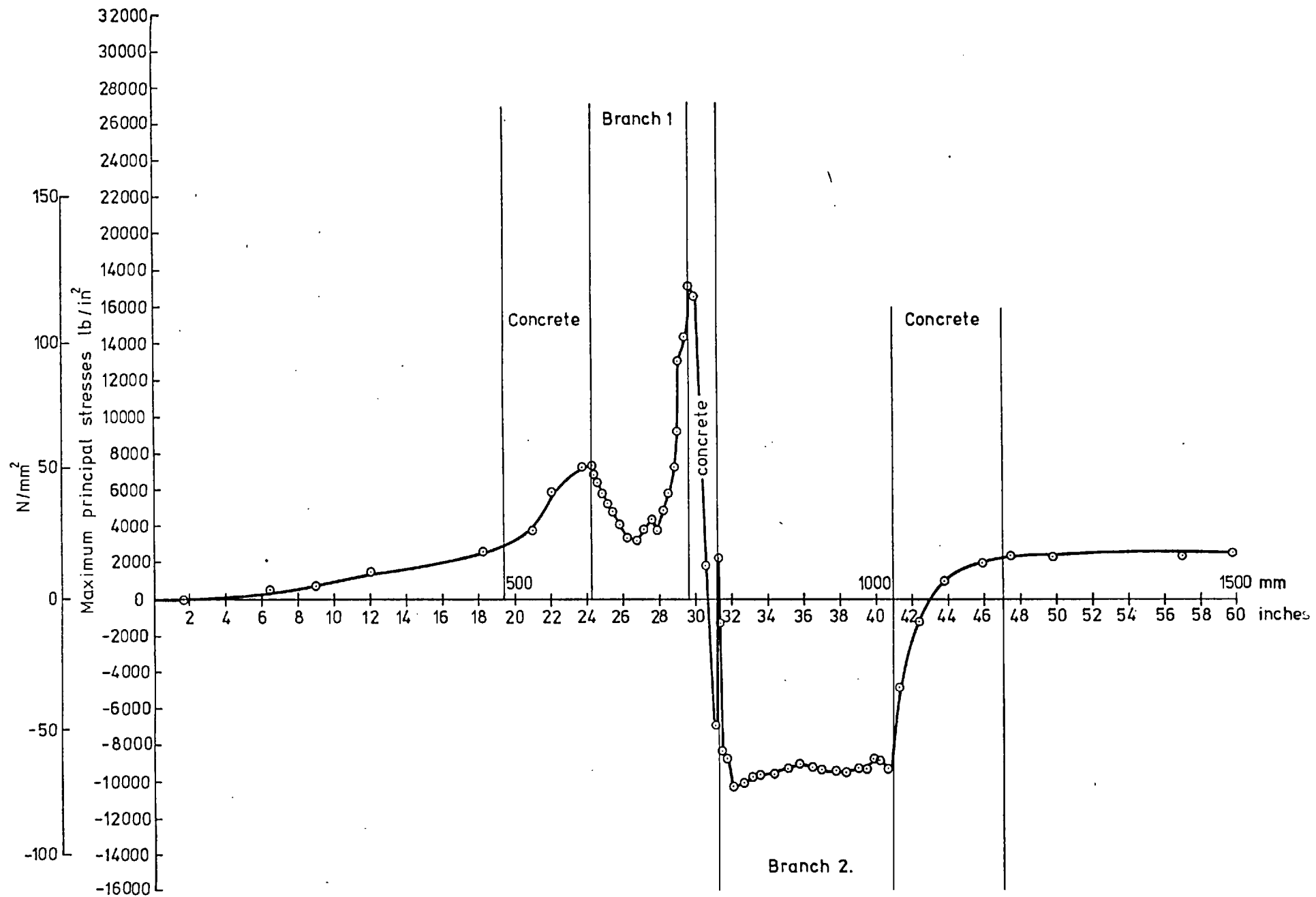


Fig (5.30) Chord surface stresses ( Along top of chord )

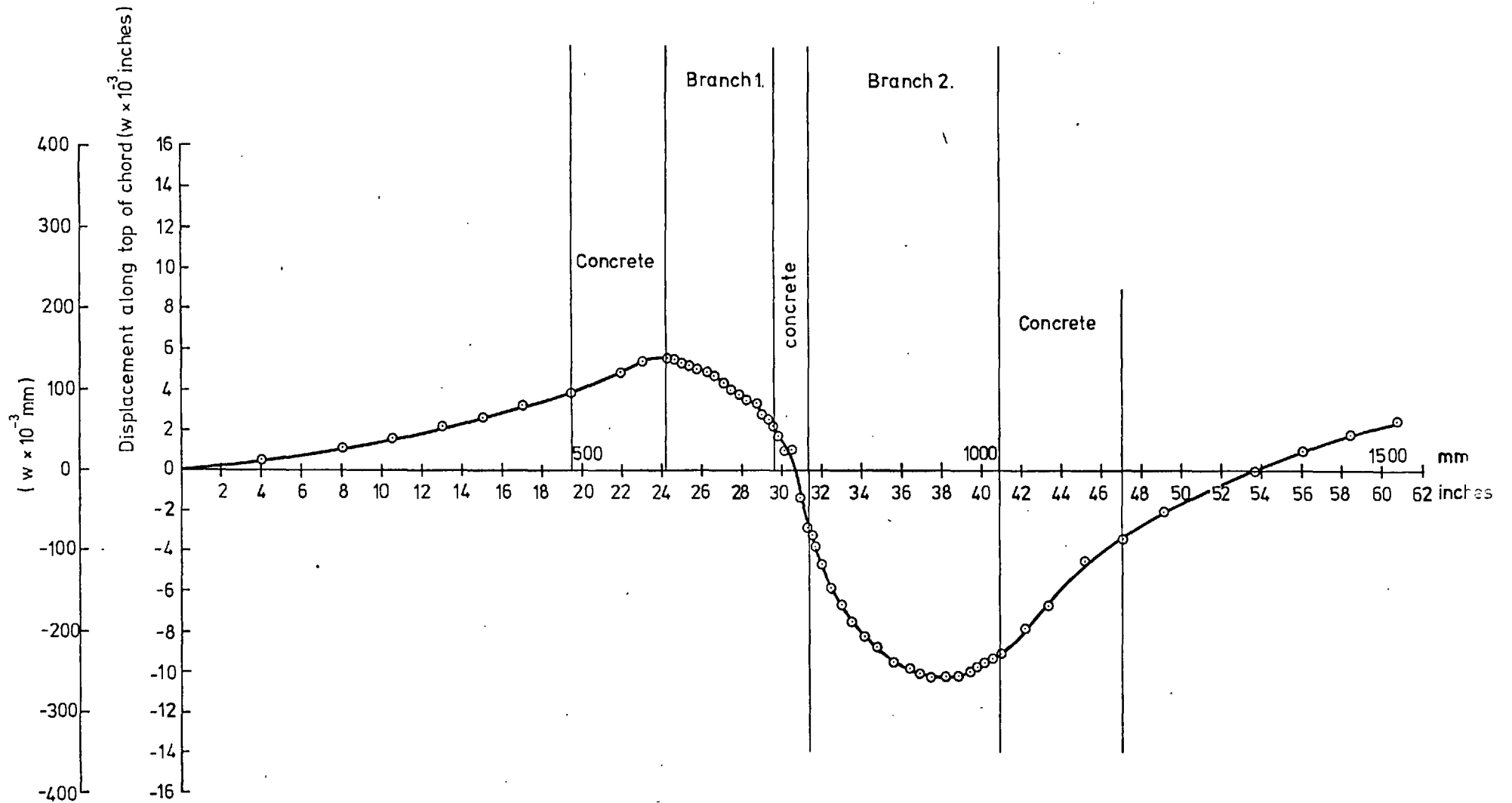
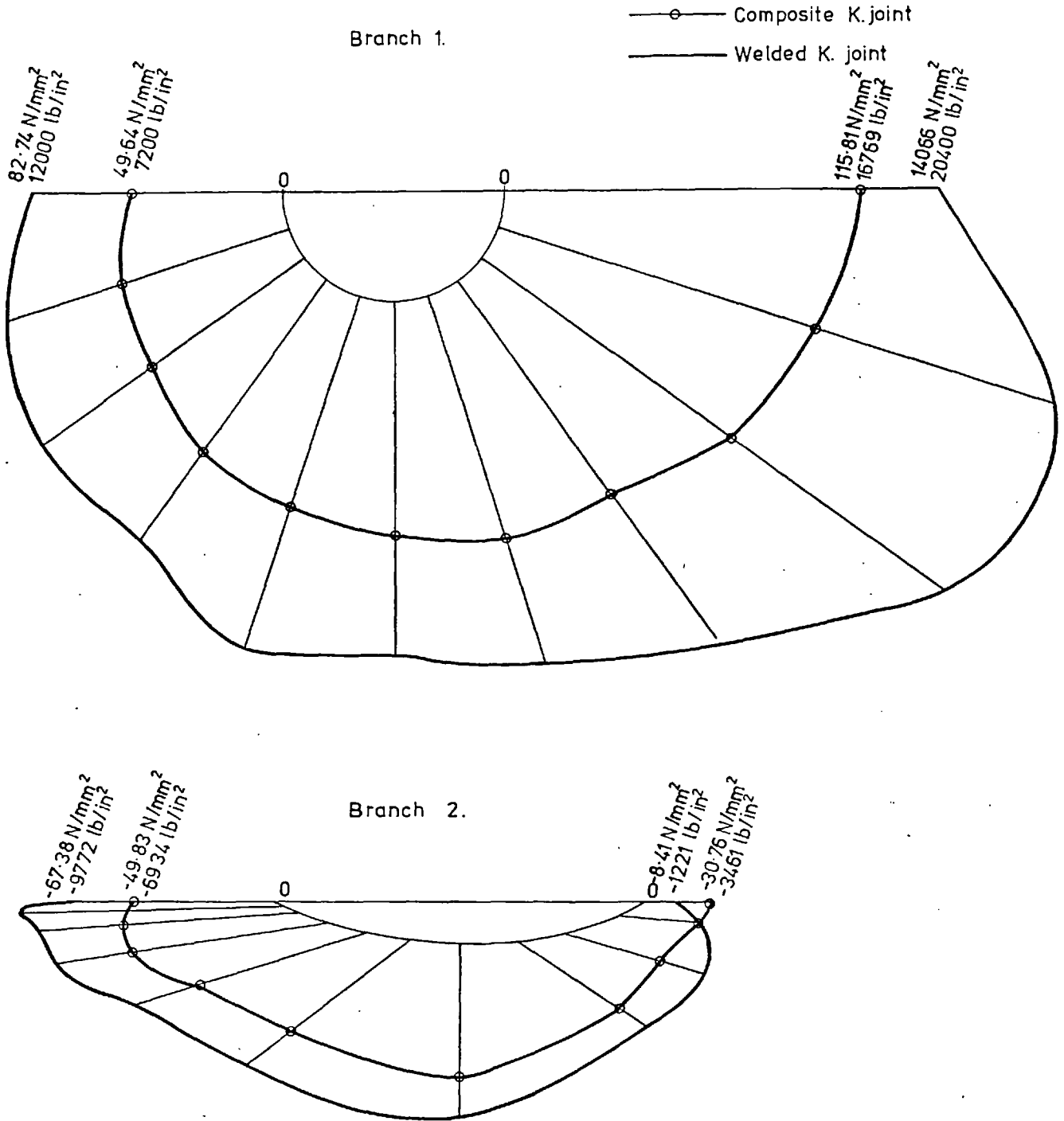
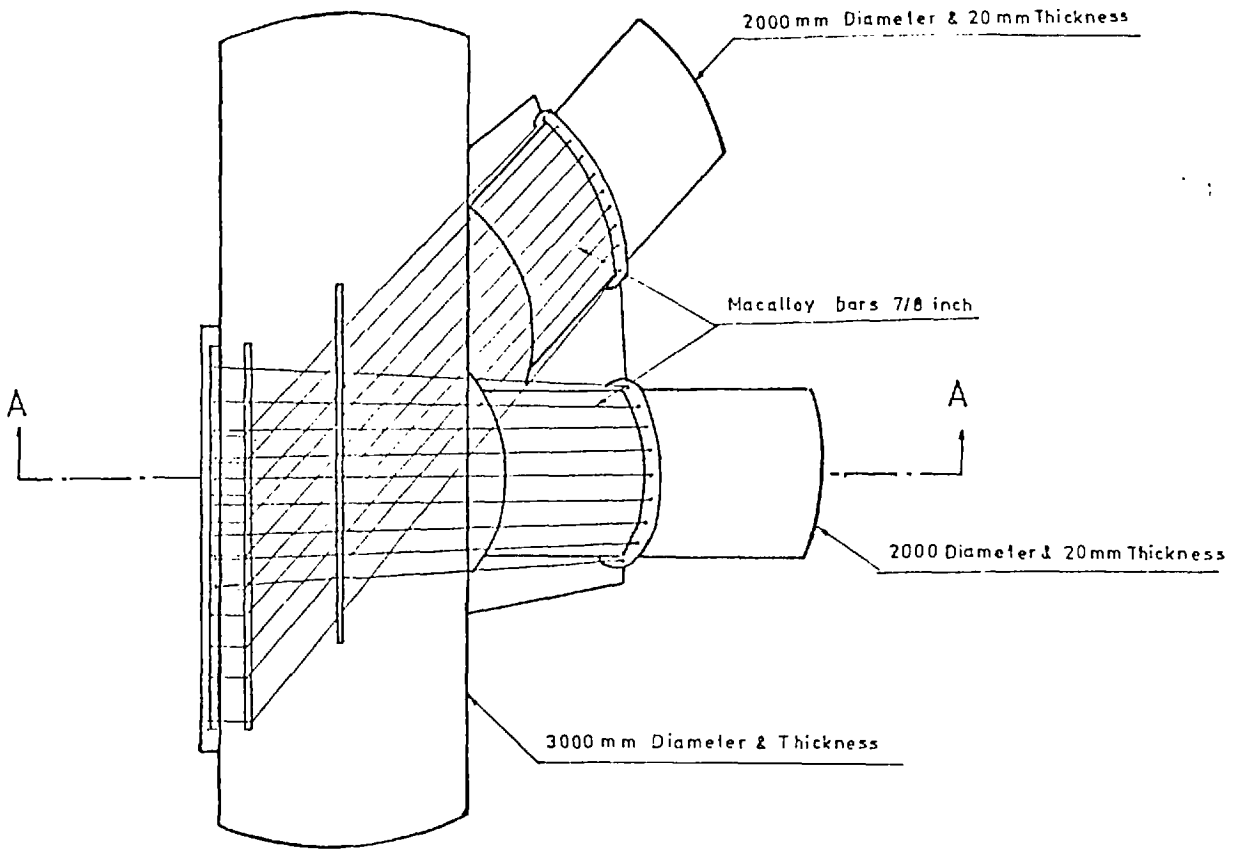


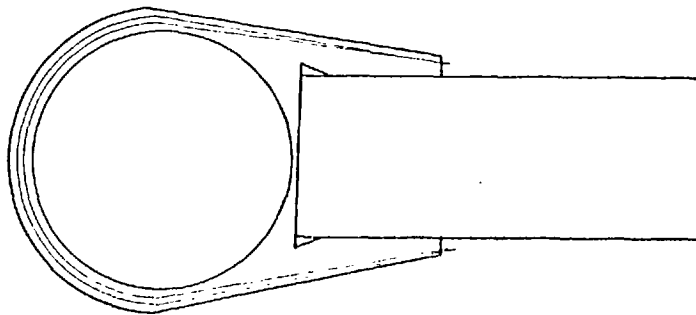
Fig (5,31 ) Displacement w along top of chord



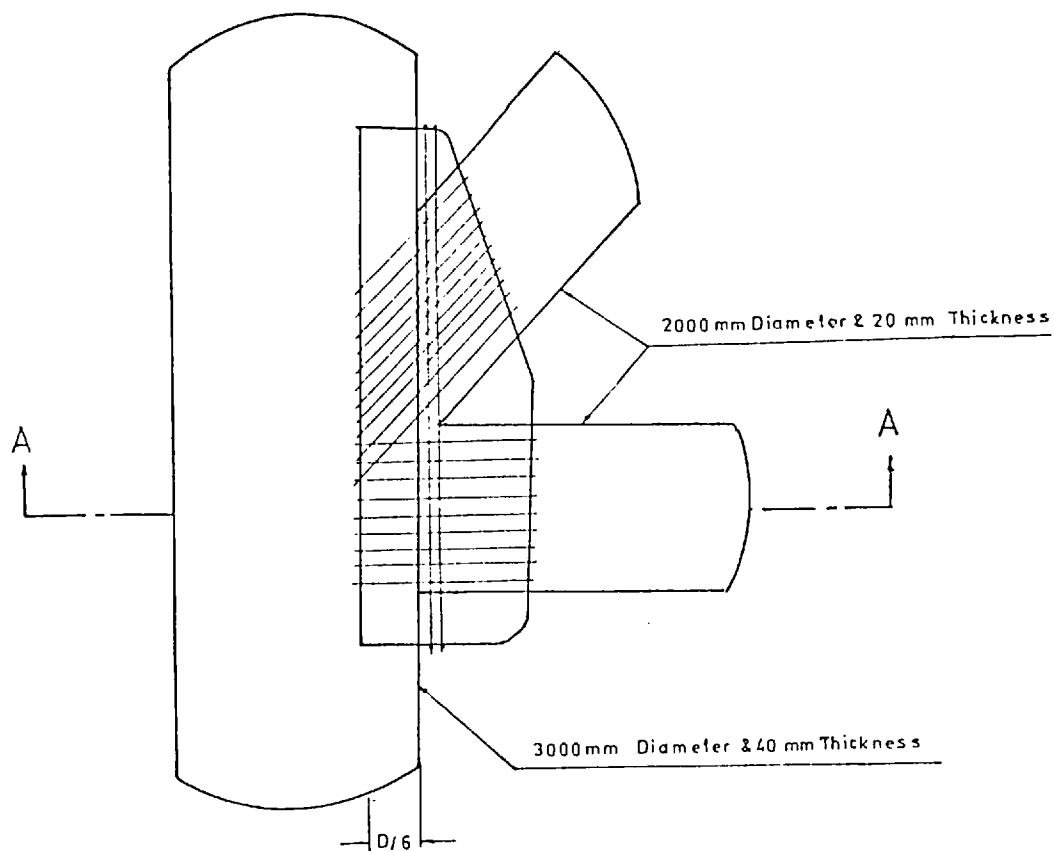
Fig(5,32) Variation of maximum principal stresses around the intersection lines



Section A - A



Fig(A3,1) Joint I



Section A - A

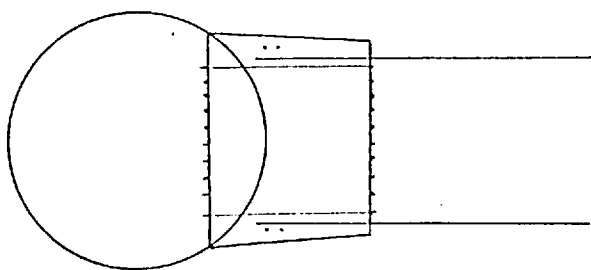
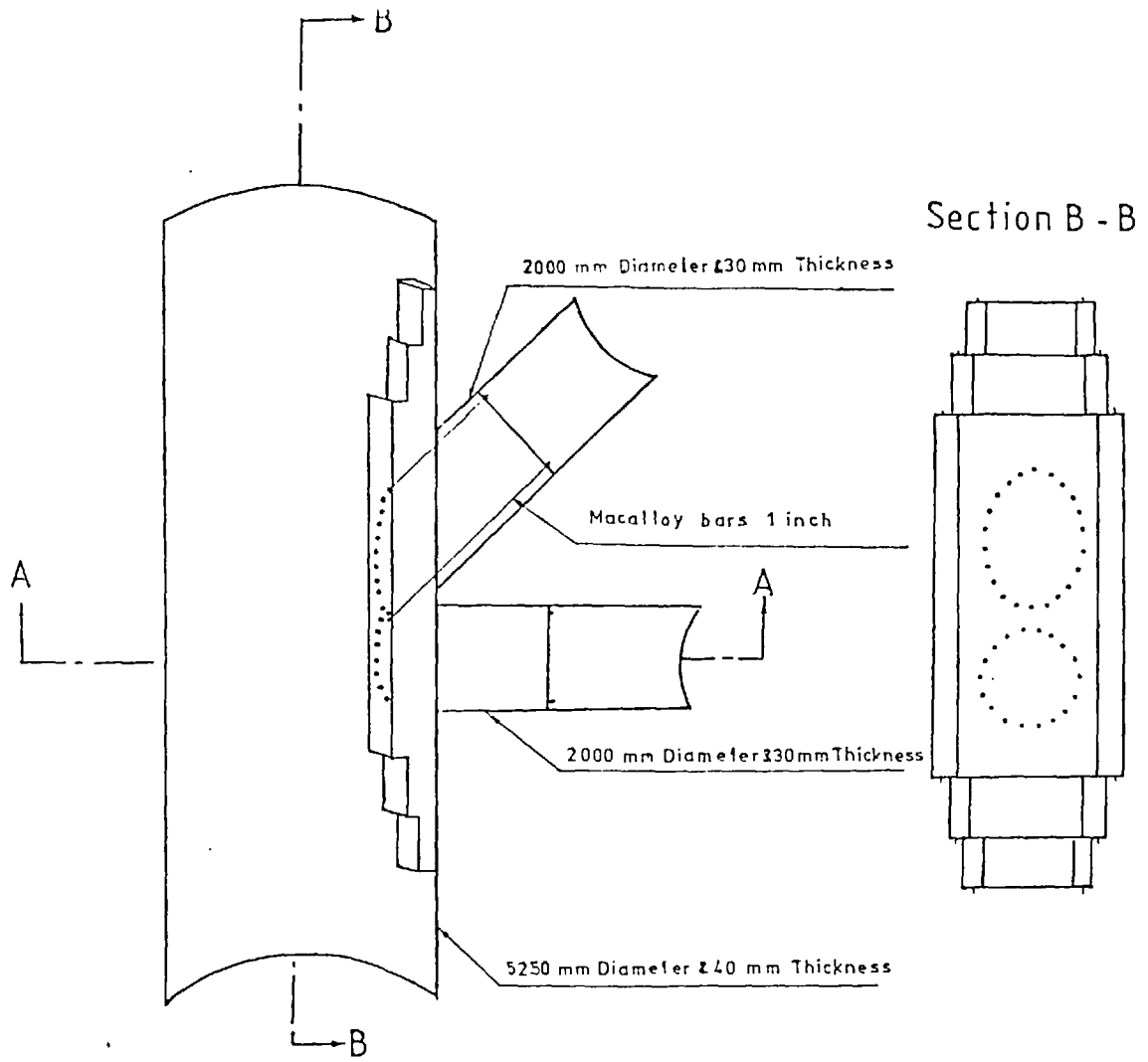
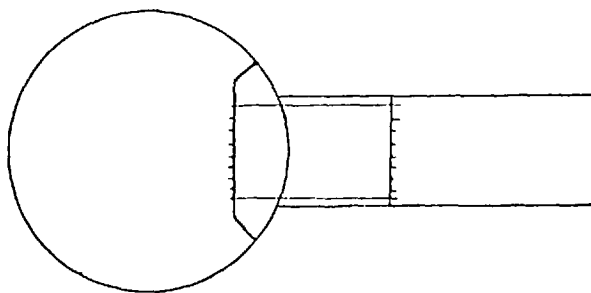


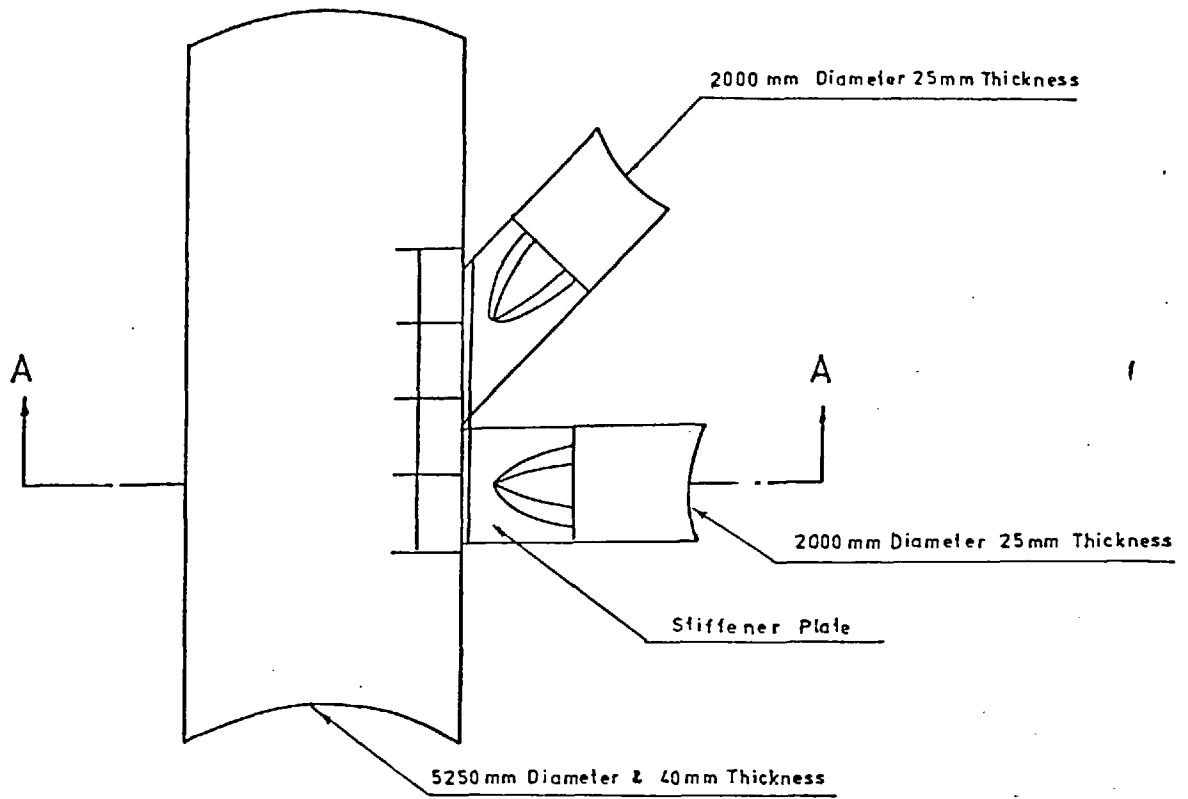
Fig (A 3,2) Joint II (with positive eccentricity  
 $D/6$ )



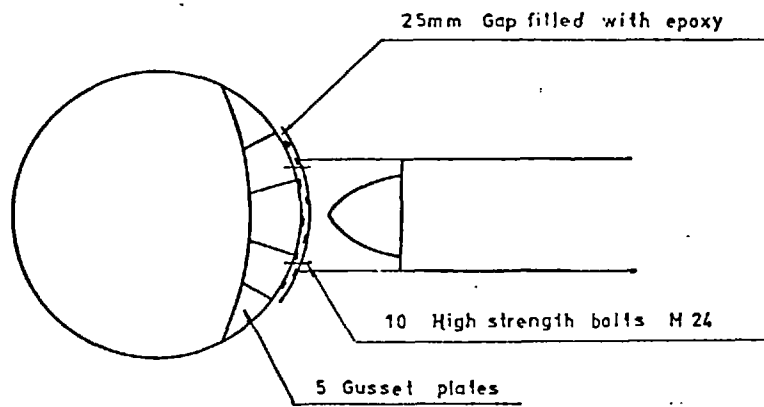
Section A - A



Fig(A3,3) Joint III

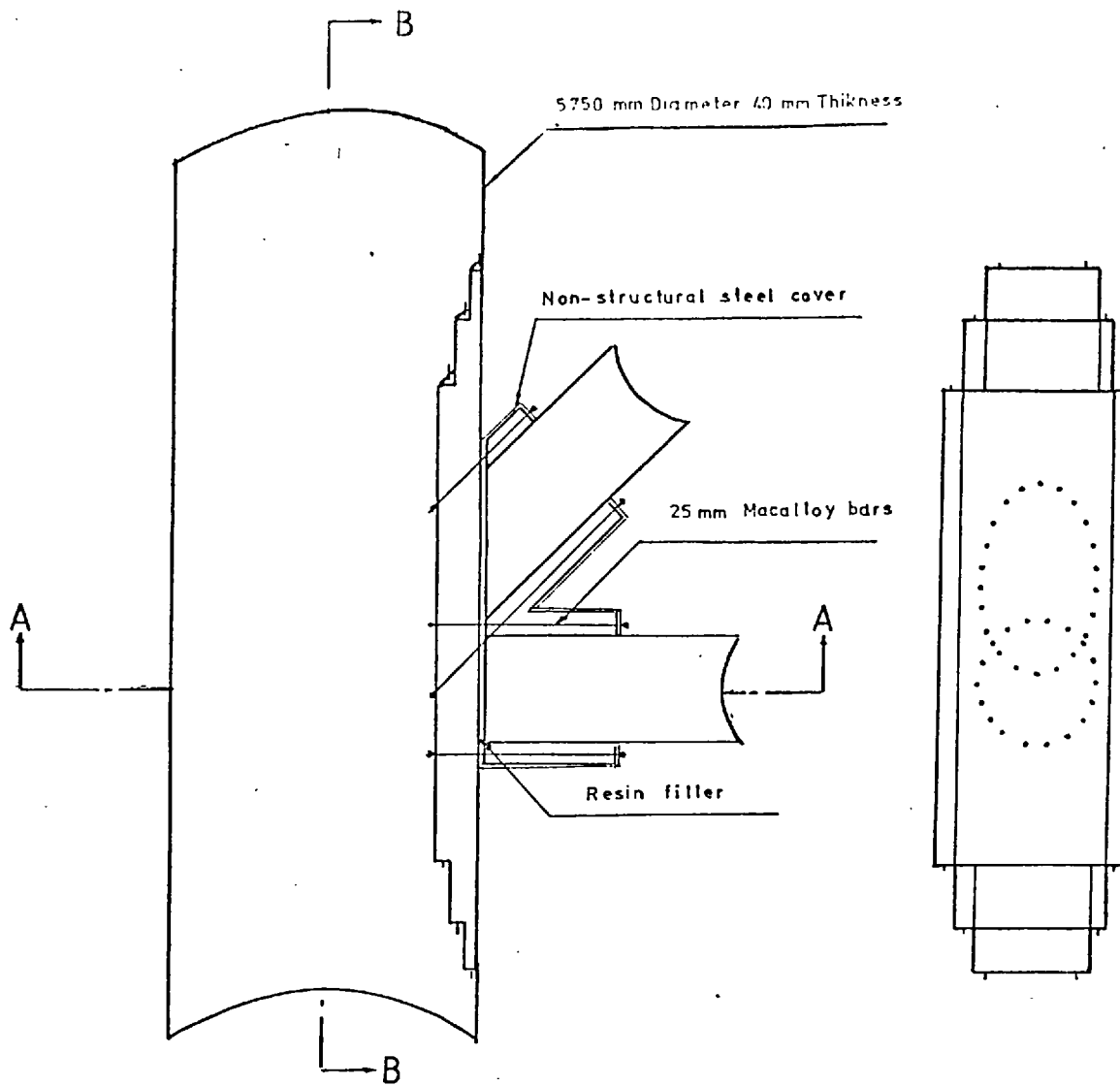


Section A - A

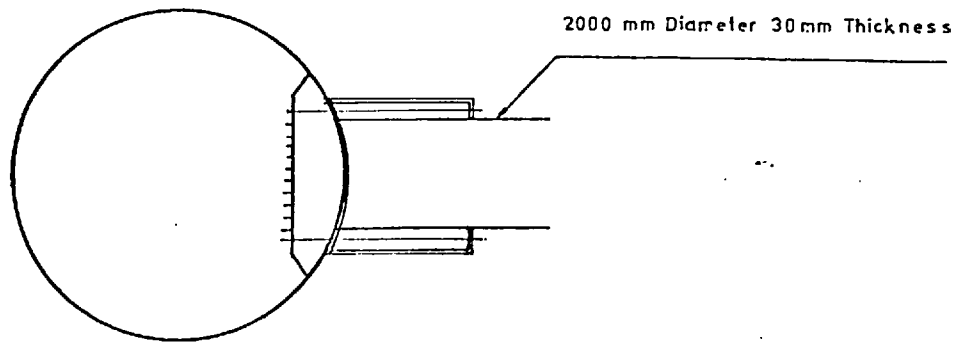


Fig(A3,4) Joint IV





Section A-A



Fig(A3,5) Joint V



Plate 1: Small scale model (Phase 1)

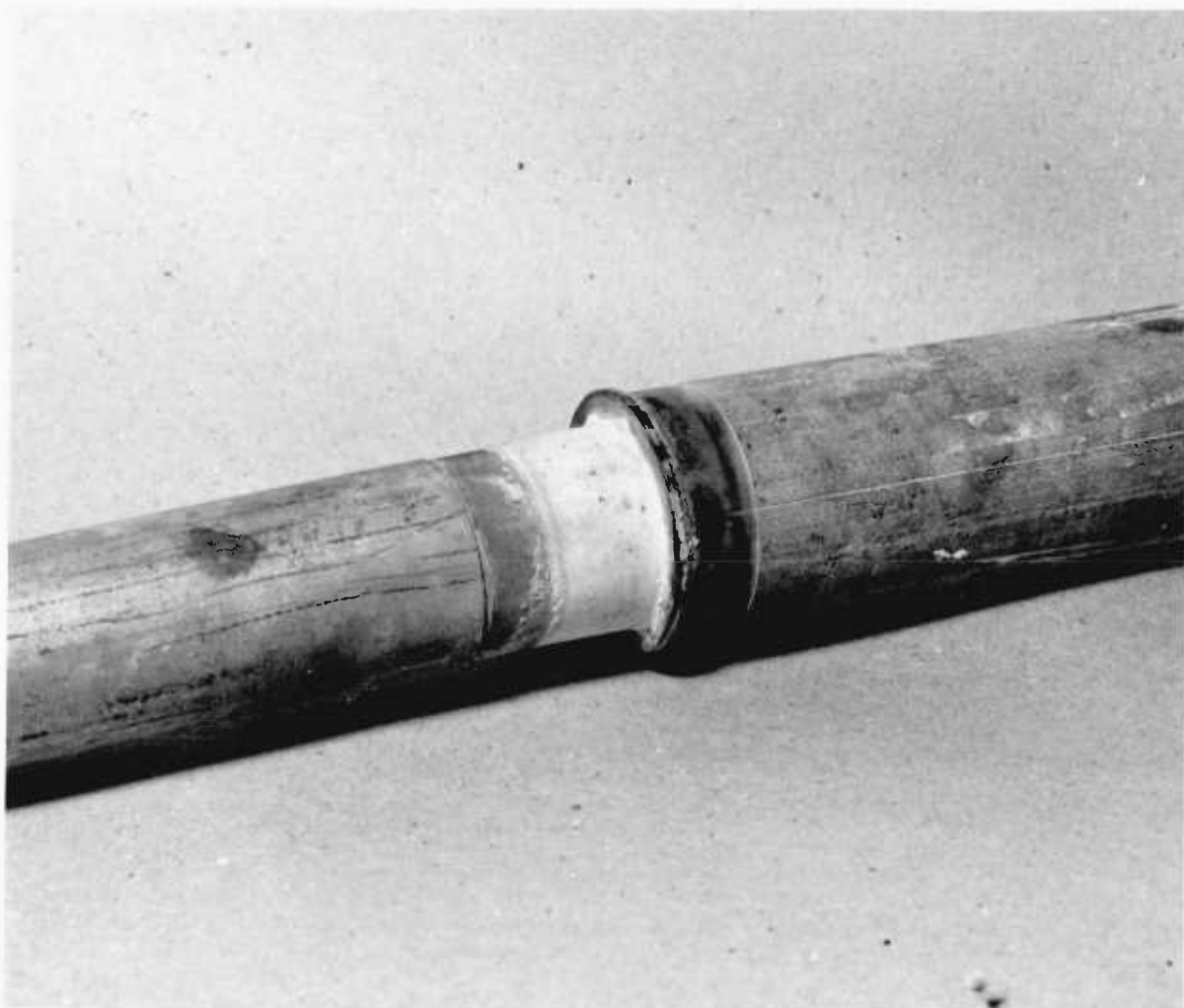


Plate 2: Small scale model with ring welded at the end of sleeve (Phase 2)

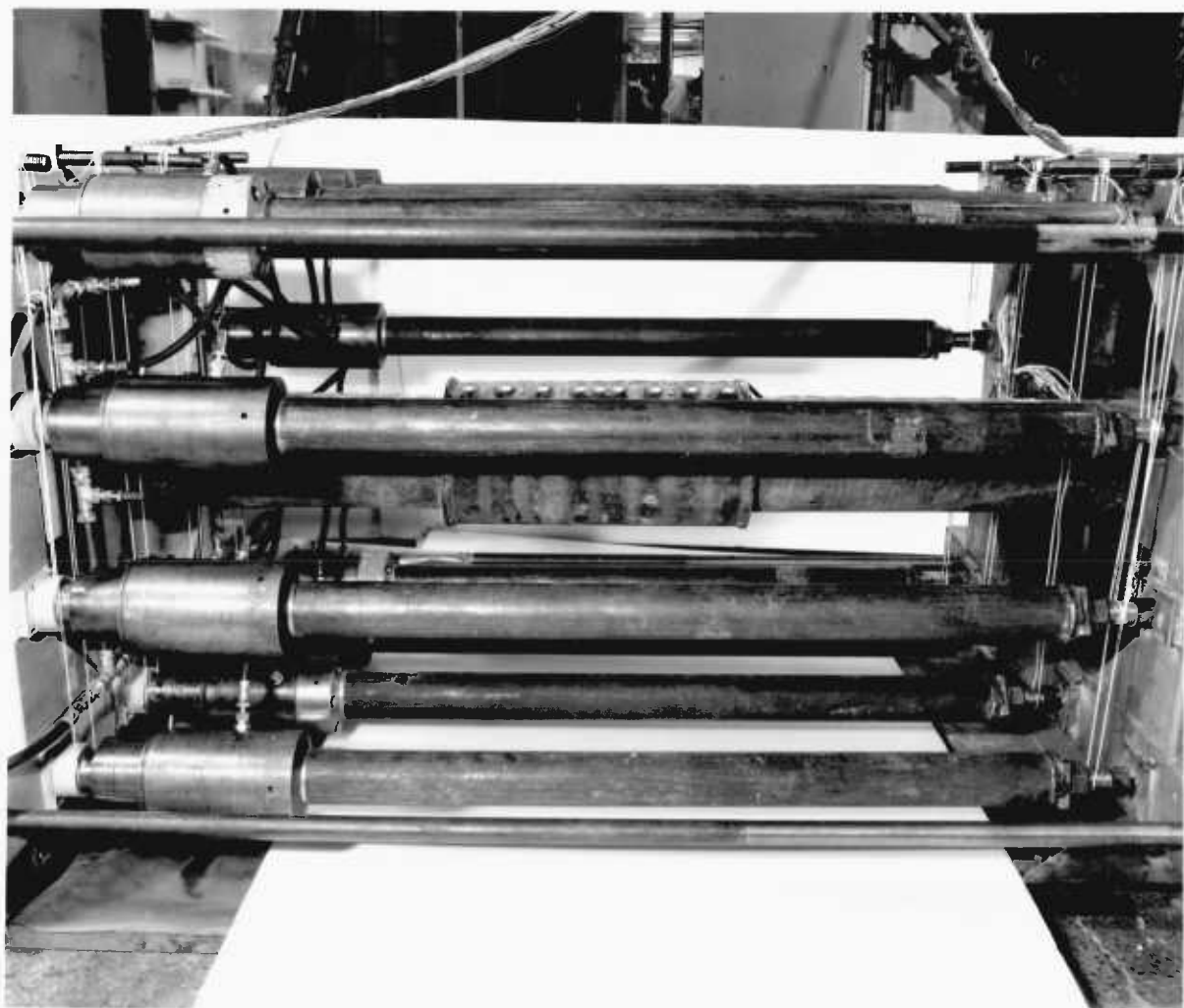


Plate 3: Large scale model (Phase 3)

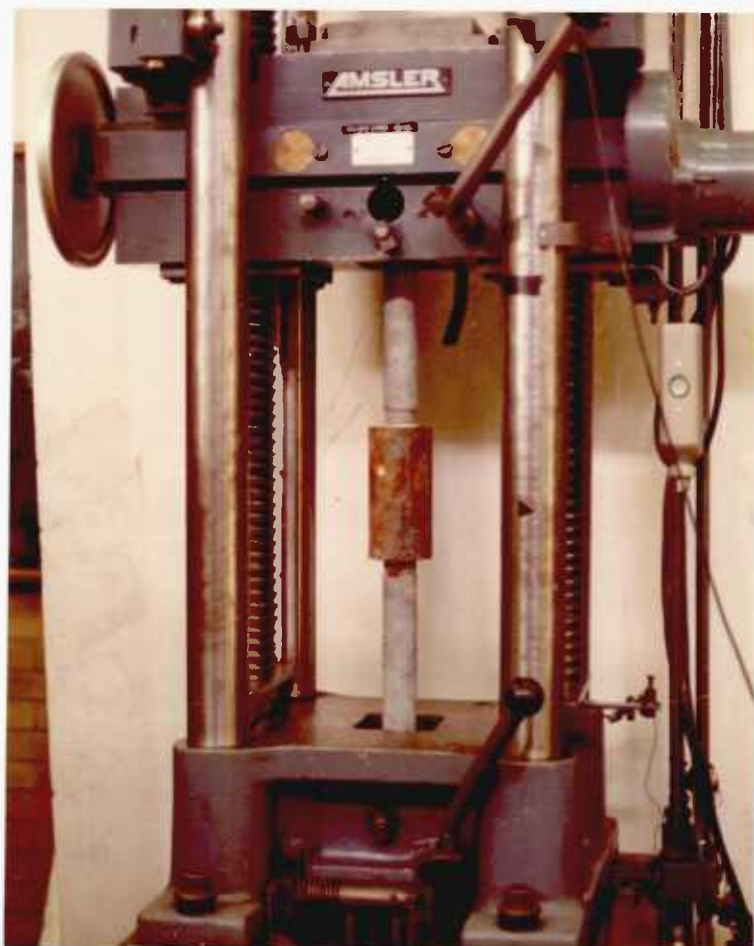


Plate 4: Loading rig of small scale model

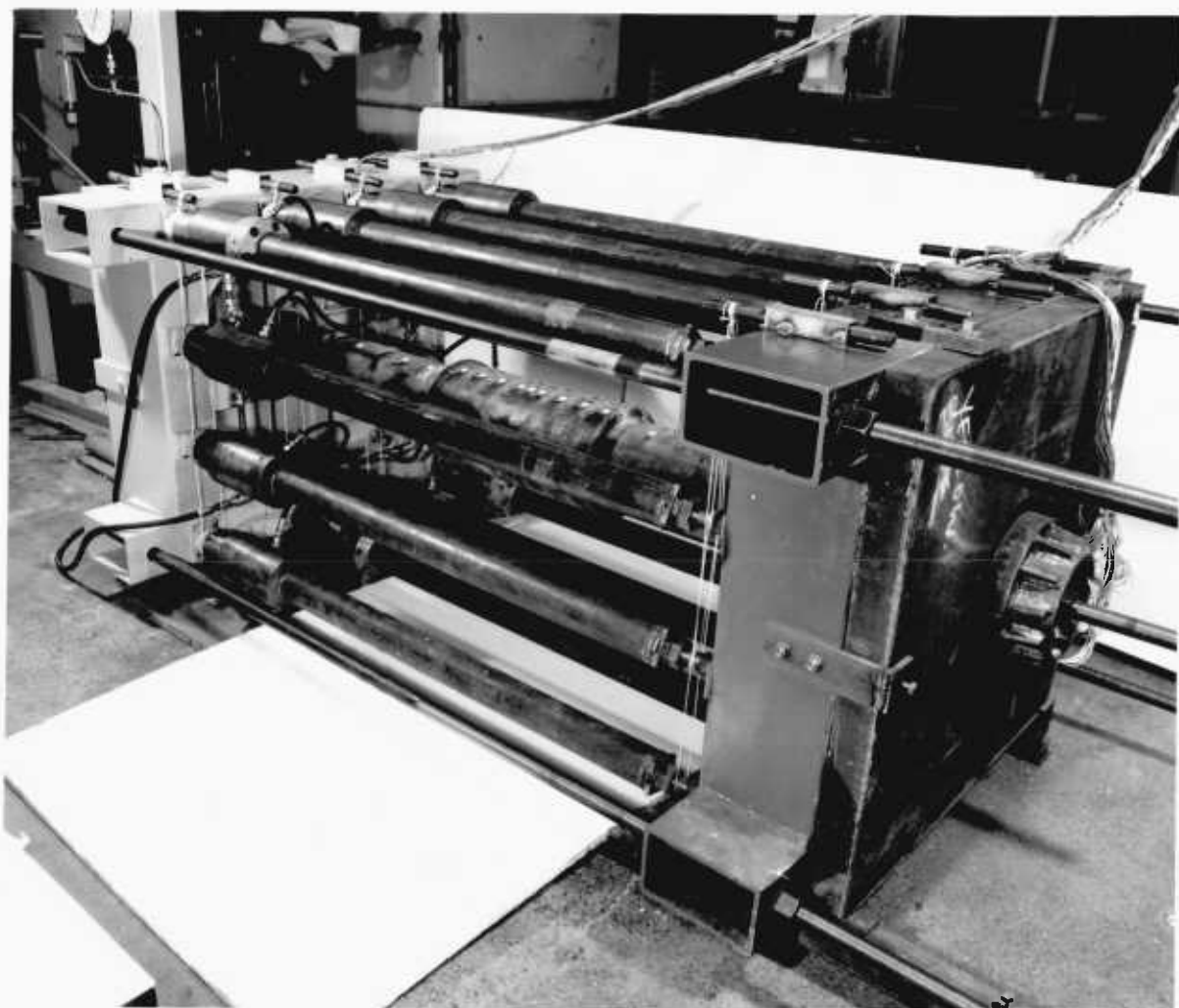


Plate 5: Loading rig of large scale model



Plate 6: The mode of failure of large scale model



Plate 7: The mode of failure of small scale model ( $L = 2D$ )





Plate 8: The mode of failure of small model ( $L = 3D$ )



Plate 9: Shear connectors in small scale model



Plate 10: Shear connectors (weld beads) on large scale model



Plate 11: Strain gauges. Layout on external surface of sleeve

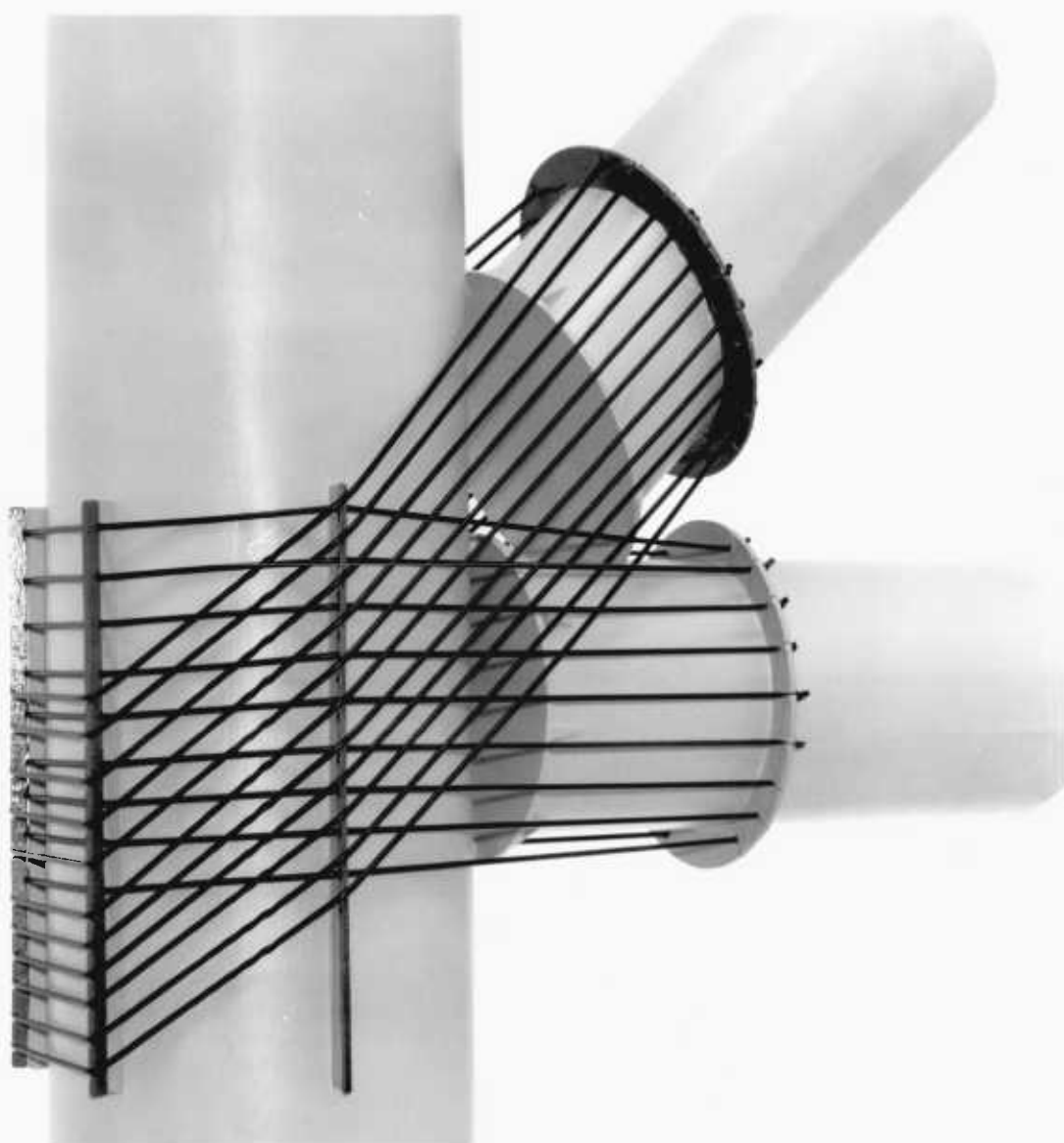


Plate 12: Joint I model

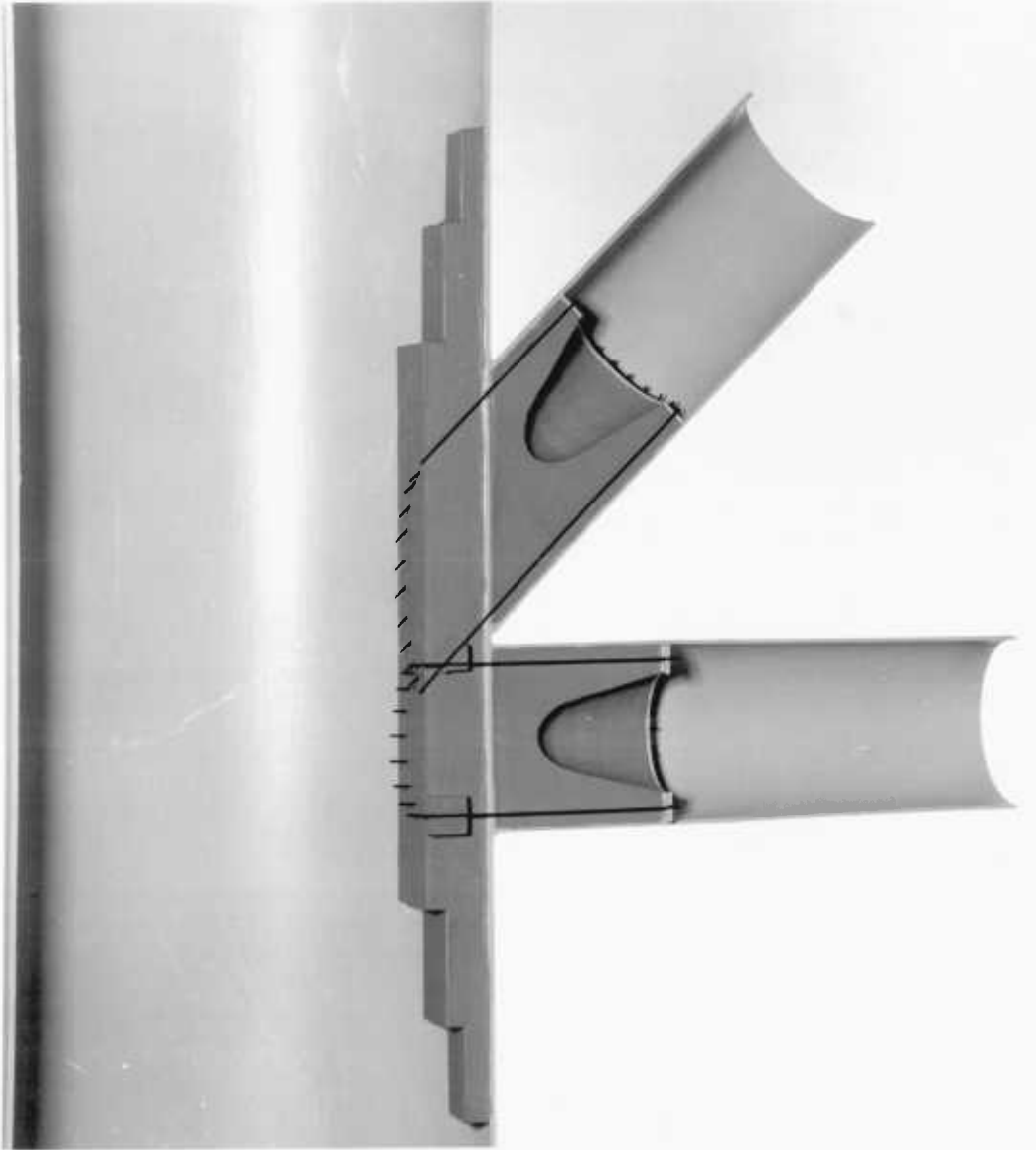


Plate 13: Joint III model